A Study on Single-cell Analysis by a Stigmatic-type Imaging Mass Spectrometer using Nanoparticle-Assisted Laser Desorption/Ionization Technique

BRIJESH

Department of Physics, Graduate School of Science,

Osaka University

March 2020

ABSTRACT

Matrix-Assisted Laser Desorption/Ionization Mass Spectrometry (MALDI-MS) imaging is a powerful and successful tool to visualize the distribution of biomolecules in the biological tissues and cells. However, a sub-cellular scale lateral resolution is still difficult to obtain by the conventional scanning-type MALDI imaging mass spectrometer because of the dependence of spatial resolution on the laser spot size, which is usually in the range of 10-100 μm. One more issue is the extremely long measurement time. Many researchers have optimized MALDI laser to smaller spot sizes, but the issue of long measurement time remains. To address this problem, a stigmatic-type imaging mass spectrometer equipped with a position- and time-sensitive detector, in which the spatial resolution is not dependent on the laser focus diameter was used in this study. In a stigmatic-type imaging mass spectrometer, the spatial distribution is determined by the combination of the magnification of the ion distribution by the ion optics and the pixel size of the detector. Thus, it has the potential to achieve a high spatial resolution. Furthermore, the measurement time can also be reduced by analyzing a large sample area in a single shot.

Other issues in MALDI are associated with organic matrices. The organic matrices, when deposited on the sample after mixing in a solution, forms large matrix-analyte co-crystals, which reduces the image resolution. Also, organic matrices are easily ionized, so they produce many interference peaks. Moreover, the deposition of the matrix in wet form can cause the migration of the analytes in the sample which results in the reduction of the image quality.

SALDI (Surface-Assisted Laser Desorption/Ionization) MS is an alternative technique to MALDI MS where inorganic nanoparticles and nanostructured surfaces are used as a matrix instead of traditional MALDI matrices. SALDI MS is getting popularity over the last decade because of the unique properties of nanoparticles and some of its advantages over MALDI MS advantages such as easier sample preparation, low background noise.

The nanoparticles, if applied as a matrix in dry form, increases the shot-to-shot reproducibility because of better homogeneity as compared to the conventional organic MALDI matrix applied in wet form. The use of nanoparticles can solve the problem of reduced image quality caused by the large size of matrix crystals. And, the deposition of the organic matrix by sublimation or deposition of the nanoparticles by sputtering can remove the wet deposition problem. The

deposition of the nanoparticles by sputtering is rather straightforward than the sublimation deposition of the organic matrix. Considering all these advantages of nanoparticles over the traditional organic matrix, nanoparticles were used as a matrix in this study.

A standard lipid 1,2-distearoyl-sn-glycero-3-phosphocholine (DSPC) using 7 nanoparticles (TiO_2, CeO_2, WO_3, Ag, ZnO, CaO, Fe_2O_3) and organic DHB matrix and, amoeba cells using the same 7 nanoparticles (TiO_2, CeO_2, WO_3, Ag, ZnO, CaO, Fe_2O_3) were analyzed by a scanning-type MALDI Spiral-TOF mass spectrometer for the selection of the appropriate nanoparticle for single-cell analysis. The metal oxide nanoparticles were deposited on the sample in the wet form after mixing in a solution using a pipette and, the Ag NPs were deposited in dry form using an ion sputtering instrument. After screening all these nanoparticles, the Fe_2O_3 NPs were found to be most effective for the analysis of lipids in the amoeba cells. Fe_2O_3 NPs and Ag NPs were selected for further analysis. Fe_2O_3 NPs were selected because they were most suitable and Ag NPs were also selected because they can be deposited in dry form which is suitable for imaging analysis. Then the imaging analyses of amoeba cells were performed using Fe_2O_3 NPs and Ag NPs. However, the spatial resolution of the images was reduced when Fe_2O_3 NPs were used because they were deposited in the wet form which may have caused the migration of the cells or the analytes in the cells.

HeLa cells were analyzed using Ag nanoparticles, which can be deposited in the dry form, by the scanning-type MALDI Spiral-TOF mass spectrometer and, a spatial resolution of 30 μm was achieved. Then, single HeLa cells were analyzed by a stigmatic-type imaging mass spectrometer using Ag nanoparticles and, a spatial resolution of 2 μm was obtained as a result.

The stigmatic-type imaging mass spectrometer equipped with a position- and time-sensitive detector and in combination with nanoparticle-assisted laser desorption/ionization technique showed the potential for high spatial resolution single-cell imaging. Since single-cell analyses are very important for understanding cell metabolism, cellular functions, and disease states, this study will be of great importance for the single-cell biologist and mass spectrometry researchers and inspire them to adopt stigmatic-type imaging mass spectrometer for single-cell analysis.

Abbreviations and symbols used in this thesis:

MALDI – Matrix-Assisted Laser Desorption/Ionization

SALDI – Surface-Assisted Laser Desorption/Ionization

DSPC – 1,2-distearoyl-sn-glycero-3-phosphocholine

PC - Phosphatidylcholines

TiO_2 – Titanium Oxide, CeO_2 – Cerium Oxide, WO_3 – Tungsten Oxide, ZnO – Zinc Oxide, CaO – Calcium Oxide, Fe_2O_3 – Iron Oxide, Ag – Silver

NPs – Nanoparticles

TOF – Time-of-flight

SCMS – Single cell mass spectrometry

MS – Mass Spectrometry

MSI – Mass Spectrometry Imaging

DHB – Dihydroxybenzoic Acid

ESI – Electrospray Ionization

SIMS – Secondary Ion Mass Spectrometry

LDI – Laser Desorption Ionization

PEDA – Post-extraction Differential Acceleration

Contents

Chapter 1

Introduction

1.1 Introduction to MALDI Mass Spectrometry Imaging

1.1.1 MALDI-MS

MALDI (Matrix-assisted laser desorption/ ionization) is an ionization technique used for the ionization of the molecules from an analyte with minimal fragmentation. The analyte is embedded in a matrix which absorbs the energy of the laser used for the ionization.[1,2]

The credit for discovering the MALDI-MS goes to two independent research groups. In 1985, Michael Karas and Franz Hillenkamp coined the term MALDI when they ionized amino acid alanine by mixing it with amino acid tryptophan using a 266 nm wavelength pulsed laser.[1] In 1987, Koichi Tanaka of Shimadzu Corporation used 30 nm size cobalt particles suspended in glycerol as a matrix to ionize proteins by using a 337 nm pulsed laser.[2] MALDI-MS was further improved by the introduction of 355 nm wavelength laser and other matrices such as DHB, CHCA, sinapinic acid.

Matrix-assisted laser desorption/ ionization (MALDI) usually coupled with time-of-flight mass analyzer is a soft ionization technique, in which the biological sample, which is embedded in an organic matrix, is irradiated by a very short laser pulse at various spot sizes to ionize biological sample, that allows sensitive detection and identification of a variety of chemical species.[1,2] The organic matrix absorbs the laser energy and transfer it to the analyte which results in the ionization of the analyte with little or no fragmentation thus making MALDI a soft ionization technique.[1,2] MALDI MS has many advantages such as 1) High-throughput 2) High sensitivity 3) High tolerance towards salts 4) small sample consumption 5) simple sample preparation.

MALDI-MS has been applied to the analysis of biomolecules (biopolymers such as DNA, proteins, peptides, metabolites, amino acids, lipids, carbohydrates, and nucleotides and sugars) and large organic molecules (such as polymers, dendrimers, and other macromolecules), which tend to be fragile and fragment when ionized by more conventional ionization methods.[3-7]

1.1.2 Time of Flight MS

Like other mass spectrometry methods, TOF-MS[8] also analyze ions based on their mass-to-charge ratio. Time of flight mass spectrometry utilizes a vacuum chamber. An electric field is applied to accelerate the ions through the chamber but once the ions enter the chamber they are in an electric field-free region and they move only by the kinetic energy obtained when they were accelerated. Provided all ions start their journey at the same time, heavier ions of the same charge reach the detector later than the lighter ions of the same charge because of low velocity as compared to the lighter ions. The time it takes for the ions to reach the detector from their point of origin can be used to calculate their mass-to-charge ratio.

The potential energy (E_p) of an ion of mass m with electric charge q in an electric field of strength U can be written as

$E_p = qU$, where q is equal to an integer number of z of an electron charge e

Thus, $E_p = ezU$

And, when the ion is accelerated through the TOF tube by a voltage U, its potential energy is converted to kinetic energy ($E_k = ½\ mv^2$)

Hence, $½\ mv^2 = ezU$

Therefore, the unchanged velocity of the ion in the field-free TOF tube can be expressed as

$$v = (2ezU/m)^{1/2}$$

And, if the length of the TOF tube is L, then the time (T) required to traverse the length L can be written as

$$T = L(m/2ezU)^{1/2}$$

Therefore, the mass-to-charge ratio is

$$m/z = 2eU(T/L)^2$$

1.1.3 MALDI-MSI

MALDI-MS can also be used as a mass spectrometric imaging technique. MALDI-MSI (MALDI Mass Spectrometry Imaging)[7] allows the two-dimensional visualization of the spatial distribution of hundreds to thousands of molecules in a biological sample such as tissue simultaneously without the need for extraction or labeling of the analytes.

The conventional method of image construction by MALDI-MSI is as follows:

A specific region of the sample is irradiated by a pulsed laser and, a mass spectrum is recorded with the spatial information. To image a new region of the sample, either the sample plate or the laser is moved and, in this way, the whole sample is analyzed. By coupling the mass spectra obtained from all the regions, an average mass spectrum is obtained. By selecting an *m/z* peak of this spectrum, an ion image can be constructed for that particular *m/z* ion. The image represents the spatial distribution and relative abundance of that ion in the sample.

MALDI-MSI is the most popular mass spectrometric imaging technique. It has been used for

the imaging of mouse brain and kidney tissues, human tissues and fingerprints, etc.[3-7] However, MALDI-MSI has some limitations when it comes to imaging at sub-cellular scale spatial resolution. More about single-cell imaging mass spectrometry is discussed in the next section.

1.2 Single Cell Mass Spectrometry (SCMS)

1.2.1 Introduction

Cells are the fundamental structures of life. The human body contains many different types of cells and every type of cell have a separate function. Studying cells gives an insight into cellular dynamics, functions and how these cells develop. But, rather than studying a cell population, it is important to study single cells because of cellular heterogeneity. The same cell types can exhibit different biomolecular makeup depending on their surroundings and interactions, so studying a cell population can lead to a wrong conclusion. Analysis of the chemical composition and content of a single cell can provide a better understanding of cell metabolism, cell cycle, adaptation, disease states, etc. However, it is not easy to analyze single cells because of the following reasons 1) very small size of each cell 2) many types of substances are present in each cell with immensely low concentration.

1.2.2 Single Cell Analysis Techniques

Although in this study mass spectrometry was used for single-cell analysis, other various techniques have been used for the single-cell analysis. Those techniques include flow cytometry[9-10], fluorescence microscopy[11-12], single-cell transcriptomics[13] and, Raman spectroscopy[14].[15,16] However, these techniques suffer from some drawbacks. For example, flow cytometry and fluorescence microscopy require the labeling of the sample before the analysis. Single-cell transcriptomics is a fast-growing technique but suffers from some computational challenges. Raman effect in Raman spectroscopy is usually weak, which leads to low

sensitivity.

On the other hand, mass spectrometry techniques allow simultaneous analysis of thousands of molecules with high sensitivity and without the need for labeling. Other advantages of mass spectrometry are high throughput, low sample consumption, and multiplexed detection. There are various mass spectrometry ionization techniques. The three major ionization techniques that are used for mass spectrometry imaging analysis are ESI-MS[17], SIMS[18], and MALDI-MS. MALDI and ESI are soft ionization techniques whereas SIMS is a hard ionization technique. ESI-MS has been employed for single-cell analysis in the past.[19-23] ESI-MS is well suited for single-cell profiling, but not suitable for single-cell imaging analysis because of low spatial resolution as compared to MALDI and SIMS.

SIMS can provide sub-micron level spatial resolution because the ion beam in SIMS can be collimated to the sub-micron range, there have been some studies[24-26,27-29] of single-cell imaging analysis using SIMS in recent years. Lanekoff et al.[24] performed TOF SIMS analysis of freeze fractured rat PC12 cells with 4 μm spatial resolution. Vanbellingen et al.[25] performed single-cell level chemotherapeutic drug delivery analysis by 3D-MSI-TOF-SIMS with 1 μm pixel size. SIMS provides better spatial resolution than commercial MALDI instruments. However, the mass range in SIMS is limited to less than 500 *m/z* because of the excessive fragmentation and sometimes it is also difficult to identify the peaks. MALDI is a technique that is a soft ionization technique and also provides high-spatial-resolution.

1.2.3 MALDI MSI for SCMS

Before the development of MALDI-MS, LDI-MS, developed in 1960 which uses no matrix was used as a surface analysis technique in mass spectrometry. The sample to be analyzed is

irradiated by a laser and the sample molecules absorb the laser energy at the wavelength of the laser which results in the desorption/ionization of the sample molecules. There had been some studies on single-cell analysis by LDI-MS.

Although LDI is a powerful tool for the qualitative and quantitative surface analysis of the biological samples, this method has some limitations. However, direct irradiation of the laser beam on the sample can lead to extensive fragmentation of the sample molecules and, in many cases, sample molecules are not able to directly absorb the laser energy at the wavelength of the laser.

Then, in the 1980s, Karas and Hillenkamp developed matrix-assisted laser desorption ionization mass spectrometry (MALDI-MS) which incorporated a matrix that absorbs the laser energy and transfers that energy to the sample and prevents extensive fragmentation.

Now, MALDI has become one of the most commonly used MS ionization methods for the biological tissue imaging and single-cell analysis because of its advantages over matrix-free LDI-MS.[30,31]

Although MALDI is one of the most commonly used ionization methods in biological tissue imaging, it suffers from the limitation of spatial resolution when it comes to single-cell imaging.[32,33] In MALDI, the spatial resolution depends on the laser spot size which is usually in the range of 10-100 μm in commercial instruments. Recently, many research groups have optimized MALDI for single-cell mass spectrometry imaging (MSI) and achieved a high-spatial resolution.[34–37,38-46]

Feenstra et al.[43] altered laser optics of a MALDI-MSI instrument and reduced the laser spot size from 9 μm to 4 μm. Schober et al. imaged single HeLa cells using an AP-MALDI

(Atmospheric Pressure - MALDI) source attached with an Exactive Orbitrap mass analyzer and achieved spatial resolution of 7 μm.[47] Kompauer et al. also performed AP-MALDI mass spectrometry of tissues and cells with a resolution of 1.4 μm.[48] Zavalin et al.[37] was able to image tissue protein at 1 μm laser spot diameter by integrating a transmission geometry MALDI ion source with time of flight mass spectrometry.

SIMS and these optimized MALDI instruments with very small laser spot sizes have the potential for single-cell imaging analysis, but in these methods, the spatial resolution is dependent on the laser spot size. And, because the spatial resolution is dependent on the laser spot size, smaller the laser spot size longer it takes to scan and image a sample, so the measurement time becomes extremely long with the smaller spot size lasers. In our study, a stigmatic-type MALDI imaging mass spectrometry in which spatial resolution is independent of the laser spot size is used for the single-cell imaging analysis. Also, the imaging analysis by a Stigmatic-type imaging mass spectrometer is much faster than the conventional scanning type MALDI mass spectrometer and, it has the potential of achieving sub-cellular scale spatial resolution. Heeren and co-workers first reported stigmatic-type imaging MS by modifying a commercial SIMS TOF mass spectrometer (TRIFT II; Physical Electronics, Eden Prairie, MN).[49,50] Stigmatic-type imaging mass spectrometer used in this research was constructed in our lab.[51] Stigmatic-type imaging mass spectrometer is discussed in detail in chapter 2.

1.3 SALDI (Surface-Assisted Laser Desorption/Ionization) MS

As mentioned earlier, in 1987, noble laureate Koichi Tanaka used 30 nm size cobalt nanoparticles as a matrix to ionize proteins.[1] Since then MALDI-MS was developed using various kinds of matrices. Though Koichi Tanaka used NPs for the analysis of proteins, the use of organic matrices became more common in MALDI-MS because they provide better ionization efficiency and less molecular ion fragmentation. Although MALDI-MS is a very

powerful and successful tool to study biomolecules, it is difficult to measure the molecules in the low mass range (<500 Da) because of the interference caused by the fragments of the organic matrix ions. SALDI MS is an alternative technique to MALDI MS where inorganic nanoparticles and nanostructured surfaces are used as a matrix instead of traditional MALDI matrices[52-58]. SALDI MS is getting popularity over the last decade because of the unique properties of nanoparticles and some of its advantages over MALDI MS advantages such as easier sample preparation, low background noise.

The use of an organic matrix in MALDI Imaging MS can limit the spatial resolution because of the large size of the crystals formed by the MALDI matrix. The use of nanoparticles can solve the problem of reduced image quality caused by the large size of matrix crystals.

The organic matrices and nanoparticles applied on the sample in a wet state are less homogeneous which decreases the shot to shot reproducibility and nanoparticles applied on the sample in a wet state tend to aggregate and settling out of the solution which reduces the efficiency of the nanoparticles as a matrix and reduces the image quality during imaging analysis.

The deposition of the organic matrix by sublimation or deposition of the nanoparticles by sputtering can remove the wet deposition problem. The sputter deposition of nanoparticles is more straightforward and easier as compared to the deposition of the organic matrix by sublimation. Considering all these advantages of nanoparticles, nanoparticles are used in this study instead of the traditional organic matrix.

Many researchers have used different classes of nanoparticles for MALDI mass spectrometry analysis of various types of biological samples. Muller et al.[52] did MALDI MSI of lipids in a normal rat kidney using Ag NPs. There are many more studies[59] of the use of Ag NPs for the analysis of various biological samples by MALDI mass spectrometry. Kusano et al.[53] used Iron

Oxide NPs for the LDI-MS of some standard lipids. There is an excellent review on the application of NPs as a matrix in MALDI-MS by Arakawa et al.[54] There is a study[55] of analysis of small molecules and cells by gold nanoparticles. Sakurai et al.[60] used CdTe and CuO Nanoparticles for the analysis of compounds which contains carboxyl groups. Amin M.O. et al.[61] used various metal oxide nanoparticles for the analysis of latent fingerprints and small drug molecules. Yagnik et al.[57] performed large scale screening of nanoparticles for the analysis of plant metabolites. Bernier et al.[62] used Tungsten oxide and Rhenium oxide for the ionization of small molecules.

Although there have been many studies of analysis of various biological samples by MALDI mass spectrometry using nanoparticles as a matrix, there are very few studies for the single-cell level imaging analysis by SALDI MS using nanoparticles as a matrix.

In this study, a unique combination of matrix and MALDI mass spectrometer is used. Nanoparticles are used as a matrix for the single-cell imaging analysis by a stigmatic-type MALDI mass spectrometer which has never been done before in our knowledge.

1.4 Outline of this thesis

The purpose of this thesis is to image a single cell by a stigmatic-type imaging mass spectrometer with a high spatial resolution using nanoparticle-assisted laser desorption/ionization mass spectrometry technique.

In Chapter 1, the importance of single-cell imaging analysis and the advantages of using nanoparticles as a matrix in SALDI MSI is described. The limitations of conventional scanning-type mass spectrometry imaging instruments for the single-cell analysis and solutions to overcome those limitations are also described. Single-cell analysis by a stigmatic-type

imaging mass spectrometer using SALDI is proposed.

In Chapter 2, the working mechanism of a conventional scanning-type MALDI Spiral-TOF mass spectrometer and a stigmatic-type imaging mass spectrometer is described. The advantages of a stigmatic-type imaging mass spectrometer over the conventional MALDI instruments are also discussed.

In Chapter 3, the screening of 7 nanoparticles for the selection of the appropriate nanoparticles for the single-cell imaging analysis is described. A standard phospholipid and amoeba cells were analyzed by a conventional MALDI Spiral-TOF instrument using these 7 nanoparticles. After the analyses, the two suitable nanoparticles Fe_2O_3 and Ag were selected for single-cell imaging analysis.

In Chapter 4, amoeba cells and HeLa cells imaging analysis using the selected nanoparticles by a conventional MALDI Spiral-TOF instrument is described. Amoeba cells were analyzed using Fe_2O_3 and Ag nanoparticles. Although the Fe_2O_3 nanoparticles were more suitable for the analysis of lipids in the amoeba cells, the spatial resolution of the images was reduced due to the deposition of Fe_2O_3 nanoparticles in the wet form. Therefore, HeLa cells were analyzed using Ag nanoparticles. A spatial resolution of about 20-30 μm was achieved.

In Chapter 5, the single HeLa cells imaging analysis using Ag nanoparticles by a stigmatic-type imaging mass spectrometer is described. This was the first time stigmatic-type imaging mass spectrometer was used for the single-cell imaging analysis. A spatial resolution of 2 μm was achieved, which is far better as compared to 20-30 μm obtained by scanning-type MALDI Spiral-TOF instrument.

References

[1] M. Karas, F. Hillenkamp *Anal. Chem.*,1**988**, 60, 2299.

[2] Tanaka, K.; Waki, H.; Ido, Y.; Akita, S.; Yoshida, Y.; Yoshida, T.; Matsuo, T. *Rapid Commun. Mass Spectrom.* **1988**, 2, 151−153.

[3] J. H. Jungmann, R. M. Heeren, *Journal of proteomics* **2012**, *75*, 5077.

[4] A. Svatoš, *Trends in biotechnology* **2010**, *28*, 425.

[5] N. Zaima, T. Hayasaka, N. Goto-Inoue, M. Setou, *International journal of molecular sciences* **2010**, *11*, 5040.

[6] Y. J. Lee, D. C. Perdian, Z. Song, E. S. Yeung, B. J. Nikolau, *The Plant Journal* **2012**, *70*, 81.

[7] P. M. Angel, R. M. Caprioli, *Biochemistry* **2013**, *52*, 3818.

[8] Stephens W. E., **1946**, *Phys. Rev. 69* (11–12): 691

[9] J Picot, CL Guerin, C Le Van Kim, CM Boulanger, *Cytotechnology*, **2012**, 64(2), 109-130.

[10] S. Muller, G. Nebe-von-Caron, *FEMS Microbiology Reviews*, **2010**, 34(4), 554-587.

[11] M. J. Sanderson, I. Smith, I. Parker, M. D. Bootman, *Cold Spring Harb Protoc.*, **2014**(10).

[12] D. Muzzey, A. van Oudenaarden, *Annu Rev Cell Dev Biol.*, **2009**, 25:301-27.

[13] I. Kanter, T. Kalisky, *Frontiers in Oncology*, **2015**, 5:53.

[14] M. Li, J. Xu, M. Romero-Gonzalez, S. A. Banwart, W. E. Huang, *Curr Opin Biotechnol.*, **2012**, 23(1):56-63.

[15] L. Armbrecht, P. S. Dittrich, *Anal. Chem.*, **2017**, 89, 2-21.

[16] L. Yin, Z. Zhang, Y. Liu, Y. Gao, J. Gu *Analyst*, **2019**, 144, 824-845.

[17] CS Ho, MHM Chan, RCK Cheung, LK Law, LCW Lit, KF Ng, MWM Suen, HL Tai, *Clin Biochem Rev.*, **2003**, 24(1), 3-12.

[18] R. W. Odom, *Applied Spectroscopy Reviews*, **1994**, 29:1, 67-116.

[19] HM Bergman, I. Lanekoff, *Analyst*, **2017**, 142, 3639.

[20] H. Li, B.K. Smith, B. Shrestha, L. Mark, A. Vertes, *Methods Mol Biol.*, **2015**, 1203:117-127.

[21] S.A. Stopka, R. Khattar, B.J. Agtuca, C.R. Anderton, L. Pasa-Tolic, G. Stacey, A. Vertes, *Front Plant Sci.*, **2018**, 9:1646.

[22] H. Mizuno, N. Tsuyama, T. Harada and T. Masujima, *J. Mass Spectrom*., **2008**, 43, 1692–1700.

[23] A. F. Gonzalez-Serrano, V. Pirro, C. R. Ferreira, P. Oliveri, L. S. Eberlin, J. Heinzmann, A. Lucas-Hahn, H. Niemann and R. G. Cooks, *PLoS One*, **2013**, 8, e74981.

[24] I. Lanekoff, M. Kurczy, R. Hill, J. Fletcher, J. Vickerman, N. Winograd, P. Sjovall, A. Ewing *Anal Chem.* **2010**, 82(15), 6652-6659.

[25] Q. Vanbellingen, A. Castellanos, M. Rodrigues-Silva, I. Paudel, J. Chambers, F. Fernandez-Lima *J. Am. Soc. Mass Spectrom.* **2016**, 27, 2033-2040.

[26] C. Szakal, K. Narayan, J. Fu, J. Lefman, S. Subramaniam *Anal. Chem.* **2011**, 83, 1207-1213.

[27] M. K. Passarelli, C. F. Newman, P. S. Marshall, A. West, I. S. Gilmore, J. Bunch, M. R. Alexander, C. T. Dollery, *Anal. Chem.*, **2015**, 87, 13, 6696-6702.

[28] H. Jungnickel, P. Laux, A. Luch, *Toxics*, **2016**, 4(1), 5.

[29] M. Giardina, S. Cheong, C. E. Marjo, P. L. Clode, P. Guagliardo, R. Pickford, M. Pernice, J. R. Seymour, JB Raina, *Front. Microbiol.*, **2018**, 9:2847.

[30] K.J. Boggio, E. Obasuyi. K. Sugino, S. B. Nelson, N. Y. R. Agar, J. N. Agar, *Expert Rev Proteomics.* **2011** October; 8(5): 591-604.

[31] M. M. Gessel, J. L. Norris and R. M. Caprioli, *J. Proteomics*, **2014**, 107, 71–82.

[32] Q. Wu, T. J. Comi, B. Li, S. S. Rubakhin and J. V. Sweedler, *Anal. Chem*., **2016**, 88, 5988–5995.

[33] R. Bradshaw, N. Denison and S. Francese, *Analyst*, **2017**, 142, 1581–1590.

[34] T. J. Comi, M. A. Makurath, M. C. Philip, S. S. Rubakhin and J. V. Sweedler, *Anal. Chem*., **2017**, 89, 7765–7772.

[35] S. Neupert, S. S. Rubakhin and J. V. Sweedler, *Chem. Biol*., **2012**, 19, 1010–1019.

[36] S. Matsushita, E. Sugiyama, T. Hayasaka, N. Masaki, M. Setou, *J. Mass Spectrom. Soc. Jpn.*, **2014**, 62(4), 29-36.

[37] A. Zavalin, J. Yang, K. Hayden, M. Vestal and R. M. Caprioli, *Anal. Bioanal. Chem*., **2015**, 407, 2337–2342.

[38] B. Li, D. K. Bhandari, A. Rompp, B. Spengler, *Scientific Reports*, **2016**, 6:36074.

[39] W. T. Andrews, S. B. Skube and A. B. Hummon, *Analyst*, **2018**, 143, 133–140.

[40] N. E. Mascini, J. Teunissen, R. Noorlag, S. M. Willems and R. M. A. Heeren, *Methods*, **2018**, 13(6), 612–632.

[41] A. D. Feenstra, R. L. Hansen and Y. J. Lee, *Analyst*, **2015**, 140, 7293–7304.

[42] C. Keller, J. Maeda, D. Jayaraman, S. Chakraborty, M. R. Sussman, J. M. Harris, JM Ane, L. Li, *Front. Plant Sci.*, **2018**, 9:1238.

[43] A. D. Feenstra, M. E. Duenas and Y. J. Lee, *J. Am. Soc. Mass Spectrom*., **2017**, 28, 434–442.

[44] R. L. Hansen and Y. J. Lee, *Chem. Rec*., **2018**, 18, 65–77.

[45] M. E. Duenas, A. T. Klein, L. E. Alexander, M. D. Yandeau-Nelson, B.J. Nikolau and Y.J. Lee, *Plant J*., **2017**, 89, 825-838.

[46] M. E. Duenas, J. J. Essner and Y. J. Lee, *Sci. Rep*., **2017**, 7(1), 14946.

[47] Y. Schober, S. Guenther, B. Spengler, A. Rompp *Anal. Chem.*, **2012**, 84, 6293-6297.

[48] M. Kompauer, S. Heiles, B. Spengler *Nature Methods* **2017**, 14.

[49] S.L. Luxembourg, T.H. Mize, L.A. McDonnell, R.M.A. Heeren, *Anal. Chem*., **2004**, 76, 5339–5344.

[50] A.F.M. Altelaar, I.M. Taban, L.A. McDonnell, P.D.E.M. Verhaert, R.P.J. de Lange, R.A.H. Adan, W.J. Mooi, R.M.A. Heeren, S.R. Piersma, *Int. J. Mass Spectrom*., **2007**, 260, 203–211.

[51] H. Hazama, J. Aoki, H. Nagao, R. Suzuki, T. Tashima, K. Fujii, K. Masuda, K. Awazu, M. Toyoda, Y. Naito *Applied Surface Science* **2008**, 255, 1257-1263.

[52] L. Muller, A. Kailas, S. Jackson, A. Roux, D. Barbacci, J. Schultz, C. Balaban, A. Woods *Kidney Int.*, **2015**, 88(1), 186-192.

[53] M. Kusano, S. Kawabata, Y. Tamura, D. Mizoguchi, M. Murouchi, H. Kawasaki, R. Arakawa, K. Tanaka *The Mass Spectrometry Society of Japan*, **2014**, 3.

[54] R. Arakawa, H. Kawasaki *Analytical Sciences*, **2010**, 26, 1229-1240.

[55] H. N. Abdelhamid, H. Wu *Anal Bioanal Chem* (**2016**) 408: 4485-4502.

[56] Y. E. Silina, D. A. Volmer *Analyst*, **2013**, 138, 7053.

[57] Gargey B. Yagnik, Rebecca L. Hansen, Andrew R. Korte, Malinda D. Reichert, Javier Vela, Young Jin Lee *Anal. Chem.* **2016**, 88, 8926-8930.

[58] C. Chiang, W. Chen, H. Chang *Chem. Soc. Rev.*, **2011**, 40, 1269-1281.

[59] M. Dufresne, A. Thomas, J. Breault-Turcot, J. Masson, P. Chaurand *Anal. Chem.* **2013**, 85, 3318-3324.

[60] M. Sakurai, T. Sato, J. Xu, S. Sato, T. Fujino *Appl. Sci.* **2018**, 8, 492.

[61] M. Amin, M. Madkour, E. Al-Hetlani *Analytical and Bioanalytical Chemistry* **2018**.

[62] M. Bernier, V. Wysocki, S. Dagan *J Mass Spectrom* **2015**, 50(7), 891-898.

Chapter 2

Instrumentation

2.1 Introduction

As mentioned in the previous chapter, the conventional scanning type MALDI mass spectrometer is not suitable for the single-cell imaging analysis because the spatial resolution is roughly equal to the laser spot size and the laser spot size is typically 10-100 μm. To overcome this limitation, a stigmatic-type MALDI mass spectrometer, in which sub-micron level spatial resolution can be achieved independent of the laser spot size and the measurement time can also be reduced, was used in this research. In this study, a conventional scanning type MALDI Spiral-TOF mass spectrometer was used first for the nanoparticle screening to find the suitable nanoparticle for the single-cell analysis. Then the imaging analyses of two types of cells amoeba and HeLa were performed using the selected nanoparticles by the same instrument before the final analysis with the stigmatic-type MALDI mass spectrometer to compare the spatial resolution of the two instruments. In this chapter, a brief introduction about the conventional scanning type MALDI Spiral-TOF mass spectrometer and a detailed description of the stigmatic-type MALDI mass spectrometer used in the study is described.

2.2 Scanning type MALDI Spiral-TOF mass spectrometer

As the name suggests, in a Spiral-TOF MALDI mass spectrometer (Figure 2.1), the ions travel through a spiral trajectory.[1] The spiral flight path length is 17 m. The whole ion optics is packed in about 1 m. The spiral trajectory was introduced to increase the mass resolution by increasing the flight path in a compact space. The spiral trajectory was constructed by using four toroidal electrostatic sectors each consisting of 8-stories made up of 9 Matsuda plates piled up inside a cylindrical sector. The ions move through the four toroidal electrostatic sectors in a figure-

eight-shaped trajectory on a certain projection plane. After every cycle, the ion trajectory is shifted by 50 mm in a direction perpendicular to the projection plane, thus creating a spiral trajectory. The length of every cycle is 2.1 m.

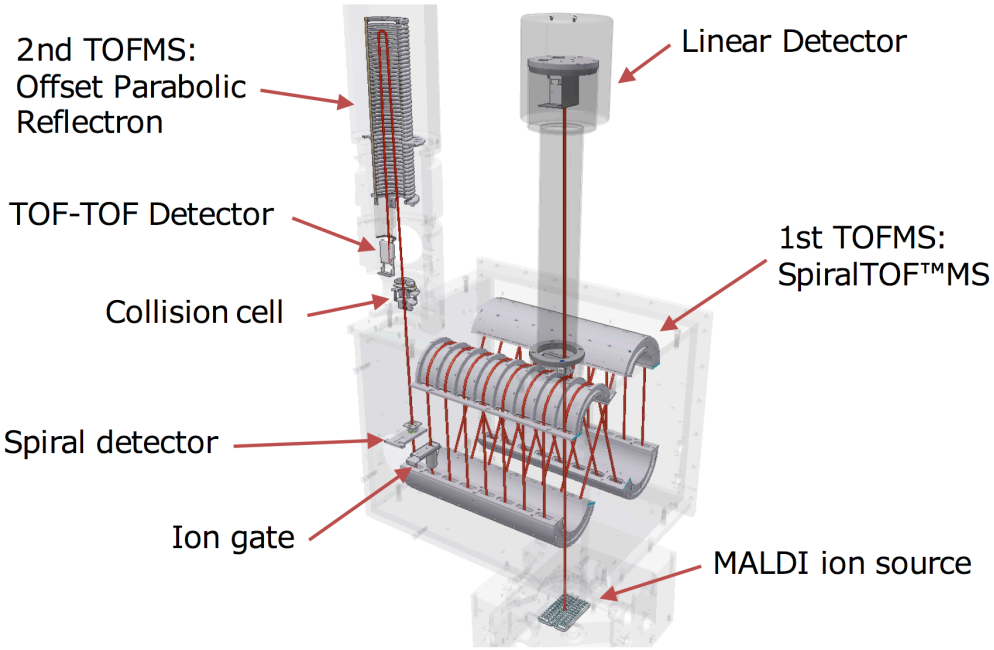

Fig. 2.1 – **Schematic of the JMS-S3000 MALDI Spiral-TOF Mass Spectrometer (**Reprinted with permission from JEOL Ltd., Tokyo, Japan**)**

The imaging analysis method is the same as other conventional MALDI-TOF mass spectrometers. A specific area of the sample is irradiated by a pulsed laser beam and, a mass spectrum is recorded with the spatial information. The laser spot size is about 20-30 µm which is not suitable for sub-cellular scale imaging analysis. To image a new area of the sample, either the sample stage or the laser is moved and, in this way, the whole sample is raster-scanned. By coupling the mass spectra obtained from all the regions, an average mass spectrum is obtained. By selecting an *m/z* peak of this spectrum, an ion image can be constructed for that particular

m/z ion. The image represents the spatial distribution and relative abundance of that ion in the sample.

2.3 Stigmatic type imaging mass spectrometer

2.3.1 Introduction

As mentioned in the previous section, in a scanning-type MALDI mass spectrometer, the spatial resolution is roughly equal to the laser spot size. Therefore, SIMS imaging MS has an advantage over MALDI imaging MS when it comes to getting better spatial resolution because the ion beam in SIMS can be focused on a narrower area than the laser beam. The smallest exposure spot size (diameter) that has been achieved in SIMS is below 100 nm, whereas that of commercial MALDI instruments is several tens of micrometers. However, SIMS has some disadvantages such as extensive fragmentation and lower mass range (<500 Da). That's why MALDI imaging MS became more popular than SIMS for the imaging of large biological samples such as tissues.

As a label-free technique, MALDI imaging MS of a single cell to observe sub-cellular structure can be of great advantage. But, it is not allowed by MALDI imaging MS due to its limited lateral resolution in the scanning mode. Also, it takes a lot of time to image a sample in MALDI imaging MS. SIMS has been applied for the single-cell imaging because it provides better lateral resolution, but it leads to extensive fragmentation as mentioned above.

To address this problem, a stigmatic-type imaging mass spectrometer[2,3] in which spatial resolution is not dependent on the laser spot size was used in this study. Heeren and co-workers first reported stigmatic-type imaging MS by modifying a commercial SIMS TOF mass spectrometer.[4,5] However, that instrument was equipped with a dual MCP phosphor screen detector. A position- and time-sensitive detector was needed for simultaneous measurements

of images from multiple types of molecules. The stigmatic-type imaging mass spectrometer used in this study is equipped with a position- and time-sensitive detector. The instrument is incorporated with a focusing lens after the extraction electrode and an electrostatic lens configuration before the detector which focused magnifies the ion distribution and projects it on the detector. This magnification of the ion distribution by the ion optics of the instrument and the pixel size of the detector determines the spatial resolution of this instrument, so the spatial resolution is independent of the laser spot size. Thus, the instrument has the potential to achieve sub-cellular scale spatial resolution.

Imaging of an area larger than the laser spot size can be performed in a similar way as the conventional raster-scanning method. Then the images from all the regions of that area can be merged to obtain the whole image. And, the merging of the stigmatic images is rather straightforward and faster than reconstructing the whole image from the mass spectral dataset. Figure 2.3 shows the comparison between a scanning probe type and a stigmatic-type imaging Mass Spectrometer.

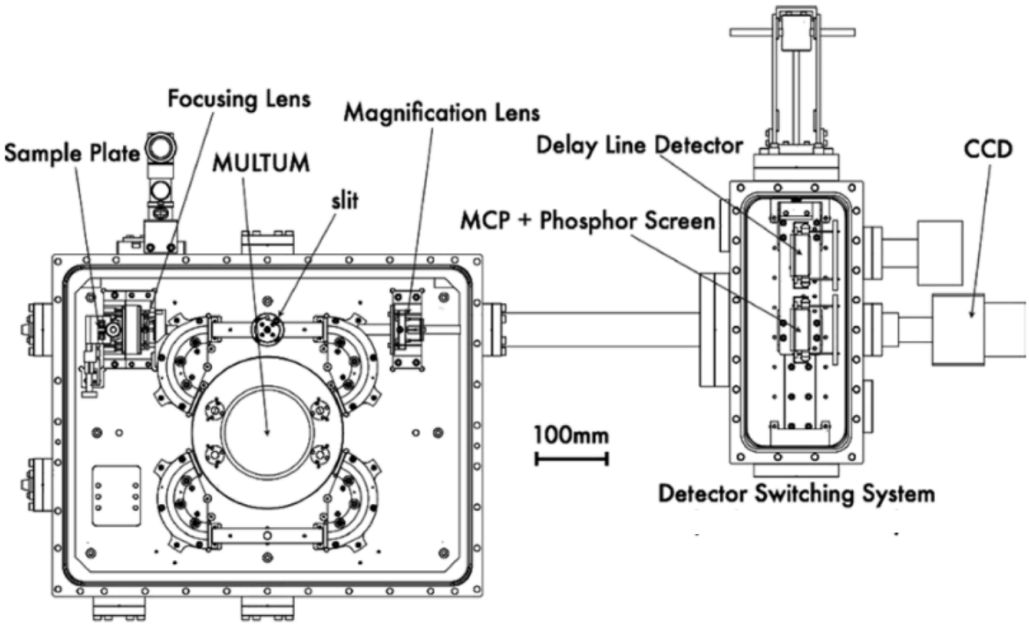

Fig. 2.2 – **Schematic drawing of the experimental apparatus for stigmatic imaging mass spectrometry (**Reprinted with permission from **Aoki, et al., *J. Mass Spectrom. Soc. Jpn.*, 2013, Vol. 61, No. 3.** Copyright 2013 **The Mass Spectrometry Society of Japan)**

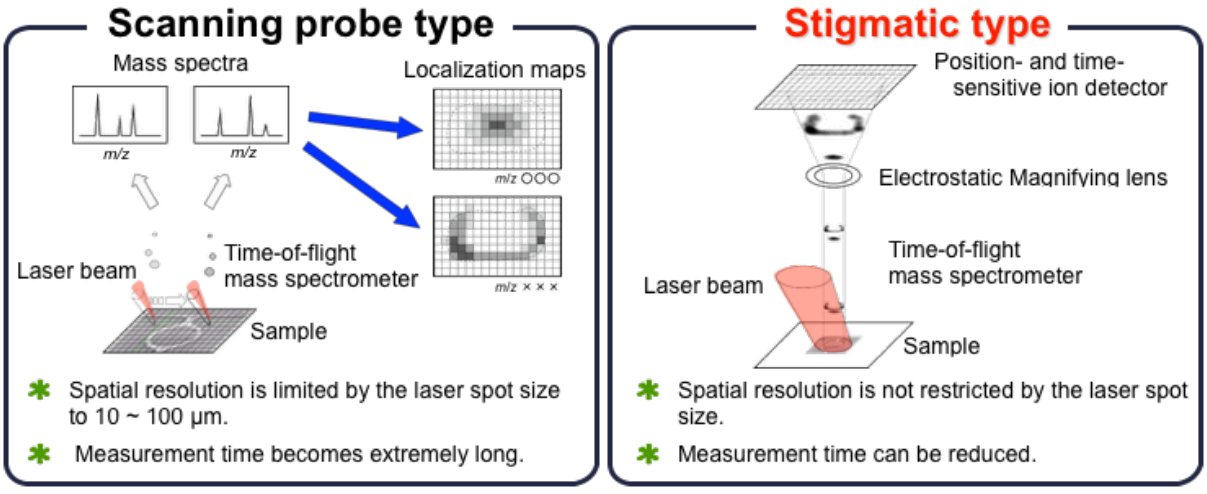

Fig. 2.3 - **Schematics of a scanning probe type and the stigmatic type MALDI mass spectrometer (**Reprinted with permission from **Aoki, et al., *J. Mass Spectrom. Soc. Jpn.*, 2013, Vol. 61, No. 3.** Copyright 2013 **The Mass Spectrometry Society of Japan)**

2.3.2 MALDI ion source

MALDI ion source of our stigmatic mass spectrometer consists of a third harmonic Nd: YAG UV laser of wavelength 355 nm with a square shape profile of that was focused onto the sample plate at 0.75 mm^2 and repetition rate of 1 kHz. The ions produced at the sample plate surface were accelerated at the ion source. The ion distribution was magnified and focused by an Einzel lens configuration.

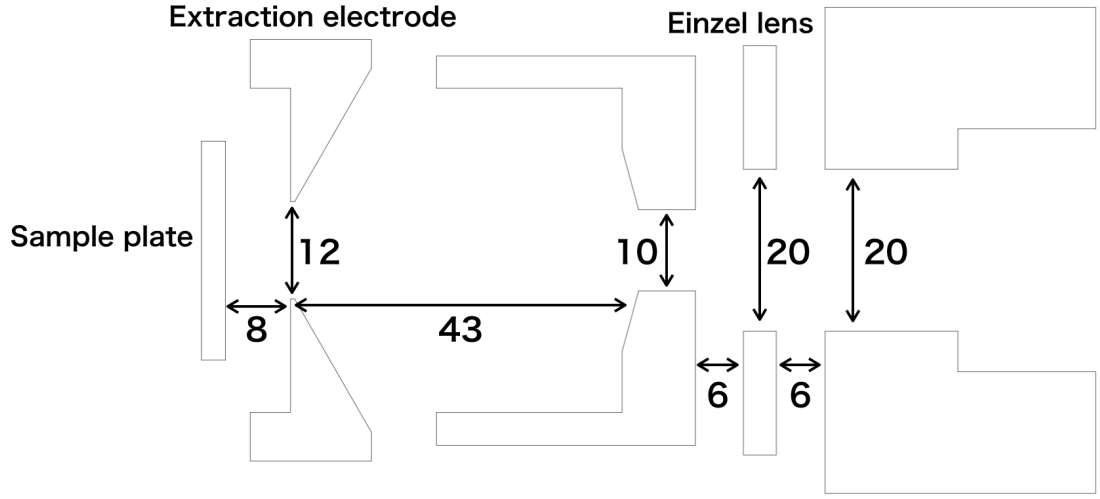

Fig. 2.4 - **Configuration of electrodes in the MALDI ion source block. Unit of length is mm.**

Figure 2.4 represents the Configuration of electrodes in the MALDI ion source block. The extraction electrode had a circular aperture of diameter 12 mm. The separation between the sample plate and the extraction electrode was 8 mm, while that of the extraction and ground electrodes was 43 mm. The acceleration voltage of up to 6 kV was applied to the sample plate and, the voltage on the extraction electrode was set to 96% of the acceleration voltage. A similar ion source with different dimensions and voltage setting is discussed elsewhere.[6] Figure 2.5 shows the Trajectory of ions in the stigmatic-type mass spectrometer. It shows the magnification and focusing of ions distribution only by the einzel lens configuration. The

magnification lens, which can be seen in figure 2.2 before the detector, was not used in this study during the experiments.

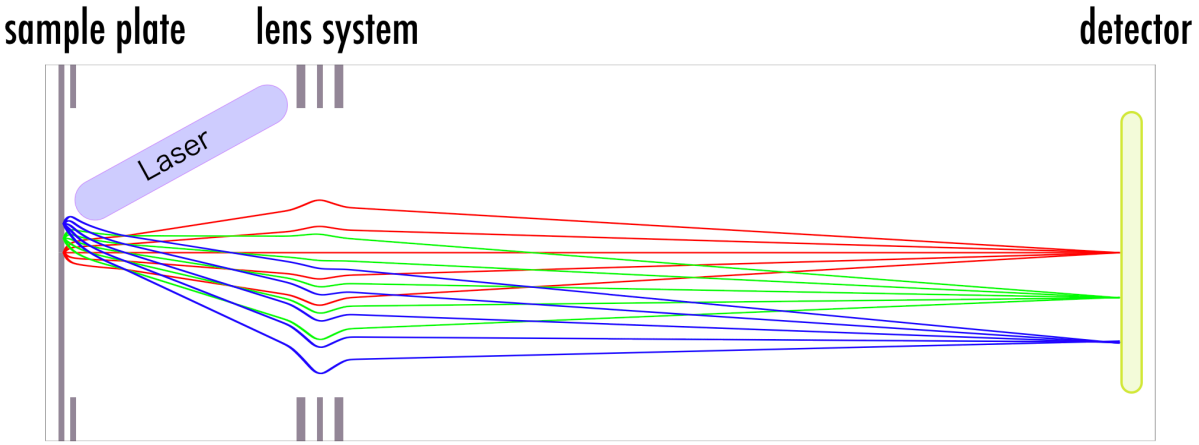

Fig. 2.5 – **Trajectory of ions in the stigmatic-type mass spectrometer (**Reprinted with permission from **Aoki, et al., *J. Mass Spectrom. Soc. Jpn.*, 2013, Vol. 61, No. 3.** Copyright 2013 **The Mass Spectrometry Society of Japan)**

2.3.3 Mass analyzer

2.3.3.1 MULTUM

A MALDI mass spectrometer is usually equipped with a TOF mass analyzer. The mass resolution of a time of flight mass spectrometer is directly proportional to its total flight path length and, the total flight path is usually about 2 m if the ions travel in a straight path. An approach to increase the flight path and, thus the mass resolution without taking a large space, is to put the ions in a closed orbit and let them pass the same orbit again and again. For this purpose, MULTUM Linear plus, in which ions travel in a figure-eight-shape trajectory, again and again, was constructed by Matsuo and co-workers[7,8]. The stigmatic-type imaging mass

spectrometer used in the study was equipped with a MULTUM mass analyzer.[9,10] Figure 2.2 is the schematic drawing of the experimental apparatus for stigmatic imaging mass spectrometry. The position of the MULTUM mass analyzer can be seen in the figure. Figure 2.6 represents the trajectory of ions in a multi-turn orbit.

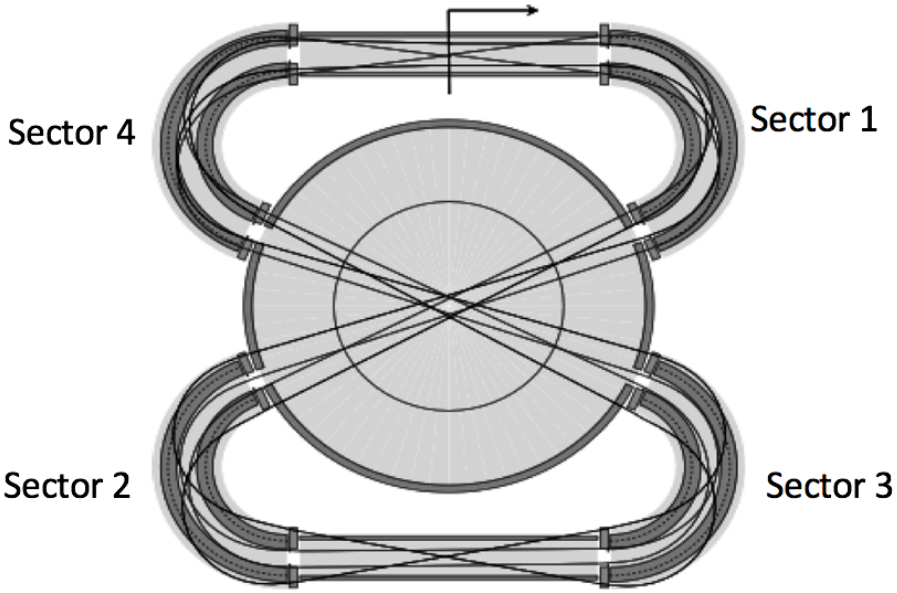

Fig. 2.6 – **Ion trajectory of multi-turn orbit (**Reprinted with permission from **Aoki, et al., *J. Mass Spectrom. Soc. Jpn.*, 2013, Vol. 61, No. 3.** Copyright 2013 **The Mass Spectrometry Society of Japan)**

The MULTUM mass analyzer consists of four electric sectors with cylindrical side plates and Matsuda plates to generate a toroidal electric field and a couple of electrostatic quadrupole triplet lenses at the entrance and the exit. When the ions enter the MULTUM, the voltage on sector 1 is turned on while that of sector 4 is turned off. The voltages to sectors 2 and 3 are statically applied during the experiment. The voltage on sector 4 is turned on when the ions start moving in the multi-turn circuit of the MULTUM. MULTUM can also be used as a linear

time-of-flight mass spectrometer (linear mode) by turning off the voltages to both sectors 1 and 4. The linear flight path length from the sample plate to the MCP was about 1 m. In this study, the experiments with stigmatic-type imaging mass spectrometer were performed in the linear mode (without the MULTUM). Figure 2.7 is the photograph of MULTUM.

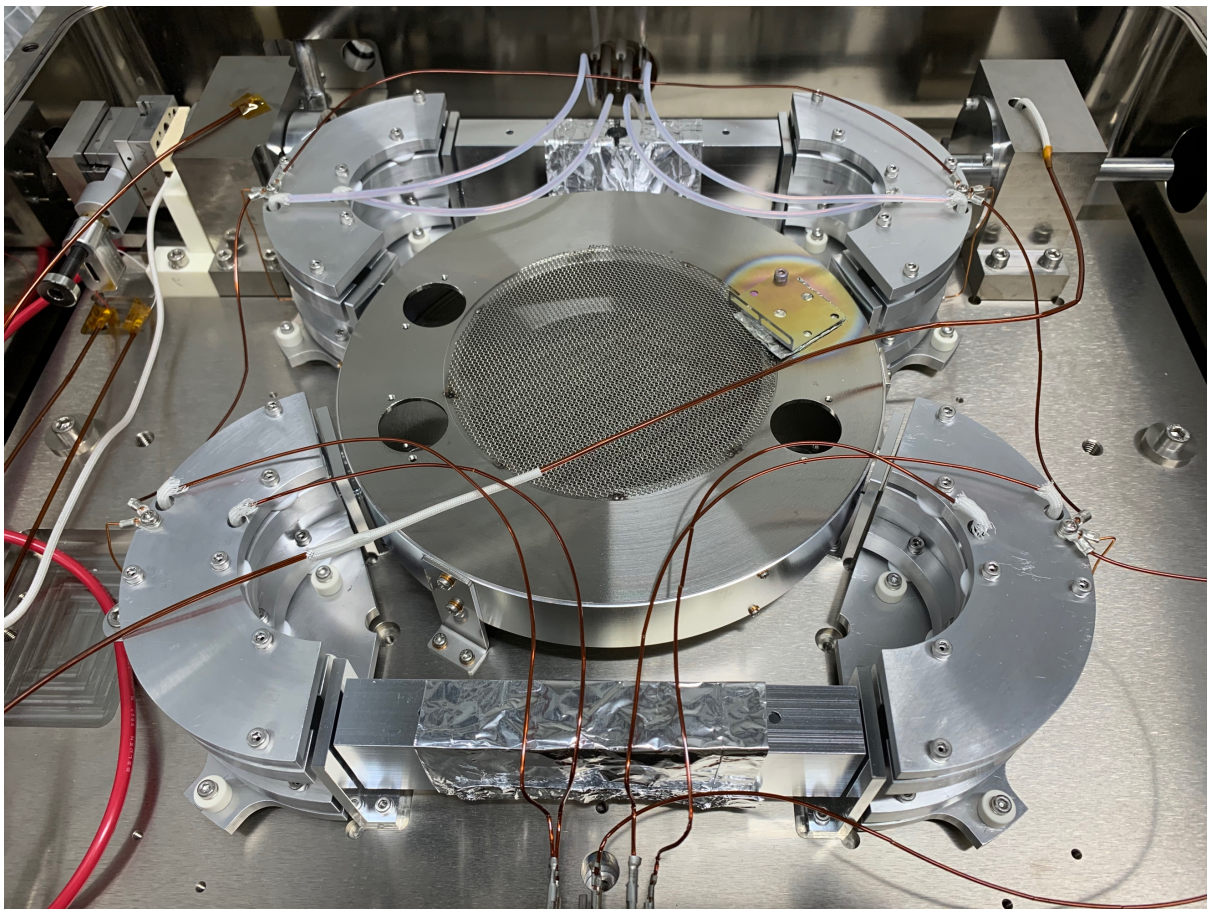

Fig. 2.7 – **Photograph of MULTUM**

2.3.4 Detector

The stigmatic-type imaging mass spectrometer is equipped with a position- and time-sensitive delay-line detector (DLD).[11] The DLD consists of a microchannel plate (MCP) and a delay-line anode behind the MCP. A delay-line anode typically consists of two layers (quadratic anode (figure 2.8)) of helical wires that are aligned at 90 degrees to one another. The role of

MCP is to amplify the ion signal. The MCP consists of an array of fine tubes with diameters equal to about 10 μm, which are called microchannels. The ions hit on the MCP after traveling through the mass analyzer, which leads to the emission of secondary electrons. These secondary electrons are accelerated towards the back of the MCP by applying a voltage on the front and the back of the channel plates. A single ion is multiplied by a factor of $10^4 – 10^7$. The electron cloud formed by the secondary emission in micro-channels is accelerated towards the delay-line anode from the MCP output by applying a voltage on the anode. When the electron cloud hits a wire in the anode, it induces an electric signal, which propagates towards both terminals of that wire. The positions of the ions (X, Y) with respect to the center of the detector is described by

$X = (t_{x1} – t_{x2}) \cdot | v_{\perp} |, \quad Y = (t_{y1} – t_{y2}) \cdot | v_{\perp} |,$

where t_{x1}, t_{x2}, t_{y1}, t_{y2} represent the signal arrival times measured at each terminal of the wires and $v_{\perp}$ stands for the effective perpendicular propagation velocity vector of the signal for the wires. It should be noted that $v_{\perp}$ is not the actual signal velocity along the wires.[11]

As shown in figure 2.2, the instrument consists of two detectors; delay line and MCP with phosphor screen, which can be switch according to the purpose of the analysis. The delay line detector was used for the imaging analysis in this study.

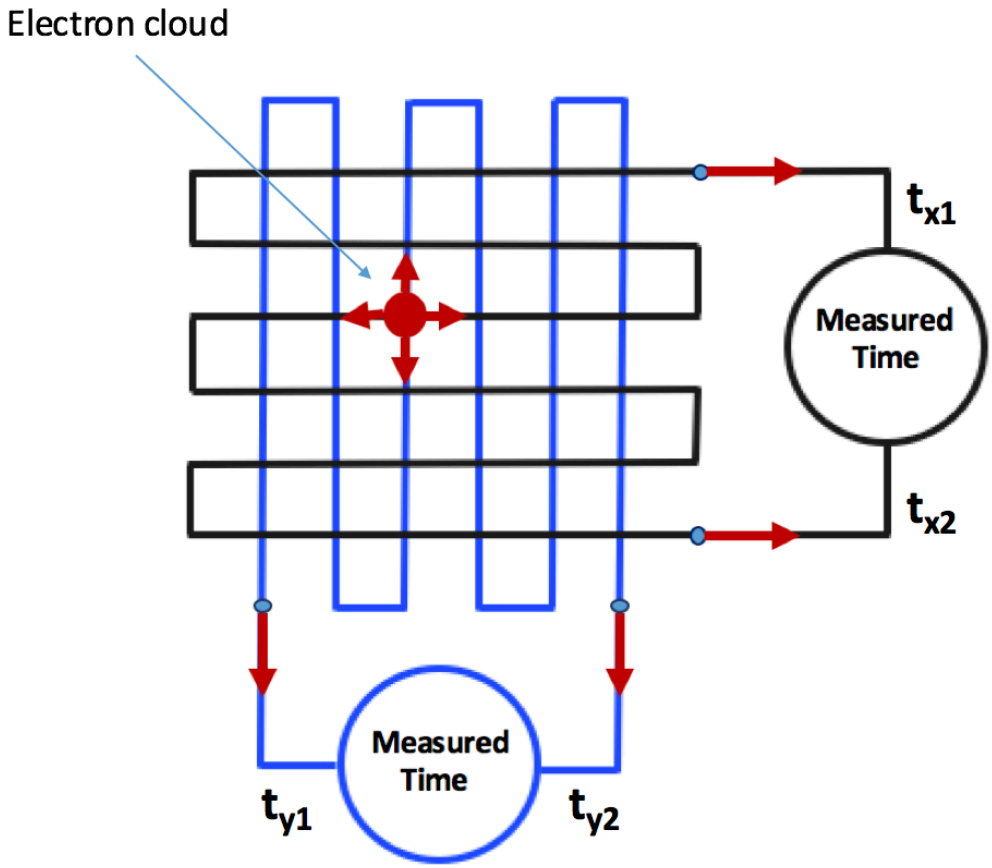

Fig. 2.8 – **Schematics of delay line detector**

2.3.5 Post-extraction differential acceleration

In conventional MALDI-TOF mass spectrometers, the delayed extraction technique is employed to improve the mass resolutions by compensating the dispersion in the initial velocity distribution, but the delayed extraction technique cannot be applied to stigmatic imaging mass spectrometers. In a stigmatic imaging mass spectrometer, ions diffuse in a plane perpendicular to the flight axis during the delay time before extraction.[12] Thus, the ion distribution is not preserved to observe as an image. Extracting the ions immediately after the formation at the sample plate without employing any method for compensating the velocity dispersion is one

option that can preserve the ion distribution, but the mass resolution will be very low. Typically, TOF mass spectrometer without employing the delayed extraction method has a mass resolution(m/Δm) of only 100, which is practically useless.[12] Aoki et al[12] developed the post-extraction differential acceleration extraction (PEDA) method for compensating the dispersion in the initial velocity distribution in stigmatic imaging TOF mass spectrometers that achieves both high-resolution imaging and a high mass resolution.

In the delayed extraction method, as the name suggests, the ions are extracted after a short time delay to compensate for the initial dispersion in the velocity. On the other hand, in the PEDA method, the ions are immediately extracted after the ionization and allowed to travel some distance in the acceleration region. Once the ions travel some distance in the acceleration region, the voltage on the extraction electrode is increased to compensate for the velocity distribution of the ions and, ions of the same *m/z* arrive at the detector at the same time. The PEDA method is discussed in detail elsewhere.[12]

However, in this study, PEDA was not applied during the experiments with stigmatic-type imaging mass spectrometer. Therefore, the mass resolution of the peaks in the spectrum obtained with stigmatic-type imaging mass spectrometer is not high. The PEDA method will be applied in the future experiments. The mass spectrum and images obtained with stigmatic-type imaging mass spectrometer are shown in Chapter 5.

References

[1] T. Satoh, T. Sato, J. Tamura *J Am Soc Mass Spectrom* **2007**, 18, 1318-1323.

[2] J. Aoki, M. Toyoda *J. Mass Spectrom. Soc. Jpn.* **2013**, 61(3).

[3] H. Hazama, J. Aoki, H. Nagao, R. Suzuki, T. Tashima, K. Fujii, K. Masuda, K. Awazu, M. Toyoda, Y. Naito *Applied Surface Science* **2008**, 255, 1257-1263.

[4] S.L. Luxembourg, T.H. Mize, L.A. McDonnell, R.M.A. Heeren, *Anal. Chem*., **2004**, 76, 5339–5344.

[5] A.F.M. Altelaar, I.M. Taban, L.A. McDonnell, P.D.E.M. Verhaert, R.P.J. de Lange, R.A.H. Adan, W.J. Mooi, R.M.A. Heeren, S.R. Piersma, *Int. J. Mass Spectrom*., **2007**, 260, 203–211.

[6] H. Hazama, H. Yoshimura, J. Aoki, H. Nagao, M. Toyoda, K. Masuda, K. Fujii, T. Tashima, Y. Naito, K. Awazu *Journal of Biomedical Optics* **2011**, 16(4), 046007.

[7] T. Matsuo, M. Ishihara, M. Toyoda, H. Ito, S. Yamaguchi, R. Roll, H. Rosenbauer, *Adv. Space Res.*, **1999**; 23: 341.

[8] M. Toyoda, M. Ishihara, S. Yamaguchi, H. Ito, T. Matsuo, R. Roll, H. Rosenbauer, *J. Mass Spectrom.,* **2000**; 35: 163.

[9] K. Jensen, T. Hondo, H. Sumino, M. Toyoda *Anal. Chem.* **2017**, 89, 7535-7540.

[10] M. Ishihara, M. Toyoda, T. Matsuo *International Journal of Mass Spectrometry* 197 (**2000**) 179-189.

[11] H. Yoshimura, H. Hazama, J. Aoki, M. Toyoda, Y. Naito, K. Awazu *Japanese Journal of Applied Physics* 50 (**2011**) 056701.

[12] J. Aoki, H. Hazama, M. Toyoda *J. Mass Spectrom. Soc. Jpn.* **2011**, Vol. 59, No. 3.

Chapter 3

Nanoparticle screening for single cell imaging analysis

3.1 Introduction

As mentioned in Chapter 1, inorganic nanoparticles were used as a matrix in this study instead of traditional organic matrices because of their advantages over the organic matrices. However, there are some challenges in using nanoparticles. When an inorganic substance is reduced from bulk size to nano-size, it can exhibit different properties as compared to the bulk of the same substance. Different nanoparticles have different structures and different physical and chemical properties, so a single type of nanoparticle is not suitable to ionize all types of molecules in the sample. These complexities make SALDI mechanism hard to understand. Therefore, SALDI MS is often used as a trial and error technique, so several nanoparticles were used for the analysis of a standard lipid and amoeba cells in this study and, based on the results suitable nanoparticles were chosen for the single-cell imaging analysis.

The goal of this thesis was to image the distribution of phospholipids present in single cells using the stigmatic-type MALDI mass spectrometer with high spatial resolution. First, a MALDI Spiral-TOF instrument was used for the nanoparticle screening and, then the imaging analyses of single cells were performed using selected nanoparticles by both MALDI Spiral-TOF instrument and stigmatic-type MALDI mass spectrometer.

The stigmatic-type imaging mass spectrometer used in this study could be operated only in the positive-ion mode, so a phospholipid, 1,2-distearoyl-sn-glycero-3-phosphocholine (DSPC), which can be ionized in the positive-ion mode was chosen for nanoparticle screening.

The screening of 7 nanoparticles (6 metal oxide nanoparticles TiO_2, CeO_2, WO_3, ZnO, CaO,

Fe_2O_3, and 1 metal nanoparticles Ag) for the selection of the appropriate nanoparticles for the single-cell imaging analysis is described in this chapter. These nanoparticles were selected based on the literature survey and discussions with researchers researching nanoparticles. A standard phospholipid 1,2-distearoyl-sn-glycero-3-phosphocholine (DSPC) and amoeba cells were analyzed by a conventional MALDI Spiral-TOF instrument using these 7 nanoparticles. MALDI Spiral-TOF instrument have previously been adopted for the structural analysis of lipids directly on tissue specimens.[1]

3.2 Sample preparation

3.2.1 Materials

The standard lipid 1,2-distearoyl-sn-glycero-3-phosphocholine (DSPC), CeO_2, WO_3, CaO, Fe_2O_3 NPs, TFA(Trifluoroacetic acid), Acetonitrile were all purchased from Sigma Aldrich Co. (St. Louis, USA). ZnO NPs and chloroform, methanol, 2-propanol were purchased from Wako Chemical Industries Ltd. (Osaka, Japan).

3.2.2 DSPC sample preparation

DSPC sample solution was prepared by dissolving DSPC in chloroform/methanol (2:1) solution. First, the stock solution with the concentration of 10mM was prepared and, then it was diluted to the working solution of 100μM concentration.

3.2.3 Amoeba cells sample preparation

Dictyostelium discoideum cells (wild type strain; Ax2) were grown in HL5 medium[2] at 21 °C. The cells were re-suspended in phosphate buffer (DB; 5 mM Na_2HPO_4, 5 mM KH_2PO_4, 2 mM $MgSO_4$, 0.2 mM $CaCl_2$, pH 6.5) at the cell density of 3 $x10^6$ cells/mL after washed with DB, and 1 ml of the cell suspension was incubated in a 35-mm plastic dish for 5 hours at 21°C. The

cells were re-suspended in 0.3-mL DB after washed with DB twice, and a 10-μL aliquot of the cell suspension was placed on a 0.1 mm thin stainless steel plate and incubated for 15 min at 21°C. After incubation, the cells were fixed with 3% glyoxal (3.13 ml glyoxal (40% stock solution), 0.3 ml acetic acid, 0.1 ml 5N NaOH, 36.47 ml ddH_2O)[3] for 15 min on ice, washed with distilled water and air-dried.

3.2.4 DHB matrix and metal oxide nanoparticles solution preparation

DHB matrix solution was prepared by mixing 20 mg of 2,5-DHB in 1 mL TA30 solvent (30:70 [v/v] acetonitrile: 0.1% TFA in water).

All the metal oxide nanoparticles (NPs) were mixed with distilled water/TFA (4:1) solution. After mixing the NPs with distilled water/TFA solution, the mixer was repeatedly vortexed and sonicated for 5 minutes. A good mixer of NPs in distilled water/TFA was obtained after 5 minutes of sonication. The concentration of the nanoparticles used was different for different nanoparticles. It was 30, 50, 50, 100, 50, 35mM for TiO_2, CeO_2, WO_3, ZnO, CaO, Fe_2O_3 nanoparticles respectively.

3.2.5 Samples and matrix/nanoparticles deposition on the MALDI plate

First, 1 μl of the DHB solution was deposited on the MALDI plate spot and allowed to slowly air dry to form matrix crystals and, then 1 μl of the DSPC solution was deposited over it and air-dried. In the same way, for the case of metal oxide nanoparticles as a matrix, 1 μl of the nanoparticle solution was deposited on the MALDI plate spot and allowed to slowly air dry and, then 1 μl of the DSPC solution was deposited over it and air-dried. In the case of Ag nanoparticles, 1 μl of the lipid solution was deposited on a 0.1 mm thin stainless steel plate

(TS50-50-005, Iwata, Japan) and air-dried and after that, Ag nanoparticles were sputtered over the sample. For the analysis, the stainless steel plate was adhered to the MALDI plate using double-sided carbon tape.

For the analysis of amoeba cells, 1.5 μl of the nanoparticle solution was deposited with a pipette over the dried amoeba cells on the stainless steel plate and allowed to slowly air dry. Ag NPs were sputtered on the dried amoeba cells sample. For the analysis, the stainless steel plate was adhered to the MALDI plate using double-sided carbon tape.

3.3 Experimental

3.3.1 MS data acquisition

A MALDI spiral-TOF mass spectrometer (JMS-S3000, JEOL, Japan) was used for the analyses. The instrument is equipped with the third harmonic generation of a Nd:YLF laser operating at 349 nm wavelength. The frequency can be adjusted to 10, 20, 50, 100, 250 Hz. The measurements were performed at 250 Hz. The spot size of the laser is oval with of length of the larger side equal to about 30 μm and that of the shorter side is about 20 μm. All the analyses were performed in the positive-ion mode.

3.3.2 Optimization of laser energy

The laser energy required for the ionization of the analytes in a sample varies according to the matrix and the sample. The laser energy required for the analysis of DSPC and amoeba cells was different for different NPs. The laser used in MALDI spiral-TOF has a wavelength of 349 nm and a power of 120 μJ per pulse. For each NPs, laser intensity was increased from 30% gradually with an increment of 5% until the optimum laser intensity was attained. After finding

the optimum laser intensity with an increment of 5%, it was adjusted again with the increment/decrement of 1%.

Table 3.1: **Optimum laser intensity for each NP for the analysis of DSPC**

Nanoparticle	**Optimum Laser Intensity (in %)**
TiO_2	60
CeO_2	55
WO_3	55
Fe_2O_3	45
CaO	60
ZnO	60
Ag	45

Table 3.2: **Optimum laser intensity for each NP for the analysis of amoeba cells**

Nanoparticle	**Optimum Laser Intensity (in %)**
TiO_2	50
CeO_2	41
WO_3	45
Fe_2O_3	36
CaO	55
ZnO	46
Ag	45

3.3.3 Optimization of Ag NPs deposition conditions

The size of the metal oxide NPs was not optimized. Commercially available metal oxide NPs were used. However, Ag NP sputter deposition conditions were optimized.

Magnetron sputter deposition technique was used to deposit the Ag nanoparticles. A sputtering instrument (MC1000 ion sputter coater, Hitachi, Japan) was used for that purpose. The size of deposited NPs changes with change in deposition time, deposition current and the distance between the NP target and the sample plate. The deposition time, deposition current and the distance between the NP target and the sample plate can be adjusted between a minimum value of 5 seconds, 5 mA, 20 mm and a maximum value of 300 seconds, 40 mA, 50 mm respectively. The deposition current, the distance between the NP target and the sample plate, deposition time were optimized to 30 mA, 30 mm, 8 seconds respectively. The size of the Ag NPs at these conditions was about 10 nm which was confirmed by SEM (Scanning Electron Microscope) analysis. The SEM image can be seen in the Fig. A in the appendix.

Table 3: **Size of the NPs used in this study**

NP	**Size**
TiO_2	~ 50 nm
CeO_2	< 5 μm
WO_3	< 100 nm
Fe_2O_3	< 50 nm
CaO	< 160 nm
ZnO	20 nm
Ag	~ 10 nm

3.4 Results and Discussion

3.4.1 Analysis of a standard phospholipid

At first, a standard phospholipid 1,2-distearoyl-sn-glycero-3-phosphocholine (DSPC) was analyzed using all the nanoparticles and also with the organic matrix DHB in the positive-ion mode. The monoisotopic mass of DSPC is 789.625 Da.

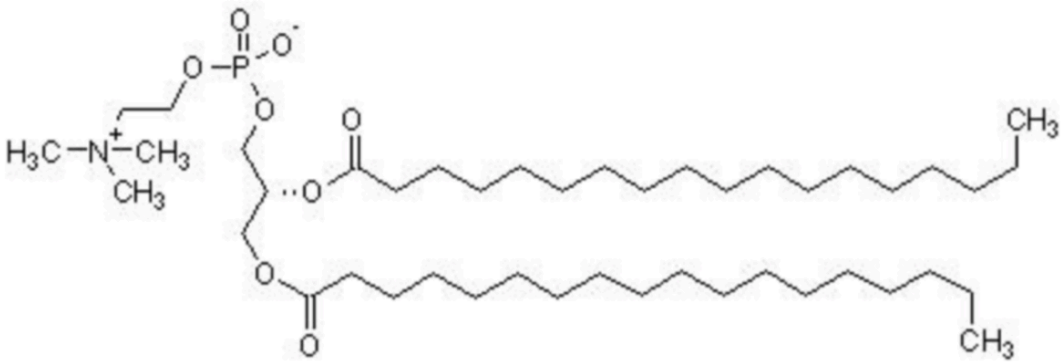

Fig. 3.1 – **Chemical structure of 1,2-distearoyl-sn-glycero-3-phosphocholine (DSPC)**

Figure 3.1 shows the Chemical structure of 1,2-distearoyl-sn-glycero-3-phosphocholine (DSPC). The peaks that are usually observed from the mass spectrometry analysis of DSPC are molecular ion peak $[M+H]^+$ at *m/z* 790, fragmentation ion peak of the phosphocholine head group at *m/z* 184, a peak at *m/z* 607 which is rest of the part of the molecule than 184, a peak at around *m/z* 284 from one of the carbon chains of the molecule, a peak at *m/z* 506 which is the rest of the part of the molecule than 284.

Figure 3.2 shows the positive-ion mode mass spectrum of DSPC obtained using DHB as a matrix. Figure 3.3, 3.4, 3.5, 3.6, 3.7, 3.8, 3.9 shows the positive-ion mode mass spectrum of DSPC obtained using Fe_2O_3, TiO_2, CeO_2, WO_3, ZnO, CaO, Ag nanoparticles as a matrix

respectively. Figure 3.10 shows the comparison view of the positive-ion mode mass spectrum of DSPC obtained using 6 metal oxide NPs (Fe_2O_3, TiO_2, CeO_2, WO_3, ZnO, CaO) as a matrix. The molecular ion peak $[M+H]^+$ of DSPC at *m/z* 790 was detected using the DHB matrix and all the nanoparticles. It was detected with Ag adduct in the case of Ag nanoparticles. Its intensity was highest with TiO_2 NPs among the nanoparticles and, its intensity was very low in the case of CaO and Ag NPs. The peak $(CH_3)_3NCH{=}CH_2^+$ at *m/z* 86 was observed with all the NPs and DHB matrix and, its intensity was lowest in the case of Ag NPs. The phosphocholine head group $PO_4H_2CH_2CH_2N(CH_3)_3^+$ at *m/z* 184 was also observed with all the nanoparticle and DHB matrix and, its intensity was low in case of CaO and Ag NPs. The peaks at *m/z* 506, 607 were also observed with the DHB matrix and all the NPs, and its intensity was low in the case of Ag and CaO NPs.

In the case of DHB, molecular ion peak $[M+H]^+$ of DSPC at 790 Da was relatively intense than the fragmentation ion peaks, but a lot of interference peaks were also observed. The intensity of the molecular ion was relatively lower than the fragmentation ion peaks at *m/z* 184 and *m/z* 86 in the case of NPs.

Although the intensity of the molecular ion peak was highest with TiO_2 NPs among the NPs, the Fe_2O_3 NPs were the most suitable for the analysis of DSPC with almost no interference or unidentified peaks. On the other hand, many interference or unidentified peaks were observed in the case of other nanoparticles.

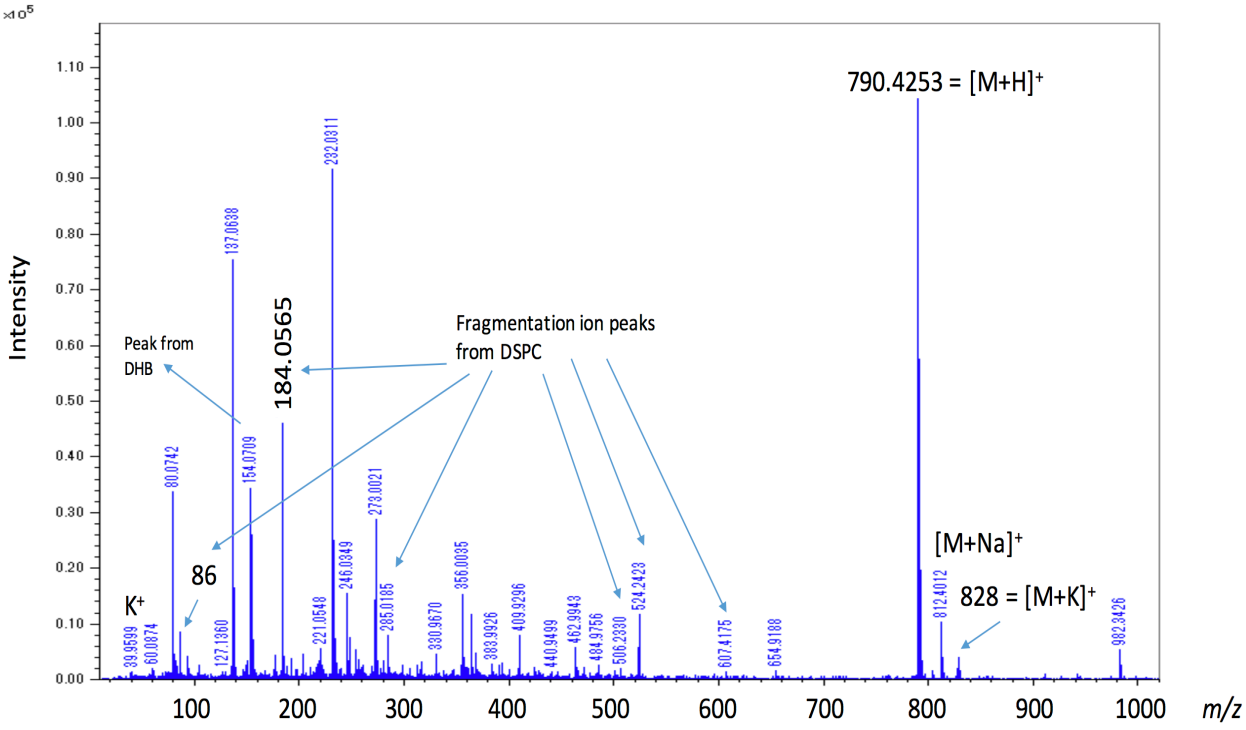

Fig. 3.2 – **Positive-ion mode mass spectrum of DSPC using DHB as a matrix and analyzed by MALDI Spiral-TOF**

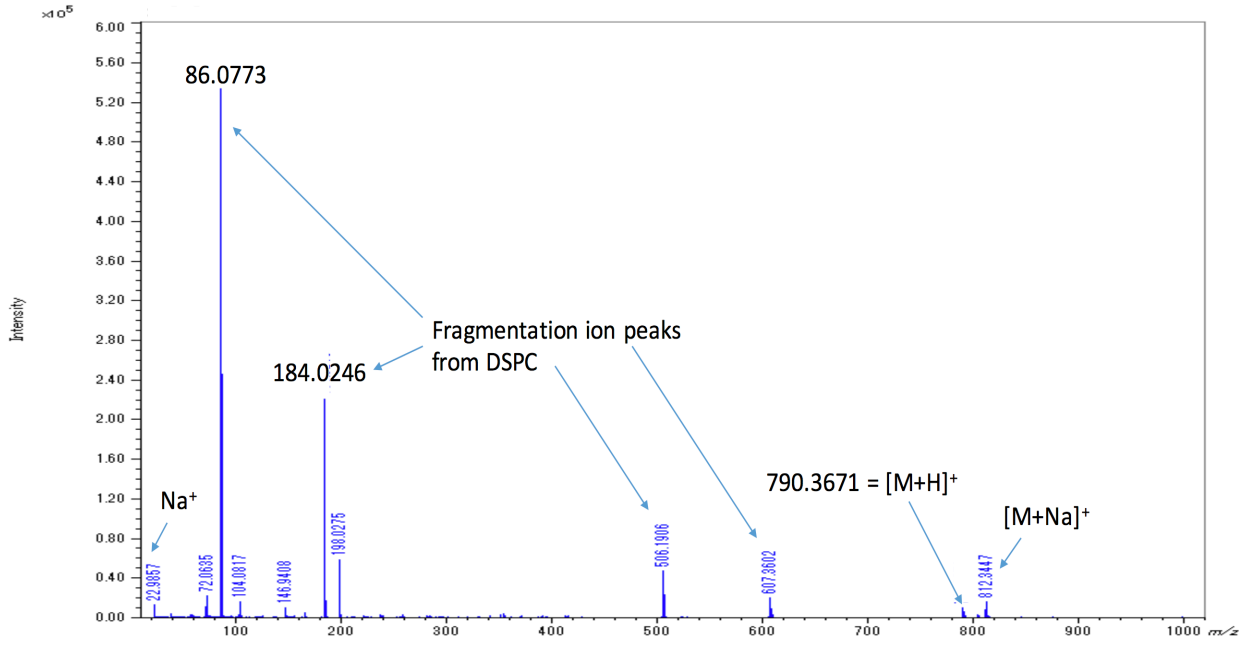

Fig. 3.3 – **Positive-ion mode mass spectrum of DSPC using Fe_2O_3 NPs as a matrix and analyzed by MALDI Spiral-TOF**

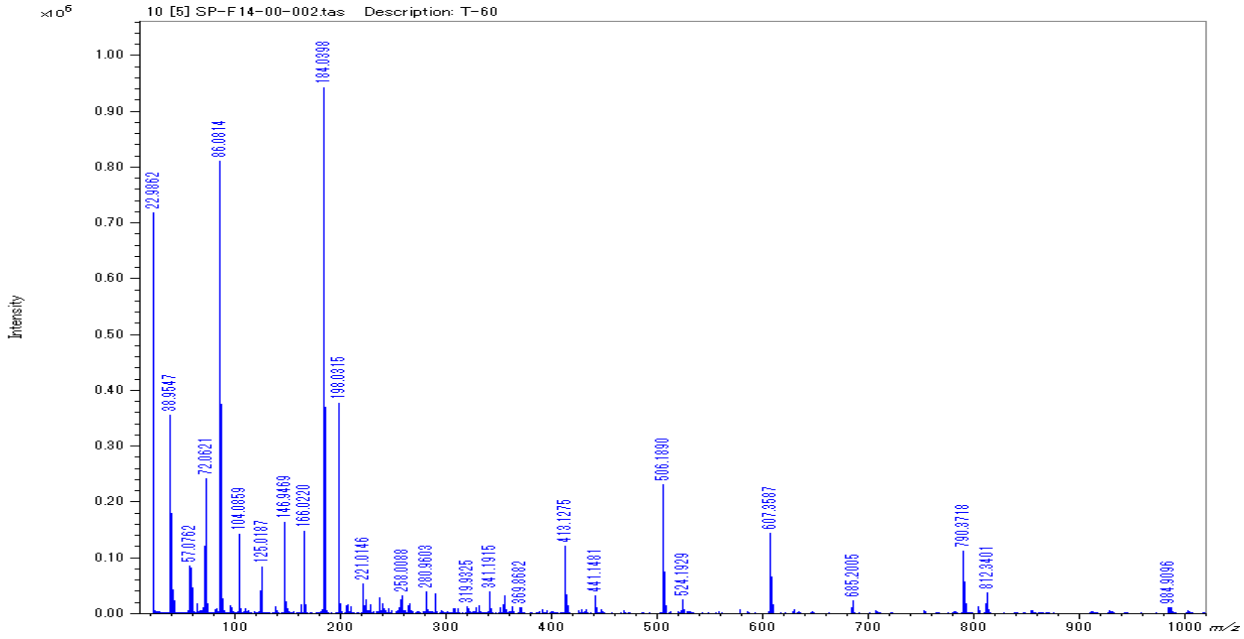

Fig. 3.4 – **Positive-ion mode mass spectrum of DSPC using TiO_2 NPs as a matrix and analyzed by MALDI Spiral-TOF**

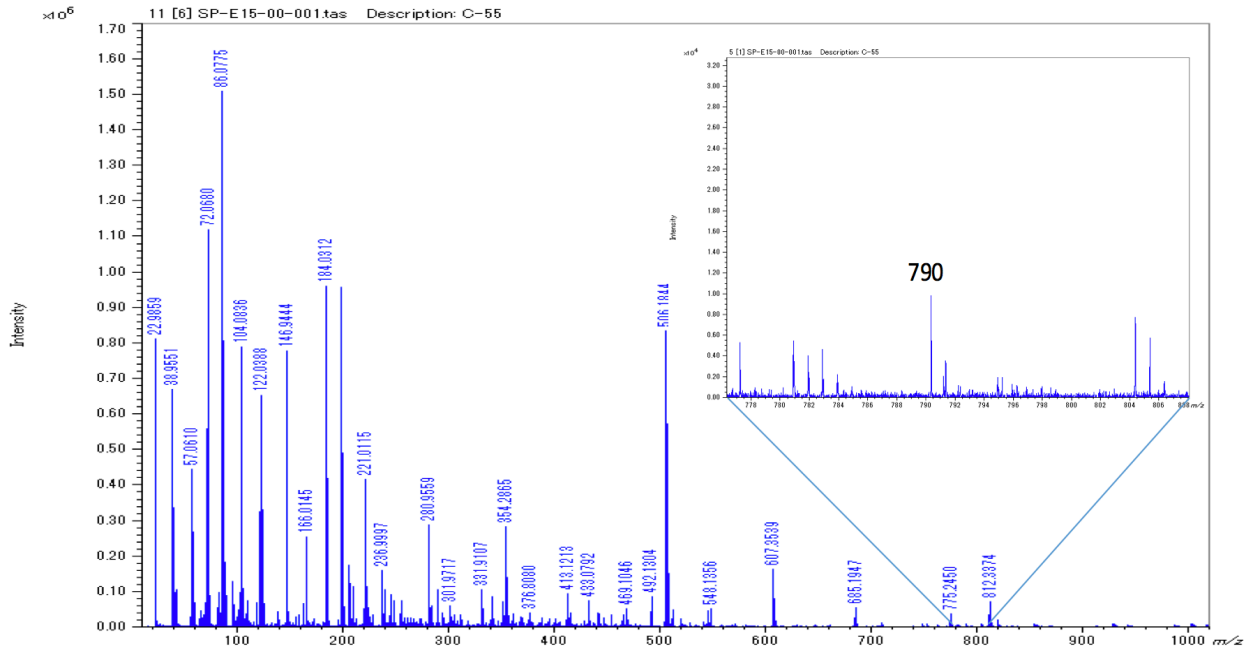

Fig. 3.5 – **Positive-ion mode mass spectrum of DSPC using CeO_2 NPs as a matrix and analyzed by MALDI Spiral-TOF**

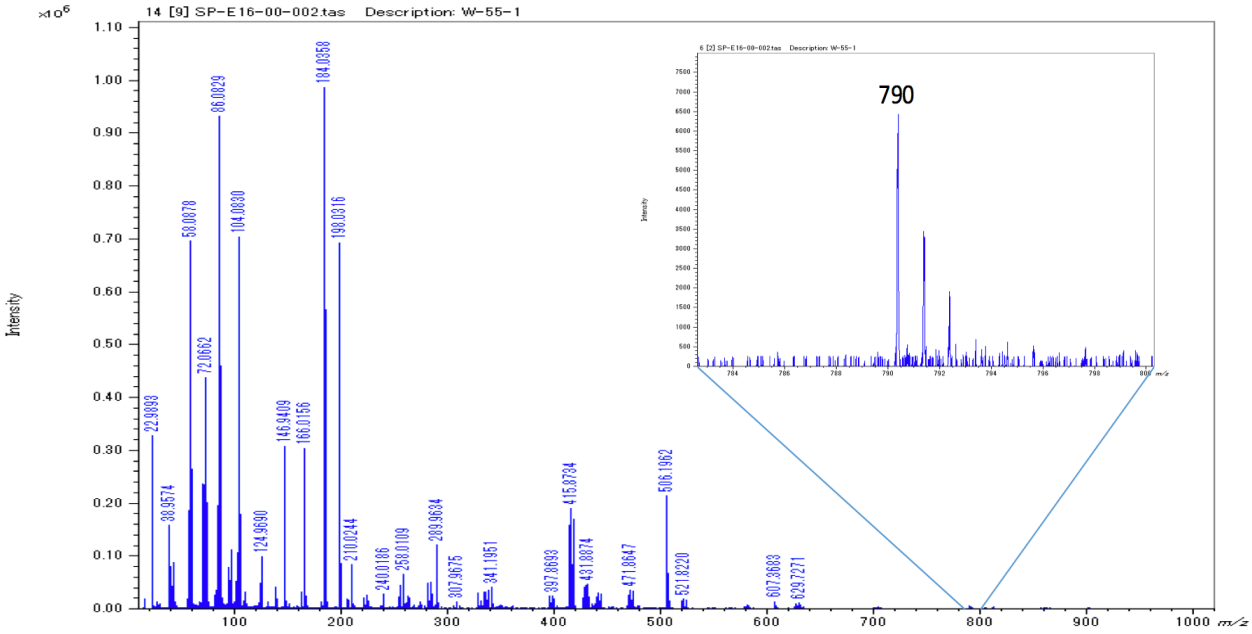

Fig. 3.6 – **Positive-ion mode mass spectrum of DSPC using WO_3 NPs as a matrix and analyzed by MALDI Spiral-TOF**

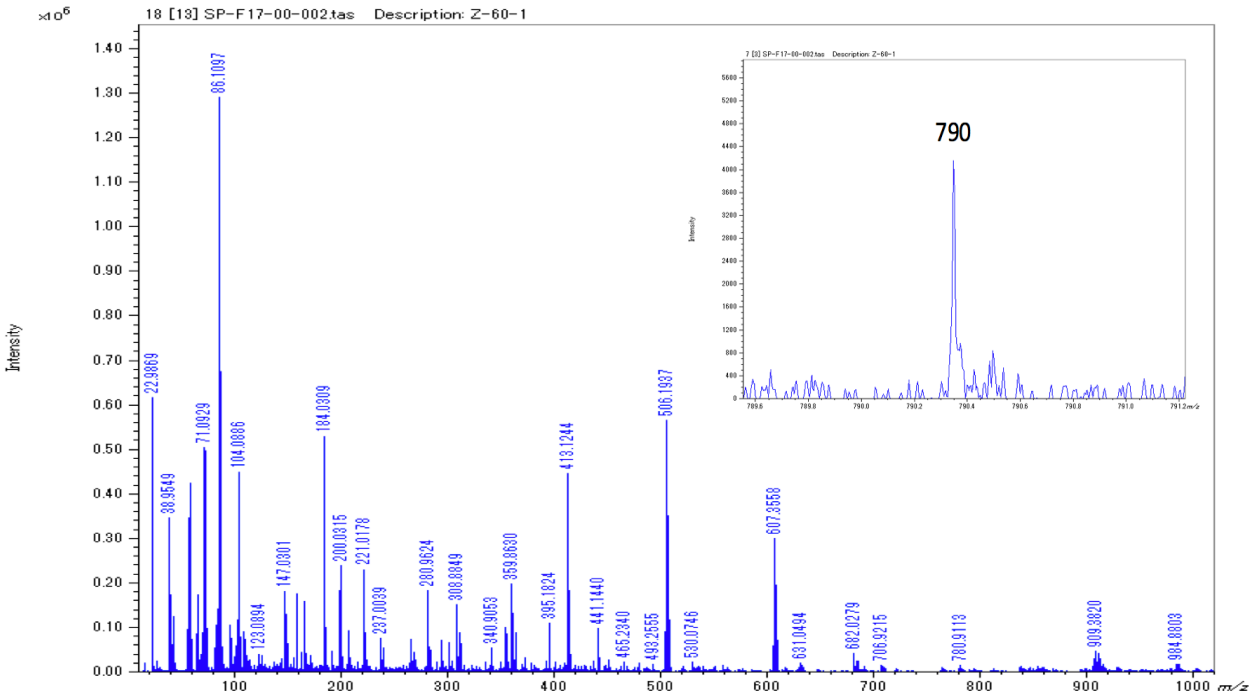

Fig. 3.7 – **Positive-ion mode mass spectrum of DSPC using ZnO NPs as a matrix and analyzed by MALDI Spiral-TOF**

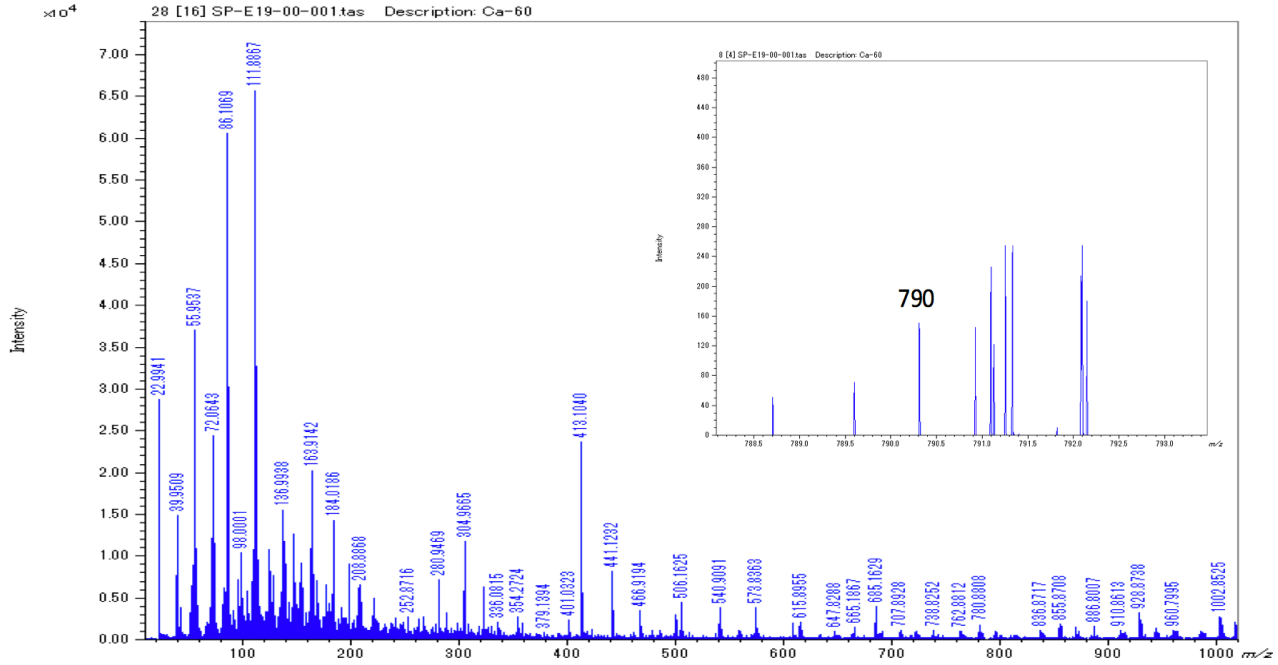

Fig. 3.8 – **Positive-ion mode mass spectrum of DSPC using CaO NPs as a matrix and analyzed by MALDI Spiral-TOF**

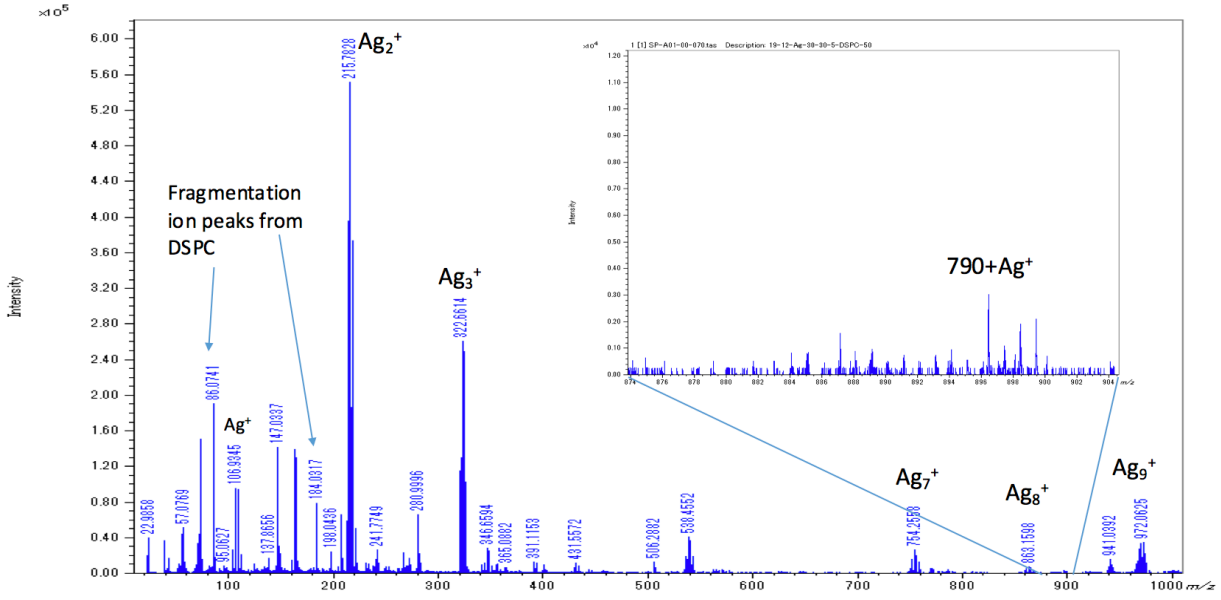

Fig. 3.9 – **Positive-ion mode mass spectrum of DSPC using Ag NPs as a matrix and analyzed by MALDI Spiral-TOF**

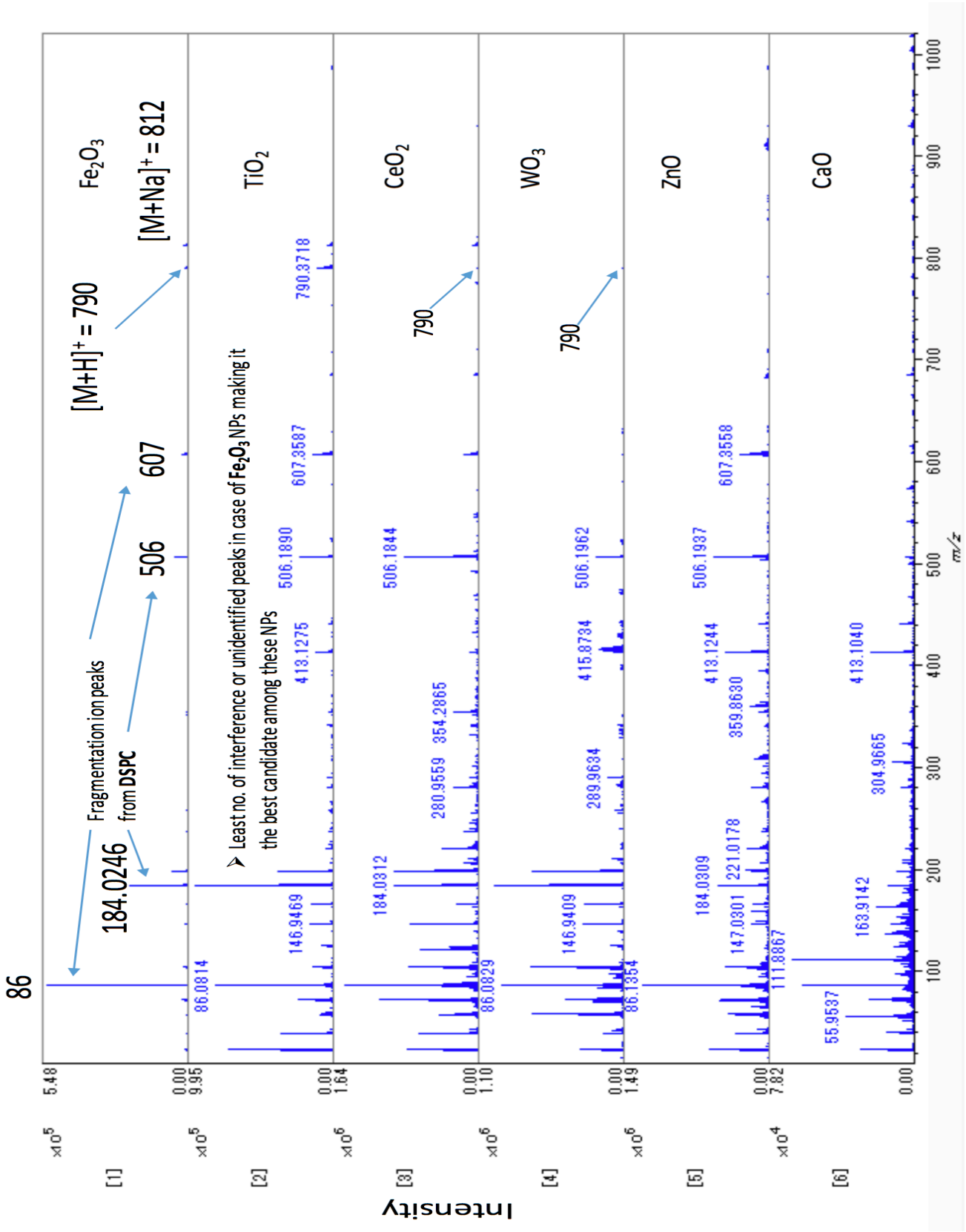

Fig. 3.10 – **Positive-ion mode mass spectrum of DSPC using 6 metal oxide NPs as a matrix and analyzed by MALDI Spiral-TOF**

3.4.2 Analysis of amoeba cells

Figure 3.11, 3.13, 3.15, 3.17, 3.19, 3.21, 3.23 shows the positive-ion mode mass spectrum of amoeba cells obtained using Fe_2O_3, TiO_2, CeO_2, WO_3, Ag, ZnO, CaO nanoparticles as a matrix respectively. Figure 3.25 shows the comparison view of the positive-ion mode mass spectrum of amoeba cells obtained using all the 7 nanoparticles used in this study as a matrix. Figure 3.12, 3.14, 3.16, 3.18, 3.20, 3.22, 3.24 shows the positive-ion mode mass spectrum of amoeba cells obtained using Fe_2O_3, TiO_2, CeO_2, WO_3, Ag, ZnO, CaO nanoparticles as a matrix respectively in the mass range 700 and above. The phosphocholine head group $PO_4H_2CH_2CH_2N(CH_3)_3^+$ at *m/z* 184 was observed with all the nanoparticles, but its intensity was low in the case of CaO and Ag NPs. The ion peak $(CH_3)_3NCH{=}CH_2^+$ at *m/z* 86, which is the further fragmentation of the phosphocholine head group, was also observed with all the NPs, but its intensity was very low in case of Ag NPs.

The molecular ion peaks of three phospholipids at *m/z* 730, 756 and 784 were observed with Fe_2O_3 NPs. The fragmentation peaks at *m/z* 184 and *m/z* 86 suggests that the phospholipids at *m/z* 756 and 784 are phosphatidylcholines. Thus, the phospholipids at *m/z* 756 and *m/z* 784 were tentatively assigned as PC(34:3) and PC(36:3) respectively. The peak at 730 is probably PE(35:2). The *m/z* of the peaks was confirmed with an online lipid database(lipidmaps.org). However, the intensity of the molecular ion peaks at *m/z* 756 and *m/z* 784 was relatively lower than the fragmentation ion peaks at *m/z* 184 and *m/z* 86. The peaks at *m/z* 744, 770, 798, 821 were also observed with Fe_2O_3 NPs, but not assigned.

The peaks at *m/z* 756 and 784 were also observed using TiO_2, WO_3 NPs with a lower relative intensity than Fe_2O_3 NPs and with even lower relative intensity using CeO_2 NPs. No significant molecular ion peak of lipids observed with ZnO NPs. Many other peaks than the peaks mentioned above in the mass range 700 and above were observed with other NPs with a low

intensity and those peaks were not assigned. Among the assigned peaks, the molecular ion peaks of two phospholipids at *m/z* 756 and 784 were obtained with the highest relative intensity using Fe_2O_3 NPs, which makes Fe_2O_3 NPs the best candidate among the nanoparticles used in this study for the analysis of lipids in amoeba cells. Also, there was almost no interference or unidentified peaks in the mass spectra obtained using Fe_2O_3 NPs. On the other hand, many interference or unidentified peaks were there in the case of other nanoparticles.

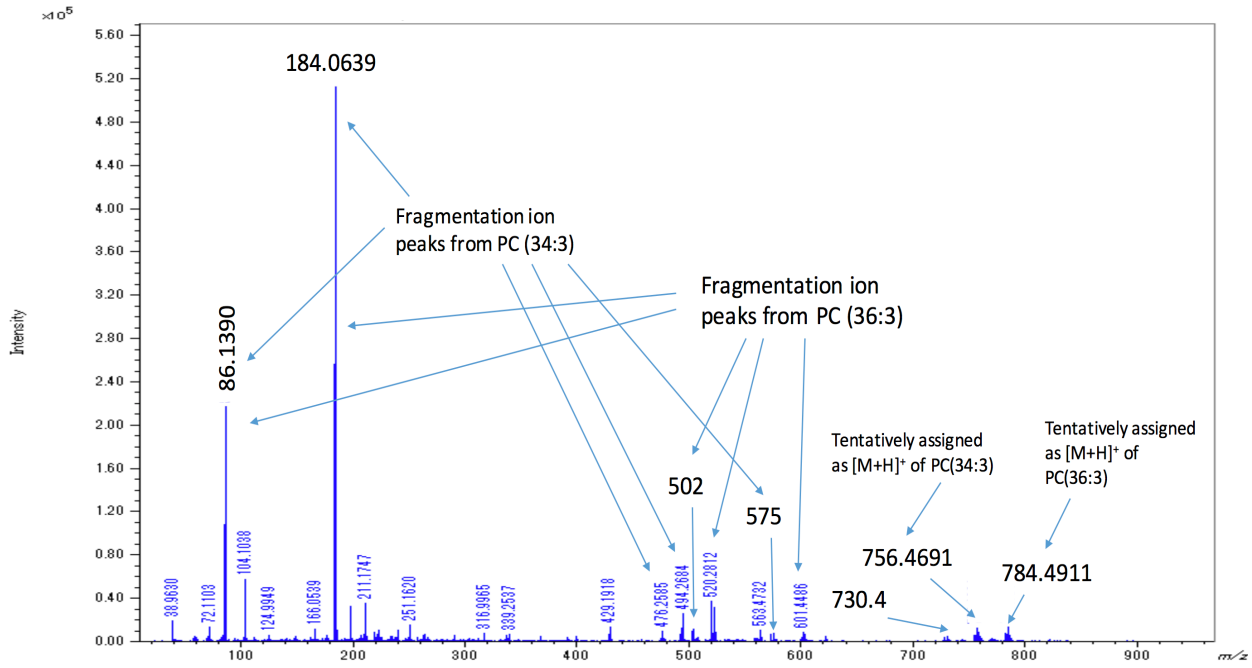

Fig. 3.11 - **Positive-ion mode mass spectrum of amoeba cells using Fe_2O_3 NPs as a matrix and analyzed by MALDI Spiral-TOF**

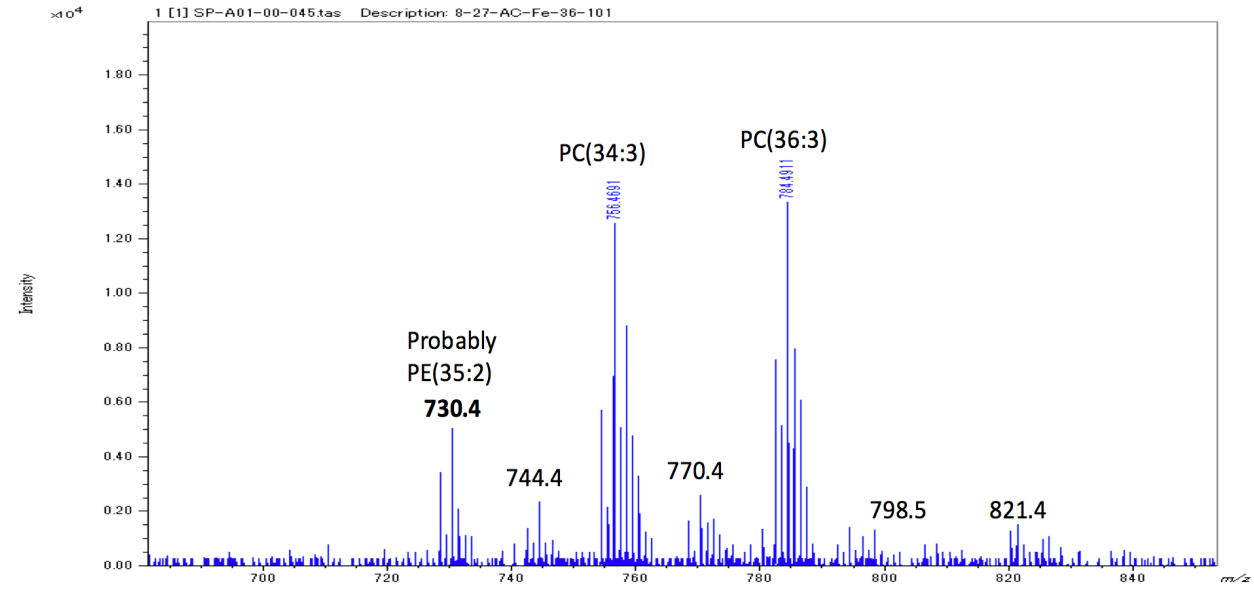

Fig. 3.12 - **Positive-ion mode mass spectrum of amoeba cells using Fe_2O_3 NPs as a matrix and analyzed by MALDI Spiral-TOF**

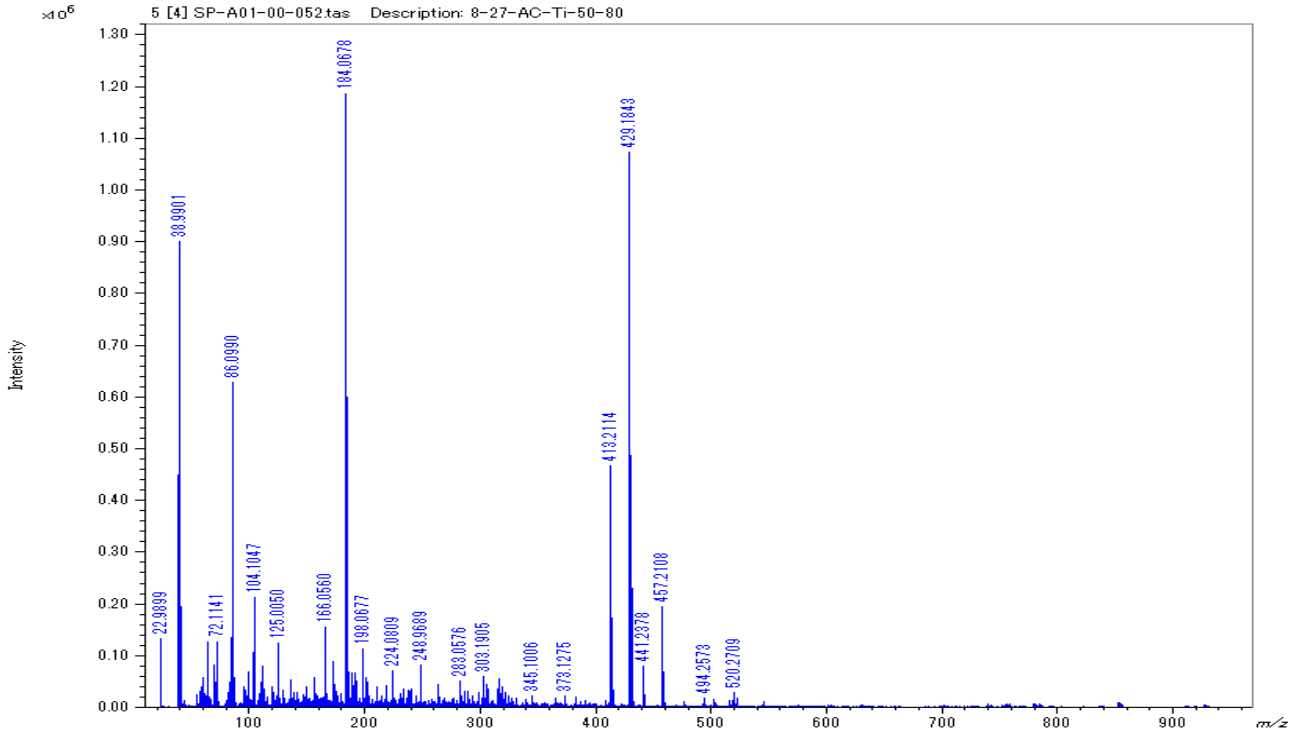

Fig. 3.13 - **Positive-ion mode mass spectrum of amoeba cells using TiO_2 NPs as a matrix and analyzed by MALDI Spiral-TOF**

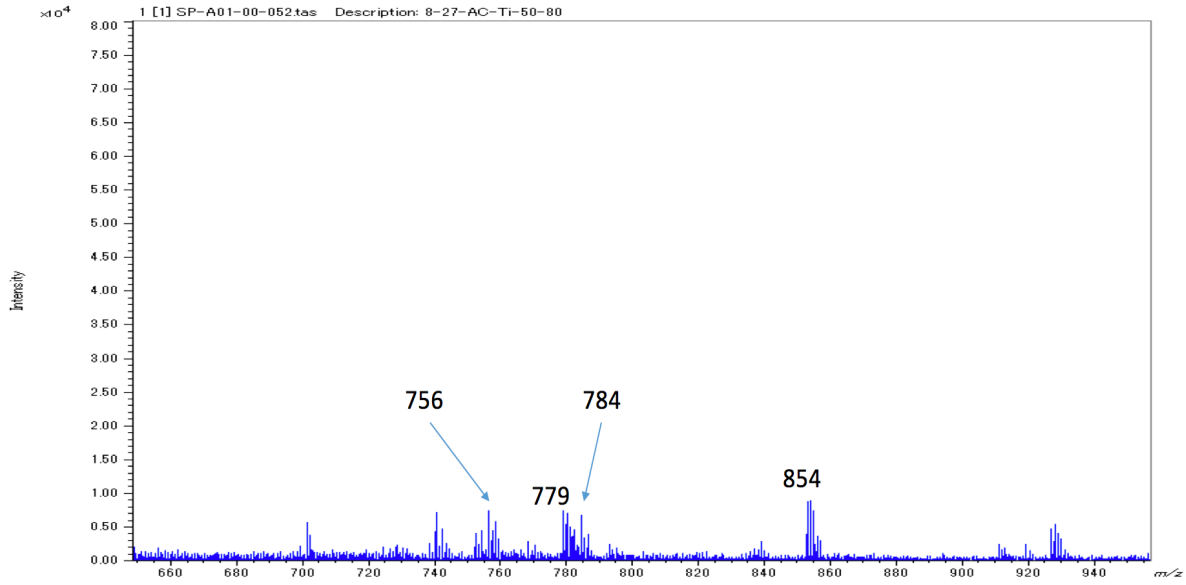

Fig. 3.14 - **Positive-ion mode mass spectrum of amoeba cells using TiO_2 NPs as a matrix and analyzed by MALDI Spiral-TOF**

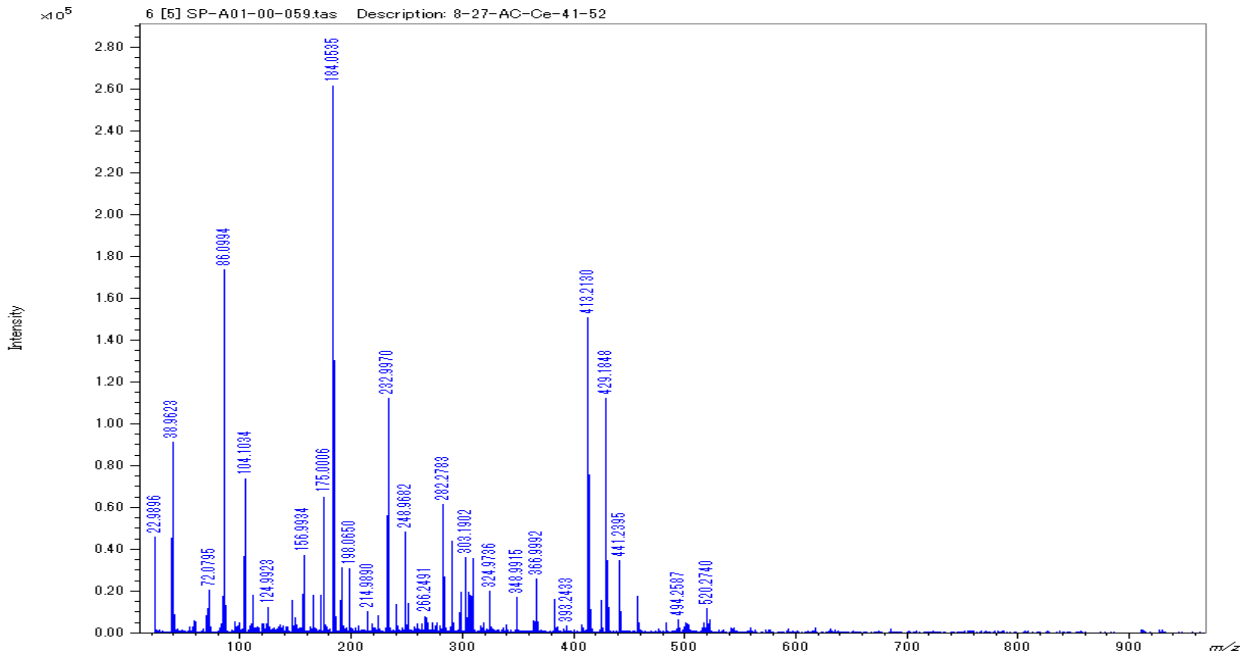

Fig. 3.15 - **Positive-ion mode mass spectrum of amoeba cells using CeO_2 NPs as a matrix and analyzed by MALDI Spiral-TOF**

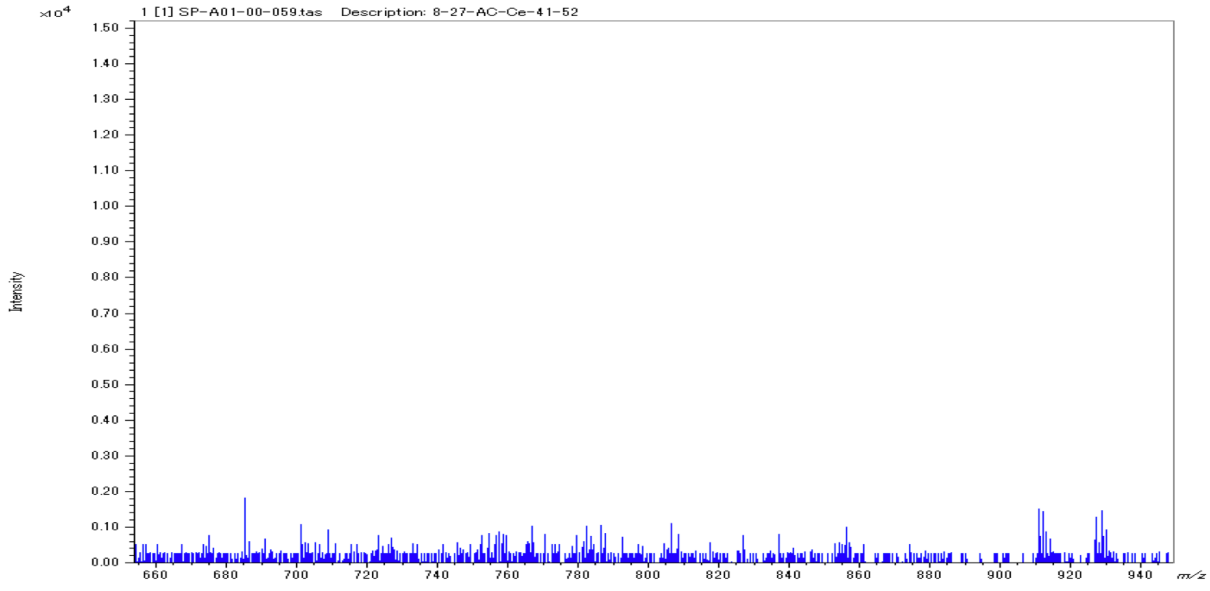

Fig. 3.16 - **Positive-ion mode mass spectrum of amoeba cells using CeO_2 NPs as a matrix and analyzed by MALDI Spiral-TOF**

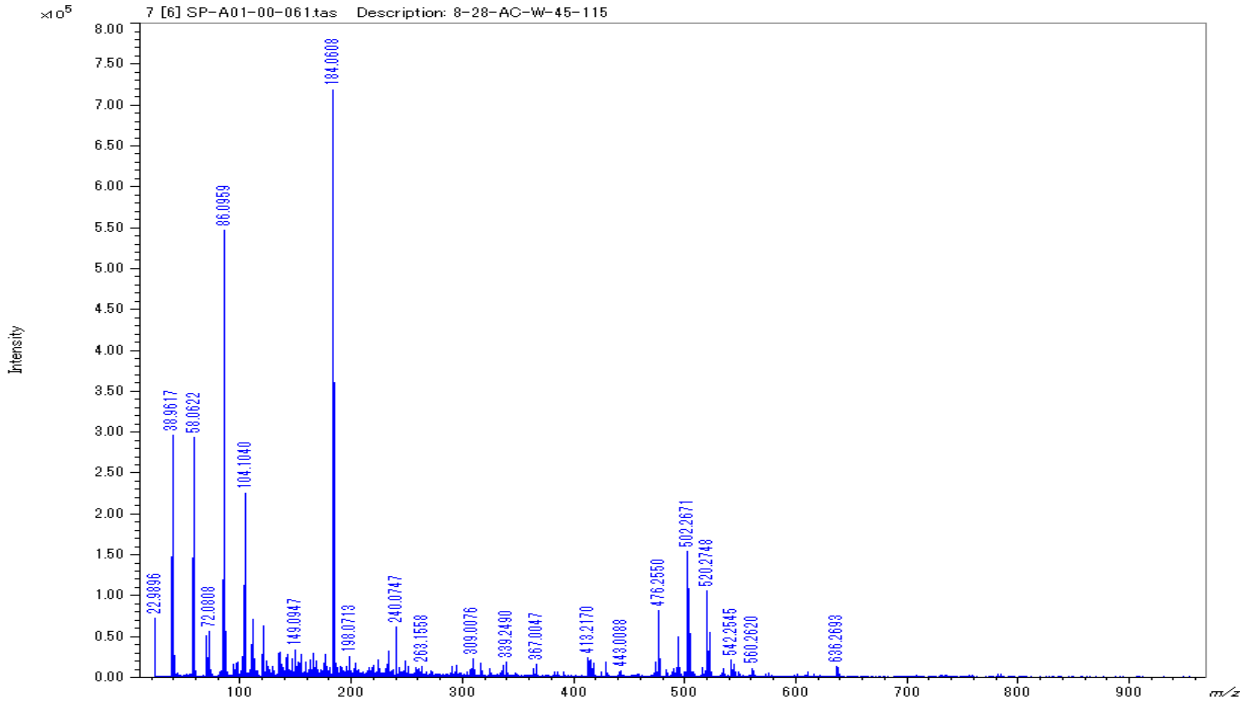

Fig. 3.17 - **Positive-ion mode mass spectrum of amoeba cells using WO_3 NPs as a matrix and analyzed by MALDI Spiral-TOF**

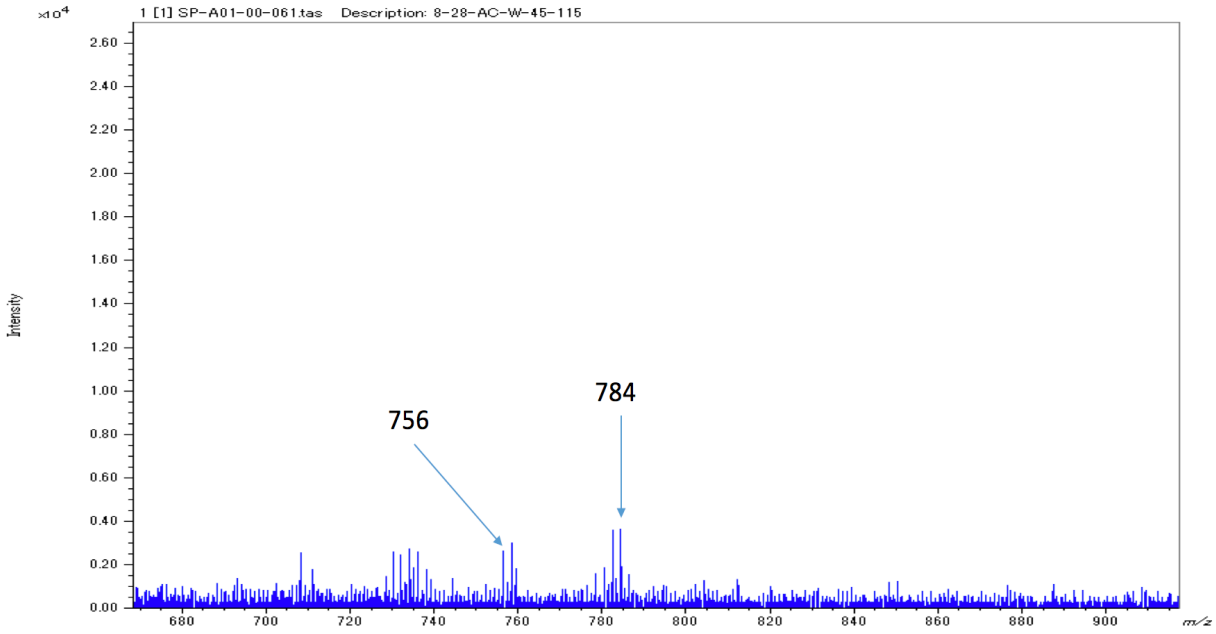

Fig. 3.18 - **Positive-ion mode mass spectrum of amoeba cells using WO_3 NPs as a matrix and analyzed by MALDI Spiral-TOF**

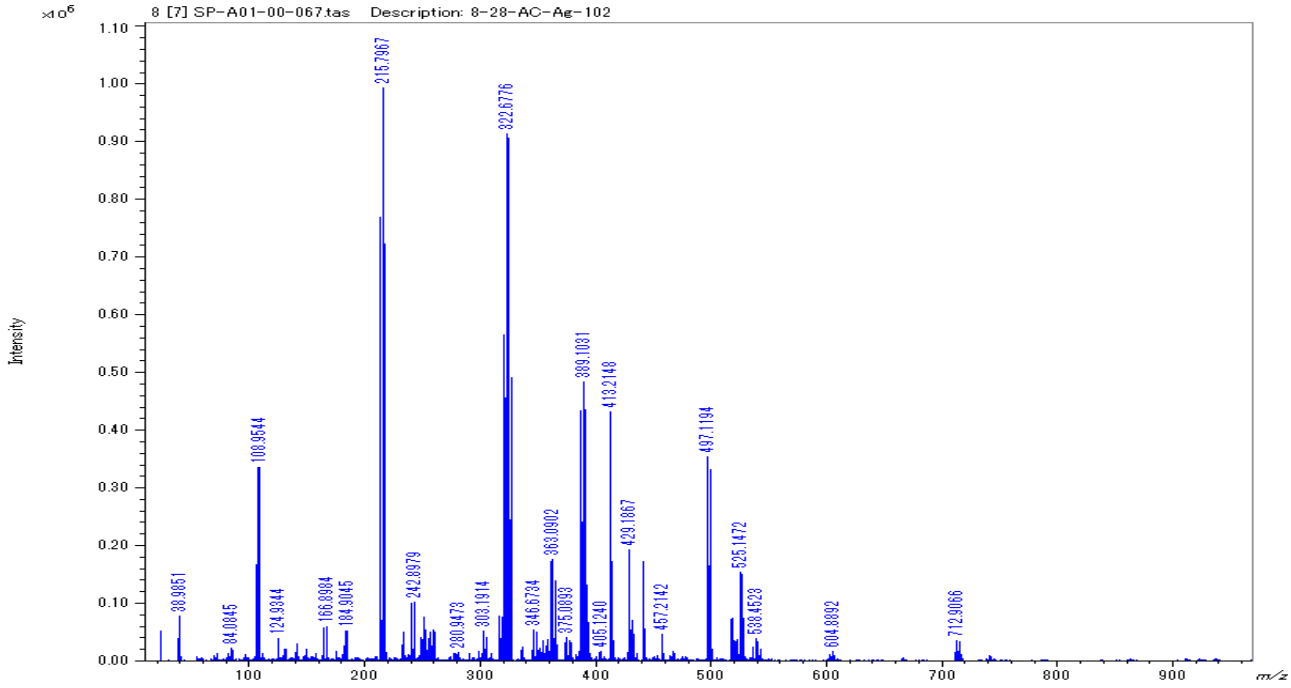

Fig. 3.19 - **Positive-ion mode mass spectrum of amoeba cells using Ag NPs as a matrix and analyzed by MALDI Spiral-TOF**

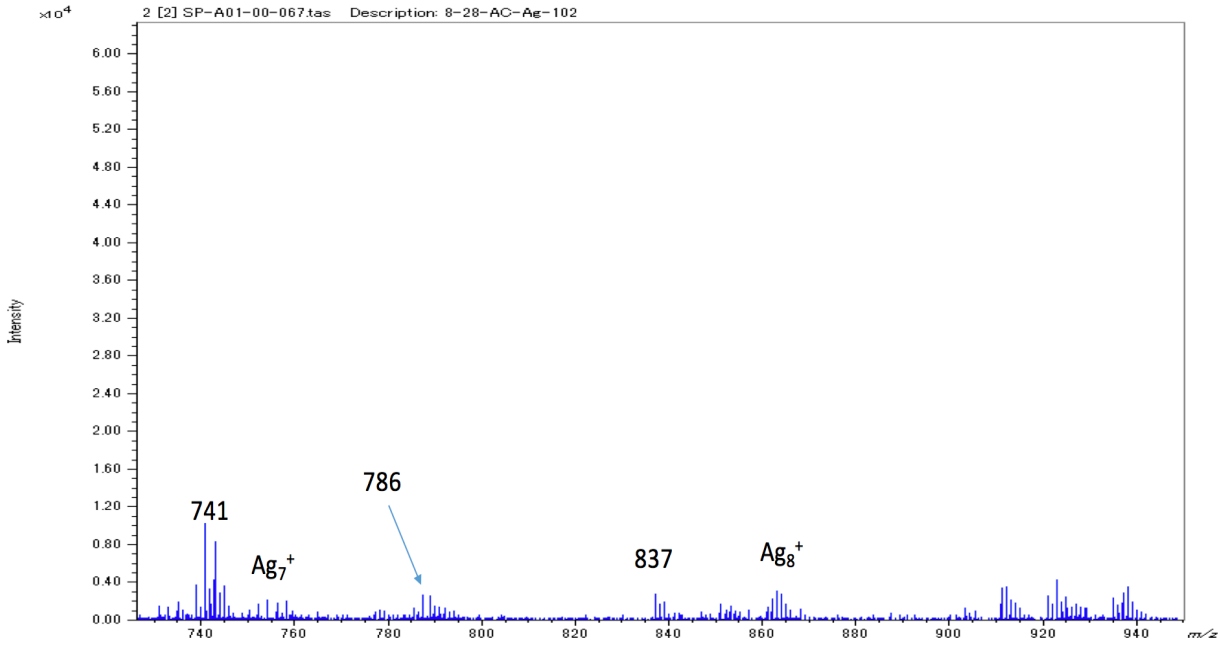

Fig. 3.20 - **Positive-ion mode mass spectrum of amoeba cells using Ag NPs as a matrix and analyzed by MALDI Spiral-TOF**

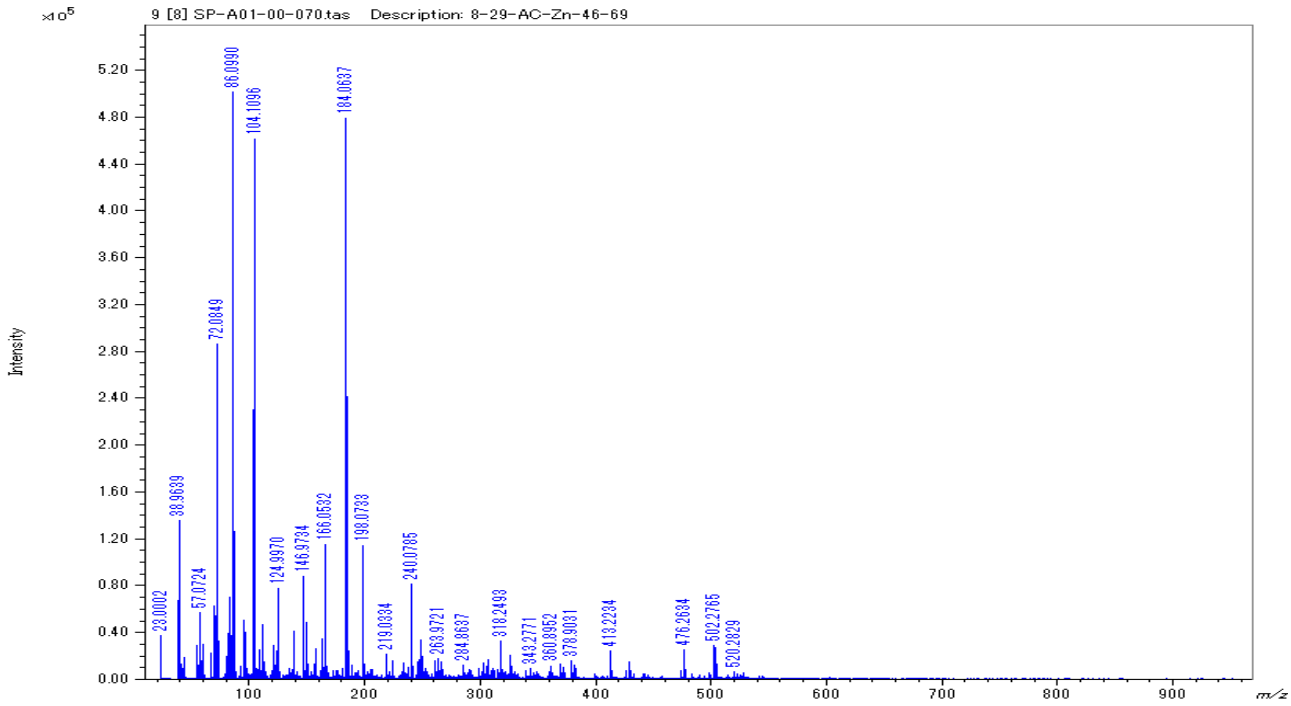

Fig. 3.21 - **Positive-ion mode mass spectrum of amoeba cells using ZnO NPs as a matrix and analyzed by MALDI Spiral-TOF**

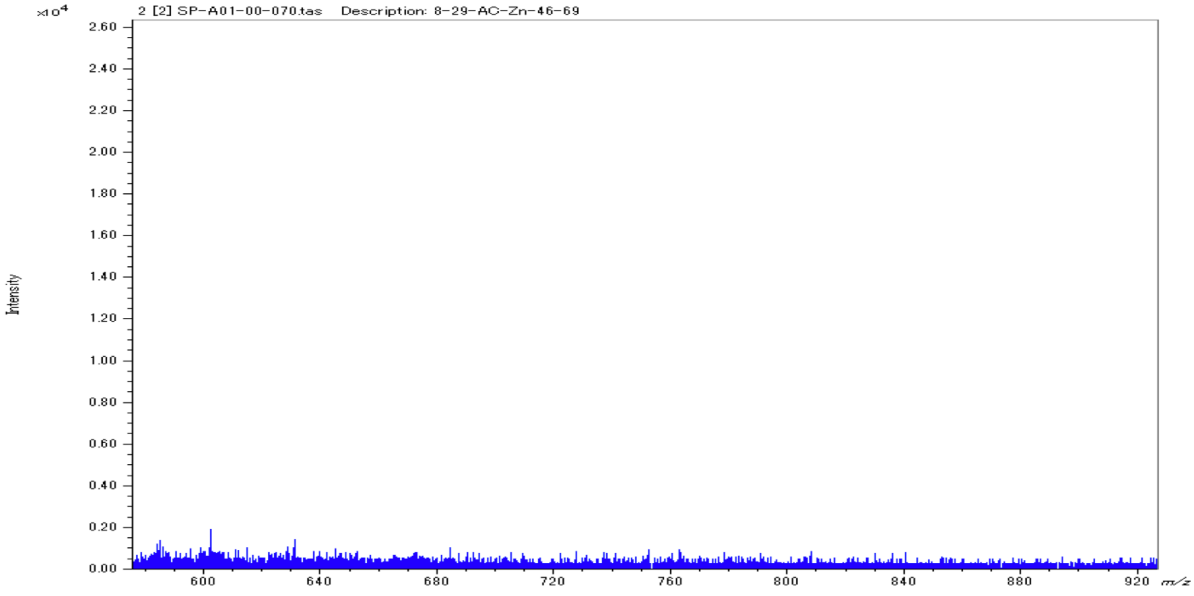

Fig. 3.22 - **Positive-ion mode mass spectrum of amoeba cells using ZnO NPs as a matrix and analyzed by MALDI Spiral-TOF**

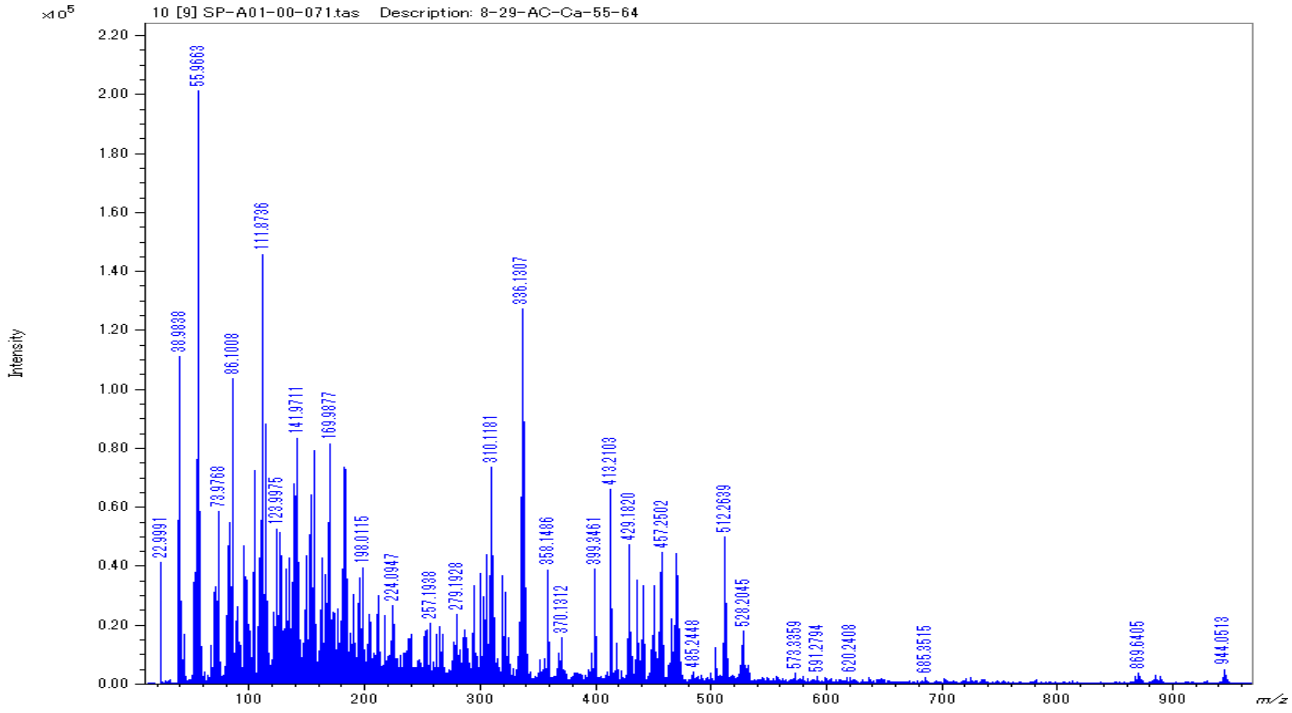

Fig. 3.23 - **Positive-ion mode mass spectrum of amoeba cells using CaO NPs as a matrix and analyzed by MALDI Spiral-TOF**

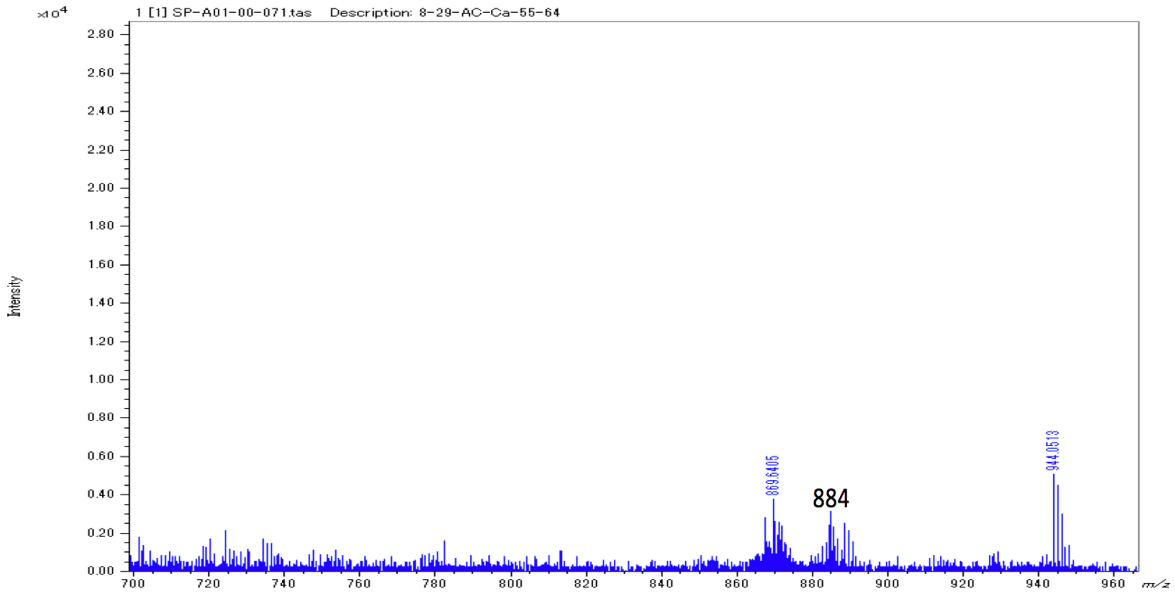

Fig. 3.24 - **Positive-ion mode mass spectrum of amoeba cells using CaO NPs as a matrix and analyzed by MALDI Spiral-TOF**

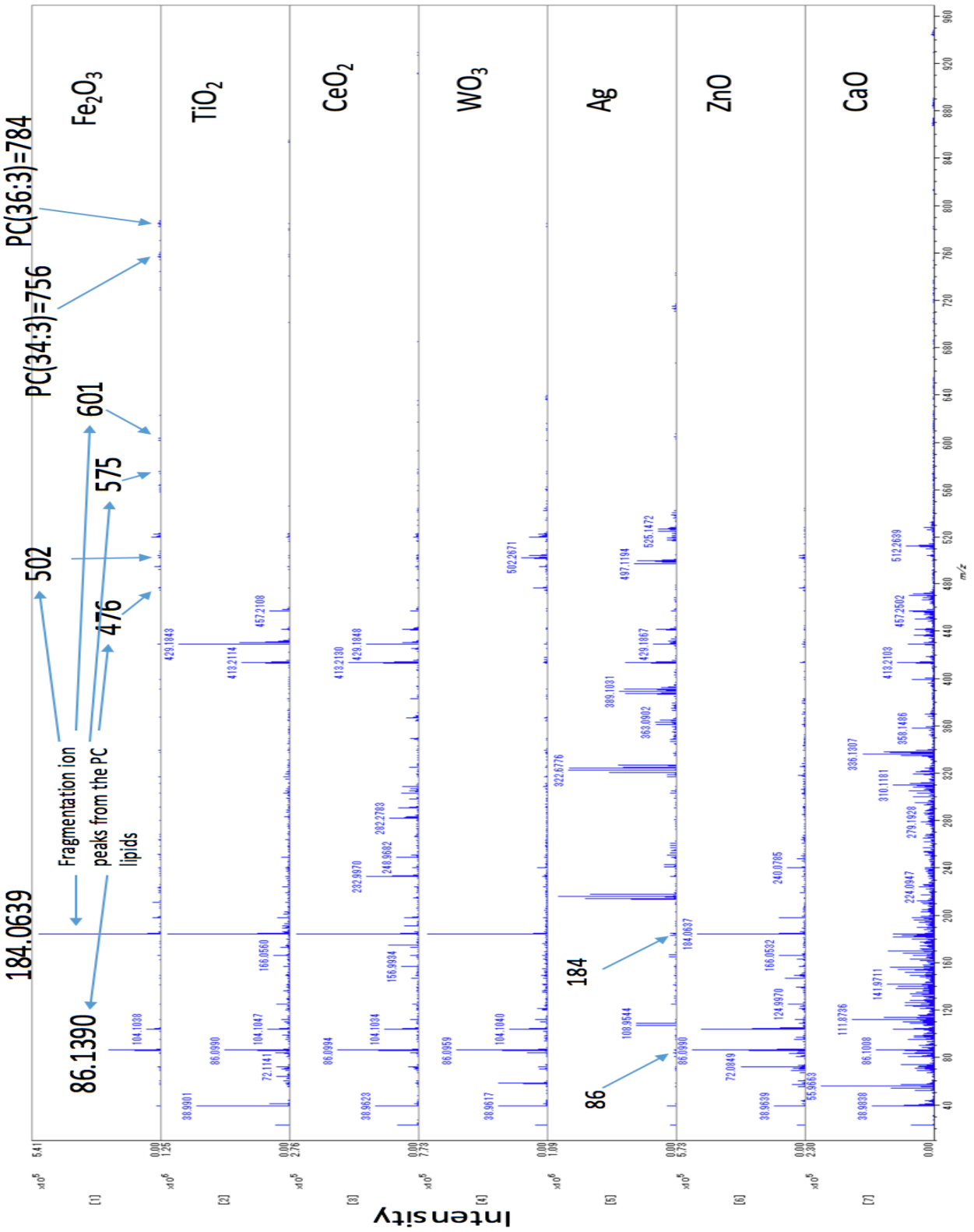

Fig. 3.25 – **Comparison view of Positive-ion mode mass spectrum of amoeba cells using all 7 nanoparticles as a matrix and analyzed by MALDI Spiral-TOF**

3.4.3 The selection of the nanoparticles for the single cell analysis

The Fe_2O_3 and Ag nanoparticles were chosen for the analysis of single cells. The Fe_2O_3 NPs were selected because it produced the least inference peaks in the analysis of DSPC and amoeba cell among all the nanoparticles used in this study. Also, molecular ion peaks of the lipids in the analysis of amoeba cells at *m/z* 756 and *m/z* 784 were observed with the highest relative intensity using the Fe_2O_3 nanoparticles.

The above results show that the Ag nanoparticles were among the least suitable nanoparticles for the analysis of lipids in the amoeba cells. However, Ag NPs were chosen because they can be deposited in dry form which is suitable for imaging analysis. The data which verifies the benefits of deposition of nanoparticles in dry form over wet form deposition is shown in the next chapter.

References

[1] S. Shimma, A. Kubo, T. Satoh, M. Toyoda, *PLoS ONE* **2012**, 7(5): e37107.

[2] D. Watts, J.M. Ashworth *Biochem. J.* **1970**, 119, 171-174.

[3] K. Richter, N. Revelo *EMBO J.* **2018**, 37(1), 139-159.

Chapter 4

Analysis of the amoeba and HeLa cells using selected nanoparticles by MALDI Spiral-TOF

4.1 Introduction

After the selection of nanoparticles, the amoeba and HeLa cell imaging analysis were performed using the selected nanoparticles Fe_2O_3 and Ag by a conventional MALDI Spiral-TOF mass spectrometer before the final analysis with the stigmatic-type MALDI mass spectrometer. At first, amoeba cells were analyzed using Fe_2O_3 and Ag nanoparticles. The Fe_2O_3 nanoparticles were deposited in wet form over the sample using a pipette and the Ag nanoparticles were deposited in the dry form over the sample using a sputtering instrument. The imaging analysis of amoeba cells using Fe_2O_3 and Ag nanoparticles were performed to show the advantages of dry deposition of nanoparticle matrix against the wet form deposition. After the analyses, Fe_2O_3 nanoparticles were found to be more suitable for the analysis of the lipids, but the spatial resolution of images was reduced because they were deposited in wet form. Therefore, HeLa cells imaging analysis was performed using only the Ag NPs later. The imaging analyses of HeLa cells using Ag nanoparticles by the conventional MALDI Spiral-TOF mass spectrometer, before the final analysis with the stigmatic-type MALDI mass spectrometer, were performed to compare the spatial resolution of the two instruments.

In this chapter, the imaging analysis of the amoeba using the two selected nanoparticles Fe_2O_3 and Ag and that of single HeLa cells using Ag nanoparticles by a conventional MALDI Spiral-TOF mass spectrometer is reported.

4.2 Sample Preparation

4.2.1 Materials

The Fe_2O_3 NPs and TFA(Trifluoroacetic acid) were purchased from Sigma Aldrich Co. (St. Louis, USA). DMEM (high glucose) was purchased from Wako Chemical Industries Ltd. (Osaka, Japan). D-PBS and glyoxal (40%) were purchased from Nacalai Tesque.

4.2.2 Amoeba cells preparation method

The amoeba cells for imaging analysis were prepared with an additional step as compared to the preparation method used in chapter 3. After the deposition of the cells on the sample plate, a 10-mm-square sheet of agarose was overlaid onto the cells to flatten the cells, which prevents the shrinkage or deformation of the cells.[2]

The whole protocol is as follows:

Dictyostelium discoideum cells (wild type strain; Ax2) were grown in HL5 medium[1] at 21 °C. The cells were re-suspended in phosphate buffer (DB; 5 mM Na_2HPO_4, 5 mM KH_2PO_4, 2 mM $MgSO_4$, 0.2 mM $CaCl_2$, pH 6.5) at the cell density of 3 $x10^6$ cells/mL after washed with DB, and 1 ml of the cell suspension was incubated in a 35-mm plastic dish for 5 hours at 21°C. The cells were re-suspended in 0.3-ml DB after washed with DB twice, and a 10-µl aliquot of the cell suspension was placed on a 0.1 mm thick stainless steel plate (TS50-50-005, Iwata, Japan) and incubated for 15 min at 21°C. A 10-mm-square sheet of agarose (2% agarose-II (Dojindo, Japan) dissolved in DB without Mg^{++} and Ca^{++}) was overlaid onto the cells, and an excess of the buffer was removed with filter paper[2]. After a 1-hour incubation, the cells were fixed with 3% glyoxal (3.13 ml glyoxal (40% stock solution), 0.3 ml acetic acid, 0.1 ml 5N NaOH, 36.47 mL ddH_2O)[3] for 15 min on ice, washed with distilled water and air-dried.

4.2.3 HeLa cells sample preparation

HeLa is an immortal cell line derived from cervical cancer cells. HeLa cells were grown on the 0.1 mm stainless steel plates (TS50-50-005, Iwata, Japan) in DMEM containing 10% fetal bovine serum (FBS) for 24 hours at 37 °C in a 5% CO_2 atmosphere. The cells were washed with phosphate buffer saline (PBS) and fixed with 3% glyoxal for 30 mins on ice. The stainless steel plates were washed with purified water and air-dried.

4.2.4 Nanoparticles preparation and deposition on cells

The Fe_2O_3 nanoparticles were suspended in a 4:1 (water/TFA) solution with a concentration of 35 mM. The Water/TFA (4:1) solution and NPs mixer solution was repeatedly vortexed and sonicated for 5 mins to obtain a well-mixed solution. 1.5 μl of the Fe_2O_3 nanoparticles suspension was deposited using a pipette over the cells prepared on a stainless steel plate. The Ag nanoparticles were sputter deposited directly on the cells by a sputtering instrument (MC1000 Ion Sputter Coater, Hitachi, Japan). After the deposition of the nanoparticles, the stainless steel plate was adhered to the MALDI plate using double-sided carbon tape.

4.3 Experimental

4.3.1 MS data acquisition

A MALDI spiral-TOF mass spectrometer (JMS-S3000, JEOL, Japan) was used for the analysis. The instrument is equipped with the third harmonic generation of a Nd:YLF laser operating at 349 nm wavelength. The frequency can be adjusted to 10, 20, 50, 100, 250 Hz. The analysis of amoeba cells using Fe_2O_3 and Ag nanoparticles was performed at 10 Hz while that of HeLa cells using Ag nanoparticles was done at 250 Hz. The spot size of the laser was known to be about 20-30 μm in diameter. All the analyses were performed in the positive-ion mode.

The step size was set to 20 μm for the analysis of amoeba cells and was set to 30 μm in the analysis of HeLa cells. The software msMicroImager^{TM} Extract (JEOL, Japan) was used to generate the images. The mass window for the images was set to 0.03.

Before the matrix application, microscopic images of the cell samples were acquired with a digital microscope (Keyence, Japan).

4.3.2 Optimization of laser energy

The laser energy required for the analysis of amoeba cells and HeLa cells were different for the two types of NPs used. The laser used in MALDI spiral-TOF has a power of 120 μJ per pulse. For each NPs, laser intensity was increased from 30% gradually with an increment of 5% until the optimum laser intensity was attained. After finding the optimum laser intensity with an increment of 5%, it was adjusted again with the increment/decrement of 1%.

For the analysis of amoeba cells, the laser intensity was set to 40% in the case of Fe_2O_3 and 45% for Ag NPs. For the analysis of HeLa cells using Ag NPs, the laser intensity was set to 60%.

4.4 Results and Discussion

4.4.1 Imaging analysis of amoeba cells using Fe_2O_3 NPs

Figure 4.1 shows the positive-ion mode mass spectrum of the amoeba cells obtained using Fe_2O_3 NPs as a matrix. Figure 4.2 shows the positive-ion mode average mass spectrum of the amoeba cells obtained using Fe_2O_3 NPs as a matrix. The average mass spectrum represents the average intensity of the ions of one pixel averaged over all the pixels, whereas the spectrum shown in figure 4.1 represents the total intensity of the ions obtained by scanning the whole sample area. Therefore, the intensity of ions is low in the average mass spectrum as compared

to the total mass spectrum shown in figure 4.1. The average spectrum is obtained by the imaging analysis and is used for generating the images.

In the average mass spectrum obtained after the imaging analysis, the most intense peaks from lipids were the phosphocholine head group $PO_4H_2CH_2CH_2N(CH_3)_3^+$ at *m/z* 184 and a fragmentation of the *m/z* 184 head group, $(CH_3)_3NCH{=}CH_2^+$ at *m/z* 86. The potassium was also detected at *m/z* 39. The other fragmentation ion peaks from the lipids have very low intensity.

Figure 4.3 is the microscopic image of the amoeba cells sample used for the imaging analysis. The big shapes in the image are not the single cells, instead, they are a large number of cells aggregated together. The small dot-like shapes are single cells.

Figure 4.4, 4.5, 4.6 shows the distributions of the potassium, phosphocholine head group fragmentation, phosphocholine head group respectively. The colored scale bar at the right of the images shows the degree of the intensity of the ions. The regions with red color show the highest intensity of ions and the pink color shows the least intensity. As shown in the spectrum, the images also show that the ion at *m/z* 86 is most intense in the amoeba cells as compared to the ions at *m/z* 184 and *m/z* 39.

The sample stage step size was set to 20 μm, which means the spatial resolution should be 20 μm, but the image quality was reduced because the Fe_2O_3 NPs were deposited in wet form using a pipette which may have caused the migration of the analytes. The images show that the shape of the cells is not maintained after the deposition of the Fe_2O_3 NPs, so it is difficult to determine the exact distribution of ions in the cells here. The size of the amoeba cells was about 10-30 μm. The pixel size (20 μm) is roughly equal to the cell size which is inadequate to observe the distribution inside a single cell.

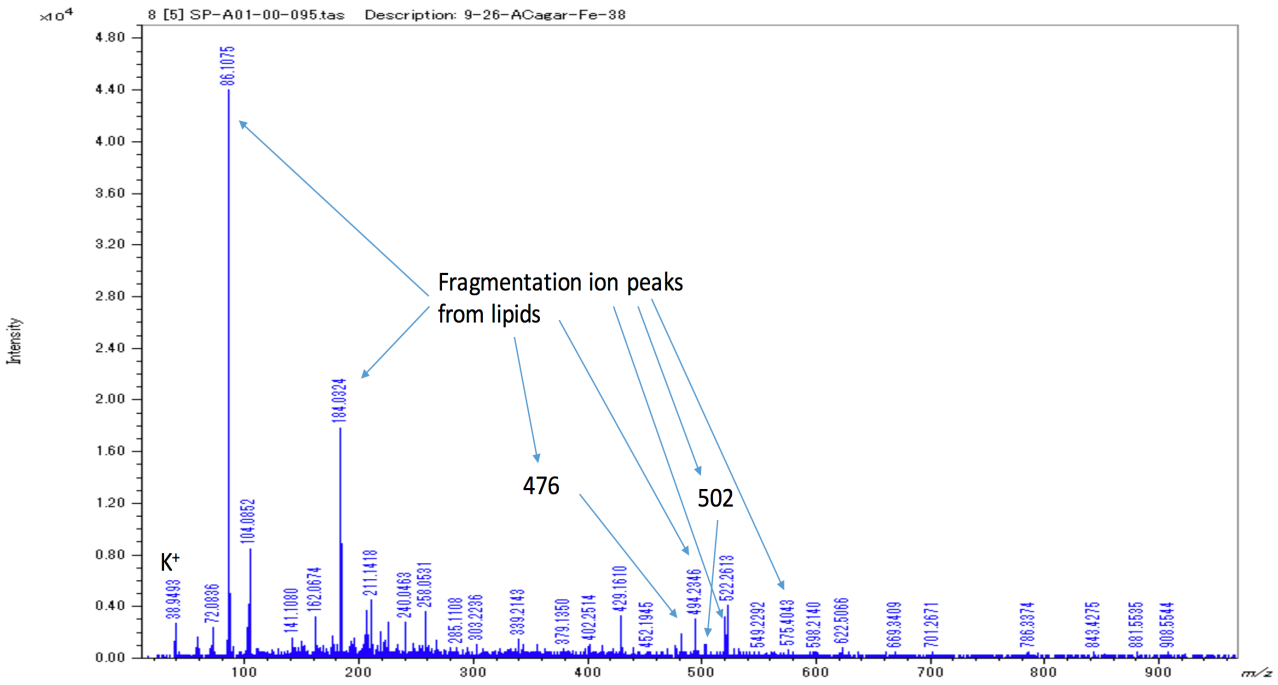

Fig. 4.1 - **Positive-ion mode mass spectrum of the amoeba cells using Fe_2O_3 NPs as a matrix and analyzed by MALDI Spiral-TOF**

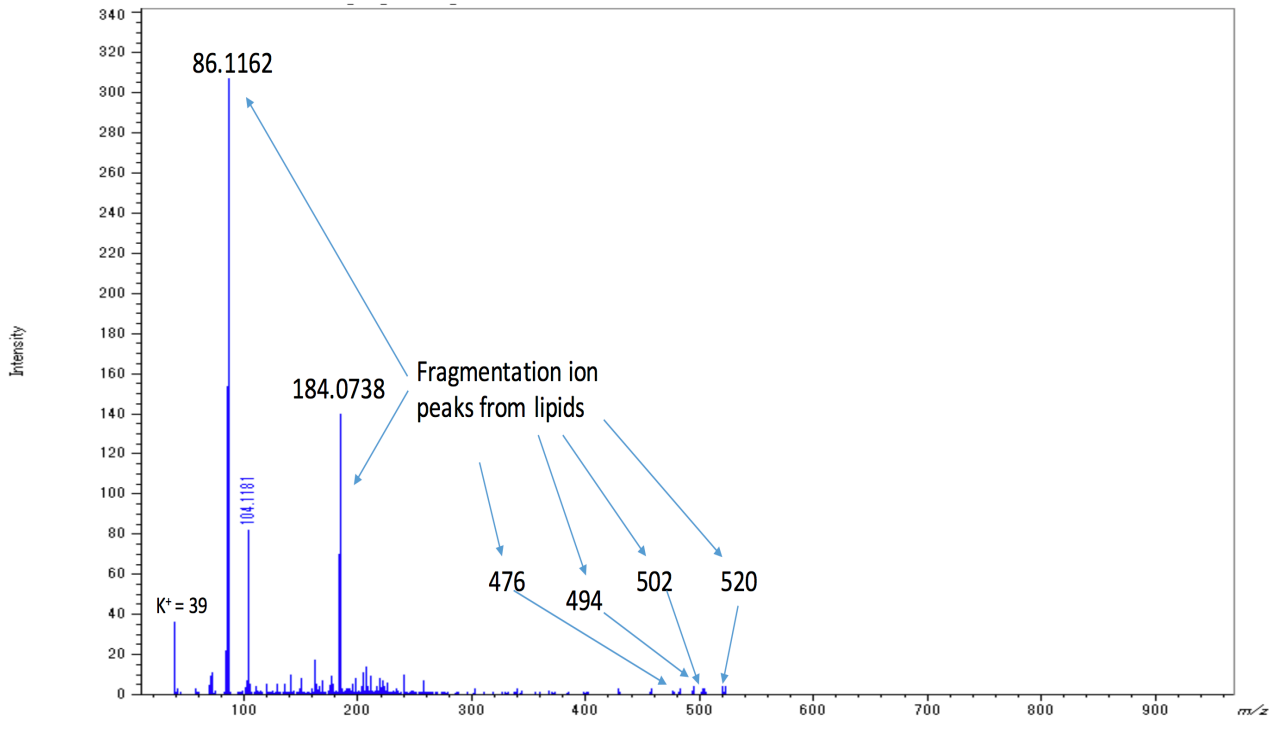

Fig. 4.2 – **Positive-ion mode average mass spectrum of the amoeba cells using Fe_2O_3 NPs as a matrix and analyzed by MALDI Spiral-TOF**

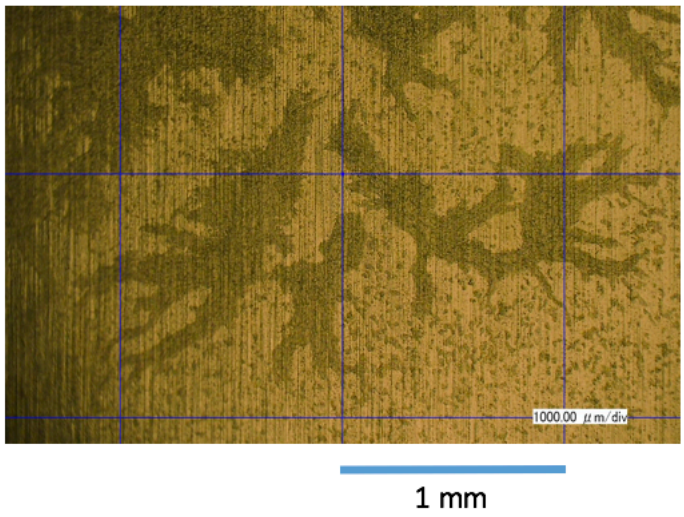

Fig. 4.3 – **Microscopic image of the analyzed amoeba cells sample**

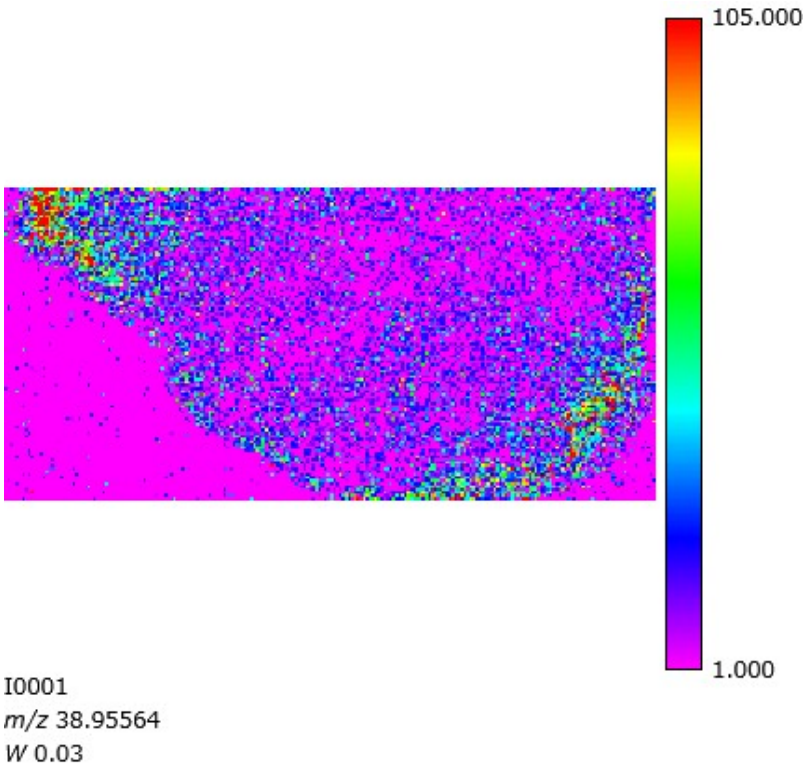

Fig. 4.4 – **Mass image of *m/z* 39**

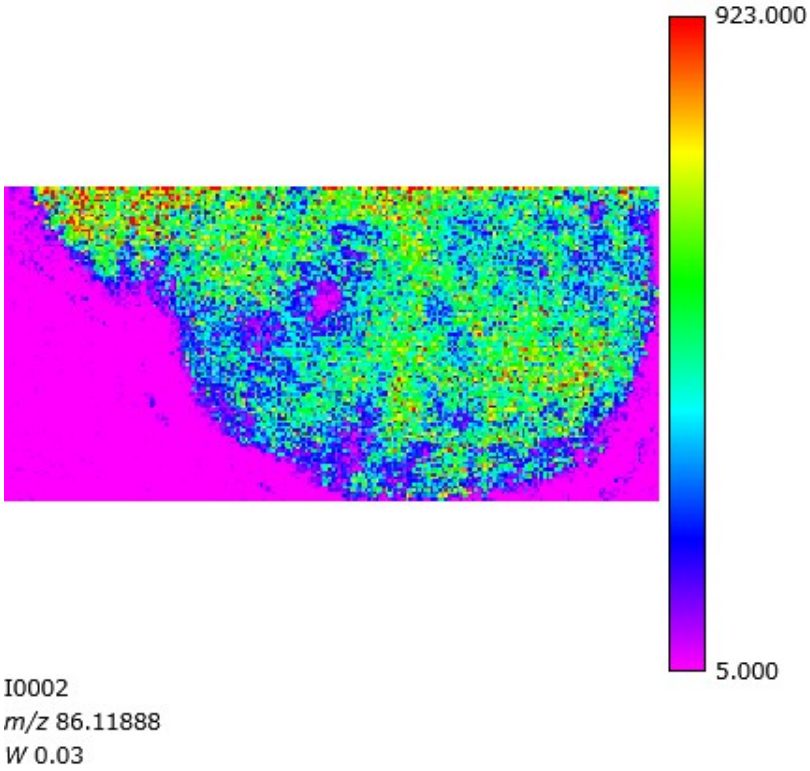

Fig. 4.5 – **Mass image of *m/z* 86**

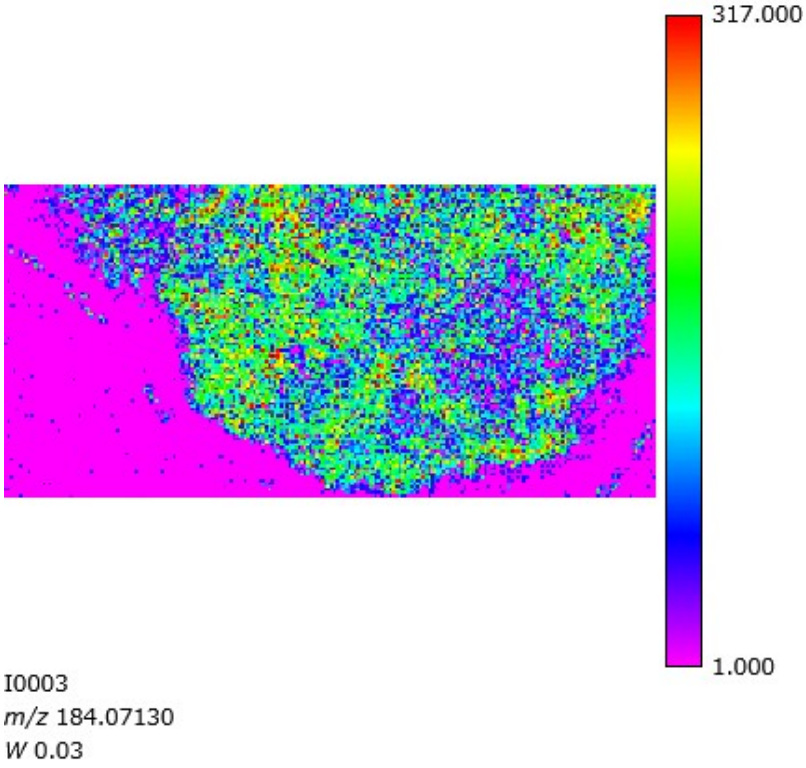

Fig. 4.6 – **Mass image of *m/z* 184**

4.4.2 Imaging analysis of amoeba cells using Ag NPs

Figure 4.7 shows the average mass spectrum of amoeba cells obtained after the imaging analysis using Ag NPs. The most intense peaks were identified at *m/z* 106.9, *m/z* 215.8, *m/z* 322.7 from the Ag nanoparticle cluster. The phosphocholine head group $PO_4H_2CH_2CH_2N(CH_3)_3^+$ at *m/z* 184 and the head group fragmentation ion peak $(CH_3)_3NCH{=}CH_2^+$ at *m/z* 86 were also observed but with low intensity. Figure 4.8 shows the average mass spectrum of amoeba cells obtained after the imaging analysis using Ag NPs in the mass range 700 to 900 *m/z*. The potassium and sodium were also detected at *m/z* 39 and at *m/z* 23 (very low intensity) respectively. The intensity of the peak at 39 was higher than that of peaks at *m/z* 184 and 86.

Figure 4.9 is the microscopic image of the amoeba cells sample used for the imaging analysis. Again, the big shape in the image is not a single cell, instead, a large number of cells aggregated together. The small dots like shapes in the image are the single cells. Figure 4.10, 4.11, 4.12, 4.13 shows the distributions of the sodium at *m/z* 23, potassium at *m/z* 38.9, phosphocholine head group fragmentation at *m/z* 86, phosphocholine head group at *m/z* 184.07 respectively. Figure 4.14 shows the distribution of the ion peak at *m/z* 785.6, which is probably from a phospholipid but was not assigned. The colored scale bar at the right of the images shows the degree of the intensity of the ions. The region with red color shows the high intensity of ions in that region and the pink color shows the least intensity. As shown in the spectrum, the images also show that the ion at *m/z* 39 is most intense in the amoeba cells as compared to the ions at *m/z* 86, *m/z* 184 and *m/z* 23. The images show that the shape of the cells was maintained after the deposition of the nanoparticles and, the spatial resolution is not affected by the deposition of Ag nanoparticles.

The sample stage step size was set to 20 µm. The diameter of the amoeba cells was about 10-30 µm. The spatial resolution of the images is 20 µm, which is inadequate to observe the distribution of ions inside the single cells.

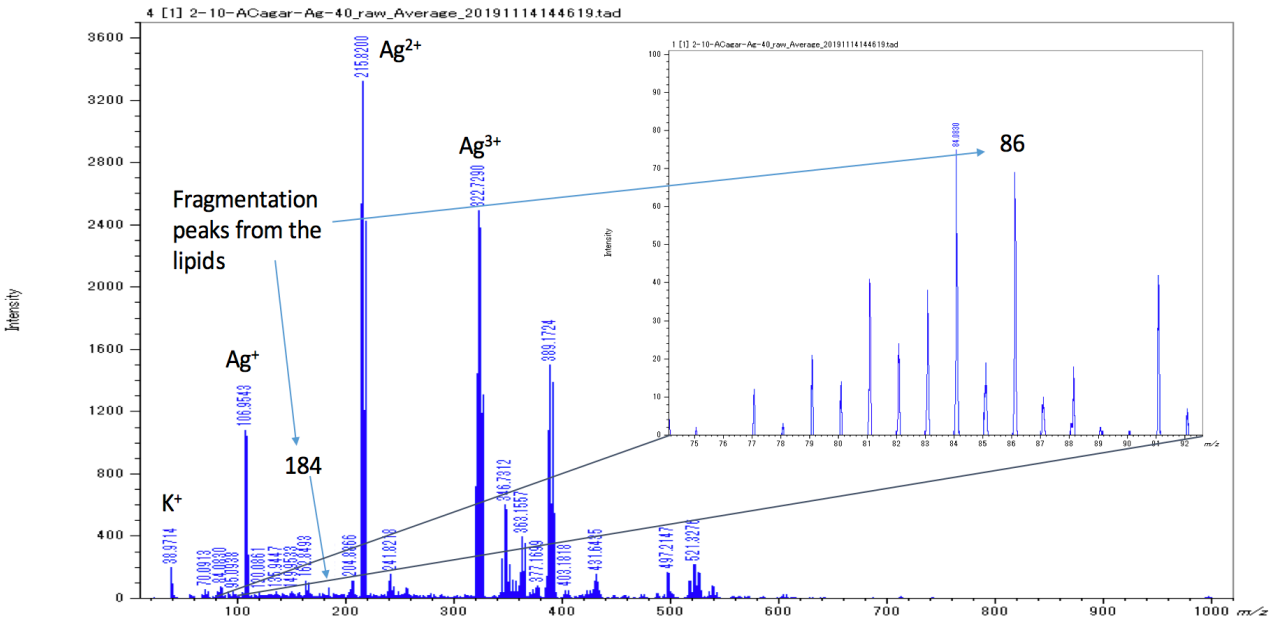

Fig. 4.7 – **Positive-ion mode average mass spectrum of the amoeba cells using Ag NPs as a matrix and analyzed by MALDI Spiral-TOF**

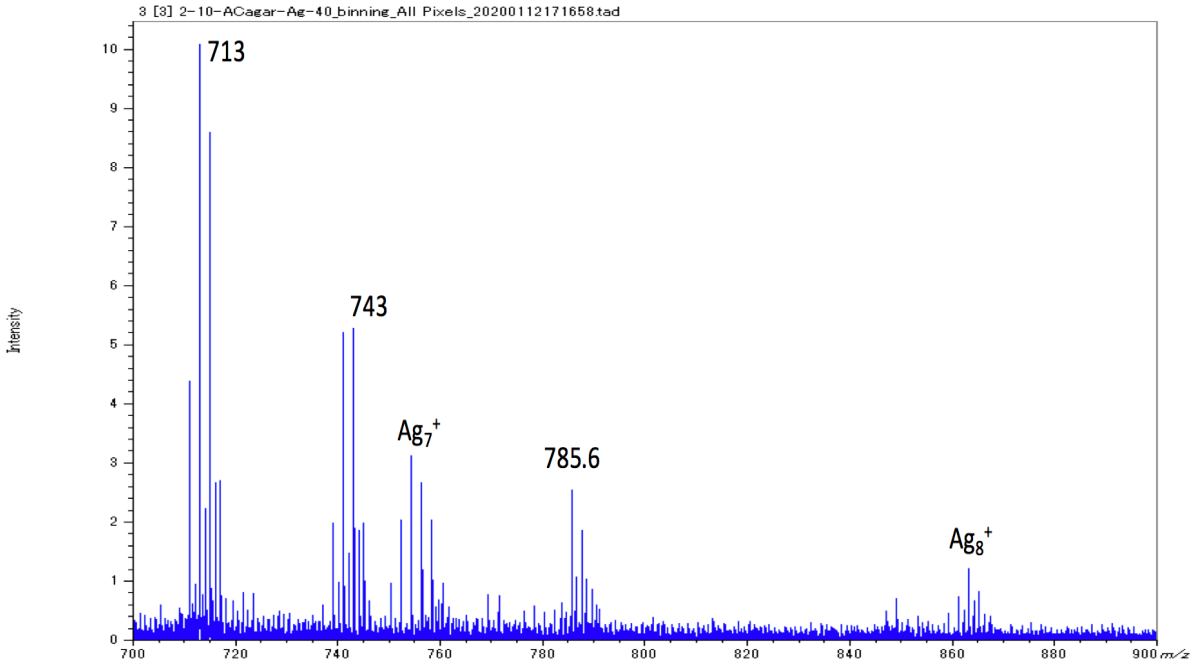

Fig. 4.8 - **Positive-ion mode average mass spectrum (mass range: 700-900) of the amoeba cells using Ag NPs as a matrix and analyzed by MALDI Spiral-TOF**

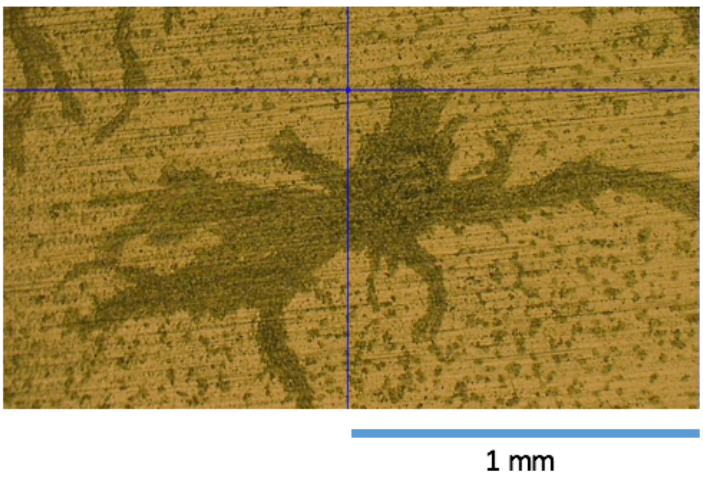

Fig. 4.9 – **Microscopic image of the analyzed amoeba cells sample**

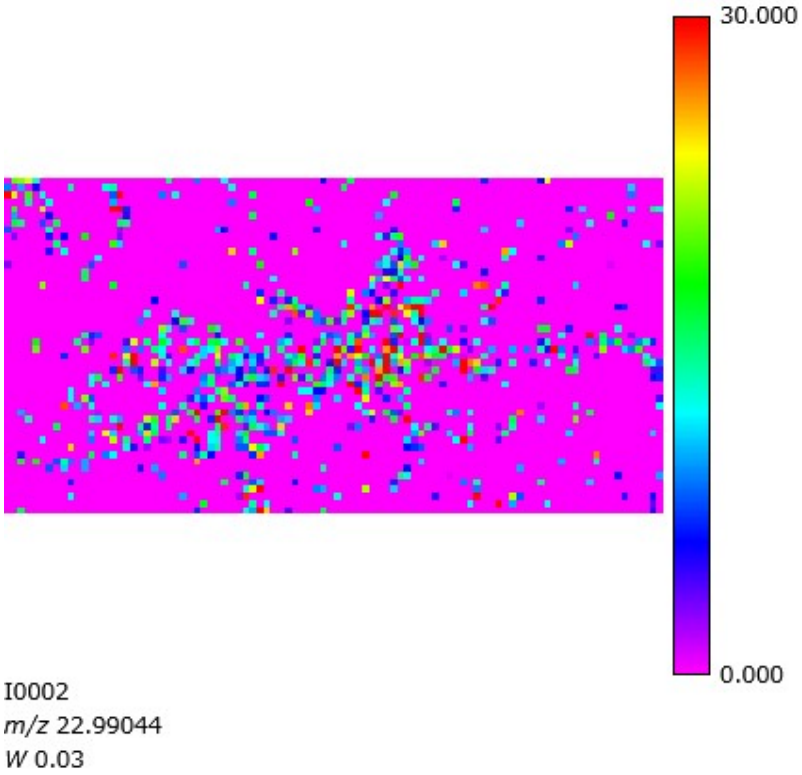

Fig. 4.10 – **Mass image of *m/z* 23**

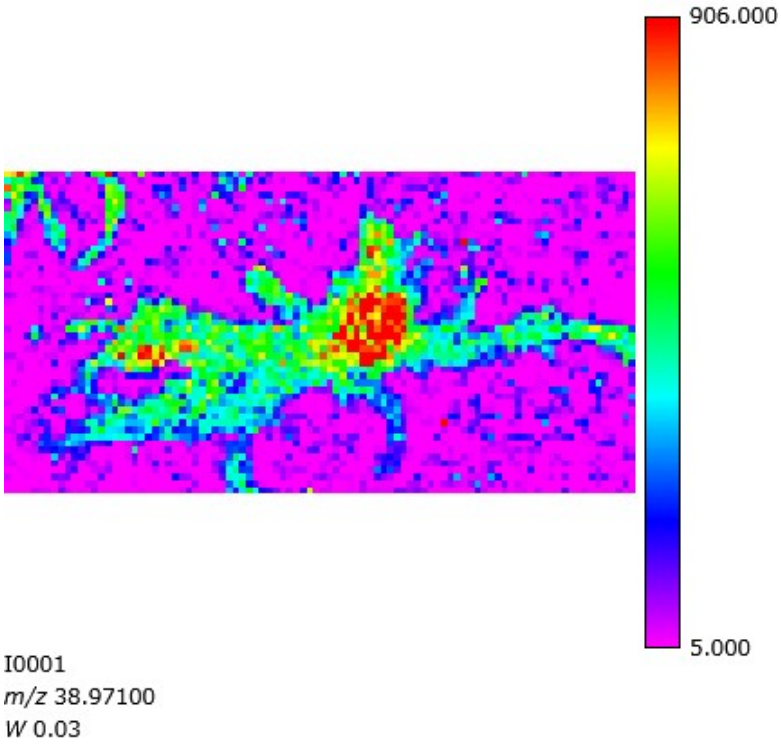

Fig. 4.11 – **Mass image of *m/z* 39**

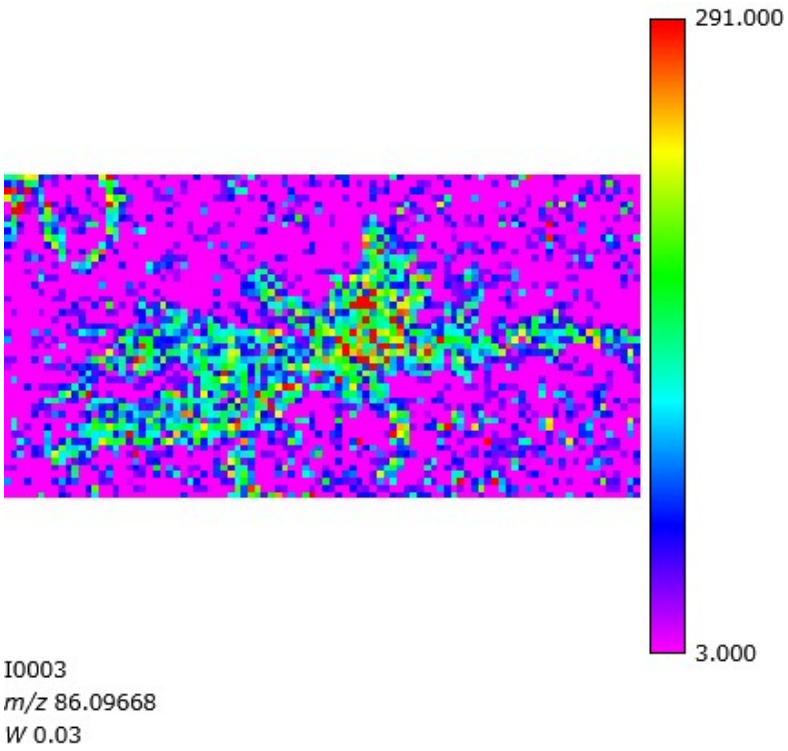

Fig. 4.12 – **Mass image of *m/z* 86**

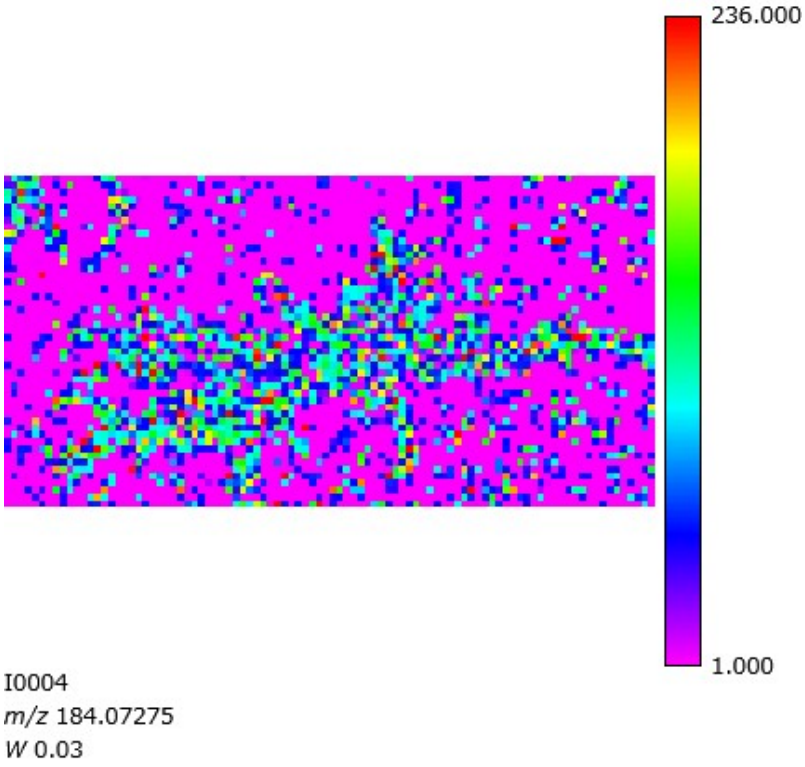

Fig. 4.13 – **Mass image of *m/z* 184**

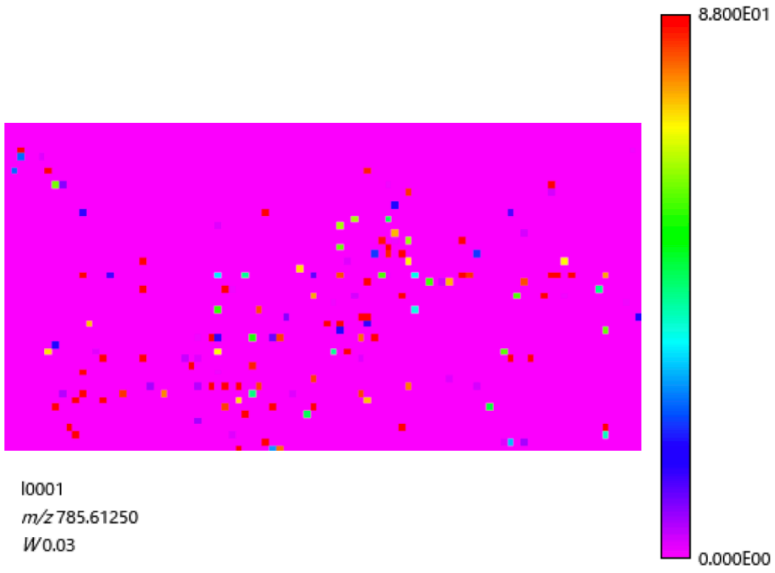

Fig. 4.14 – **Mass image of *m/z* 785.6**

4.4.3 Main conclusions from 4.4.1 and 4.4.2

The analyses of amoeba cells using Fe_2O_3 and Ag nanoparticles by the MALDI Spiral-TOF instrument lead to the two main conclusions:

1) The deposition of Fe_2O_3 nanoparticles over the sample in wet form may have caused the migration of analytes, which in result, reduced the image quality.

2) The spatial resolution of the images obtained by MALDI Spiral-TOF is not sufficient to observe the distribution of analytes inside single cells.

4.4.4 Imaging analysis of HeLa cells using Ag NPs

The size of the amoeba cells was roughly equal to the spatial resolution of the instrument which did not allow us to observe the sub-cellular structures, so a larger size cells, HeLa were adopted. HeLa cells were first analyzed using both Fe_2O_3 and Ag NPs.

Figure 4.15 and 4.16 shows the mass spectrum of HeLa cells obtained using Fe_2O_3 and Ag NPs respectively. The phosphocholine head group at *m/z* 184 and the head group fragmentation peak at *m/z* 86 were observed with both nanoparticles, but the intensity was relatively higher in the case of Fe_2O_3 nanoparticles. Molecular ion peaks of some phospholipids at *m/z* 734, 760, 786 were also observed with Fe_2O_3 nanoparticles. The peaks at *m/z* 760 and 786 were also observed with Ag NPs, but with very low intensity. The fragmentation peaks at *m/z* 86 and 184 suggest that these phospholipids are phosphatidylcholines. Thus, the phospholipids at *m/z* 734 and *m/z* 760 were tentatively assigned as PC(32:0) and PC(34:1) respectively. The phospholipid at *m/z* 786 was not assigned. The results suggest that Fe_2O_3 nanoparticles are a better candidate for the analysis of lipids in HeLa cells. However, as shown in the analysis of amoeba cells, the deposition of Fe_2O_3 NPs in wet form affects the image quality, so only Ag NPs were used for the imaging analysis of HeLa cells.

Figure 4.17 shows the average mass spectrum of HeLa cells obtained after the imaging analysis using Ag NPs. Again, same as obtained in the case of amoeba cells, the most intense peaks were from the Ag nanoparticle cluster at *m/z* 106.9, 215, 322. The phosphocholine head group at *m/z* 184 and the head group fragmentation peak at *m/z* 86 were also observed, but with very low intensity. Figure 4.18 shows the average mass spectrum of HeLa cells obtained after the imaging analysis using Ag NPs in the mass range 700 to 900 *m/z*. The potassium and sodium were also detected at *m/z* 39 and 23 respectively. The intensity of the peak at *m/z* 39 was higher than those of peaks at *m/z* 184, *m/z* 86 and *m/z* 23.

Figure 4.19 shows the microscopic image of the HeLa cells sample used for the imaging analysis. Figure 4.20, 4.21, 4.22, 4.23 shows the distributions of the phosphocholine head group fragmentation, phosphocholine head group, sodium, potassium, respectively. Figure 4.24, 4.25 shows the distributions of the ion peaks at *m/z* 786 and *m/z* 760 respectively. The

images show that the shape of the cells was maintained after the deposition of the silver nanoparticles, so the spatial resolution is not affected.

The size of the HeLa cells used was roughly equal to 50-150 µm and the sample stage step size was set to 30 µm, so an image of single-cell contains only 2 to 5 pixels, which is still inadequate to observe the subcellular distribution, so a better method was needed to obtain a better spatial resolution. For that purpose, a stigmatic-type MALDI mass spectrometer was used to image single HeLa cells using Ag nanoparticles, which is described in the next chapter.

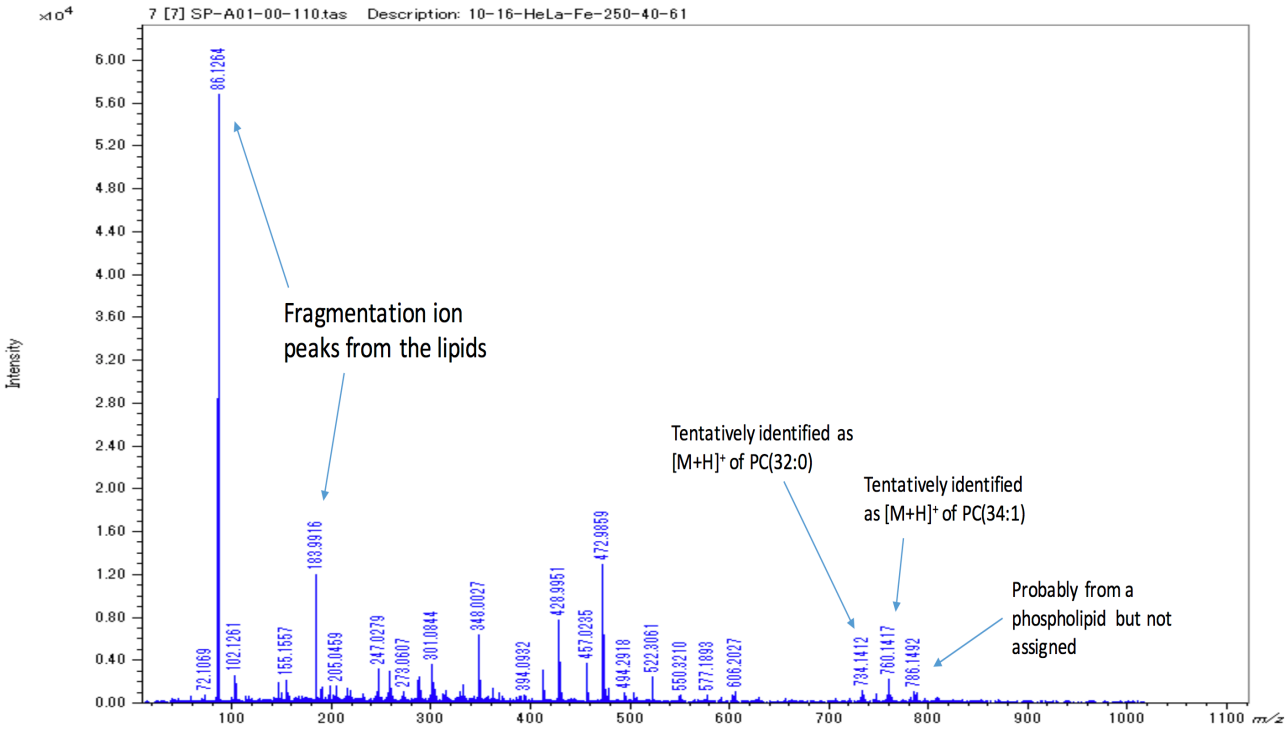

Fig. 4.15 – **Positive-ion mode mass spectrum of the HeLa cells using Fe_2O_3 NPs as a matrix and analyzed by MALDI Spiral-TOF**

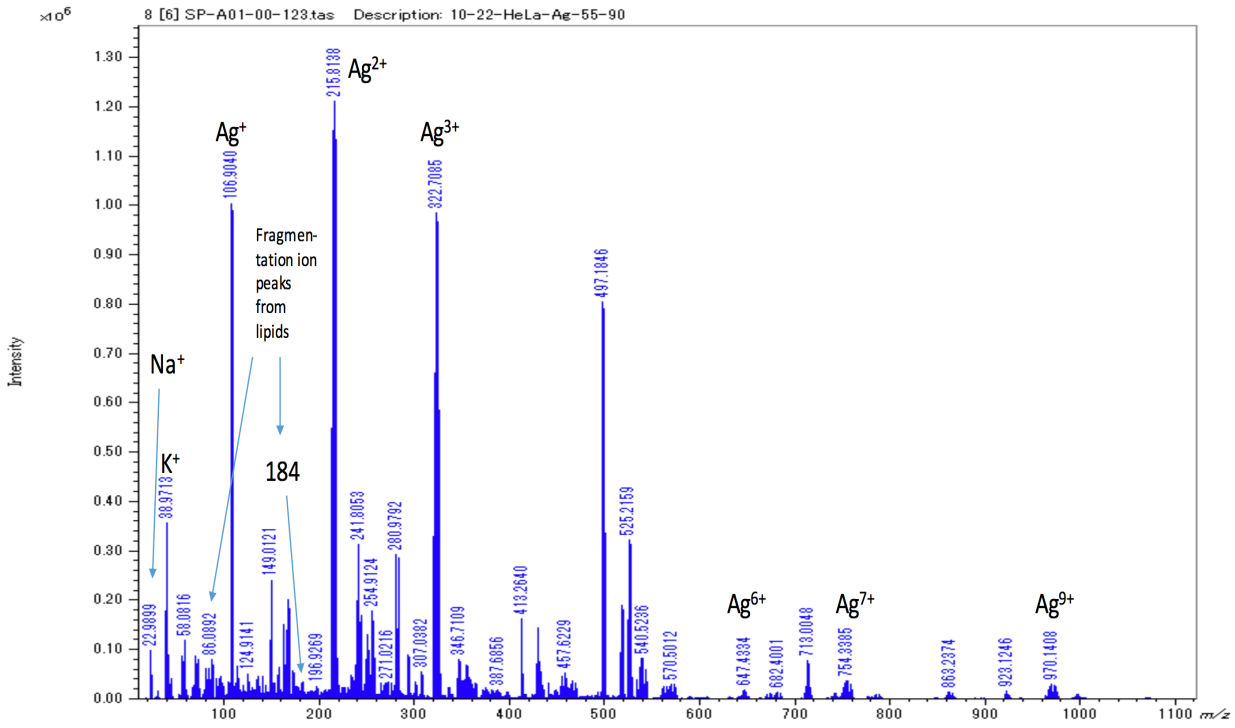

Fig. 4.16 – **Positive-ion mode mass spectrum of the HeLa cells using Ag NPs as a matrix and analyzed by MALDI Spiral-TOF**

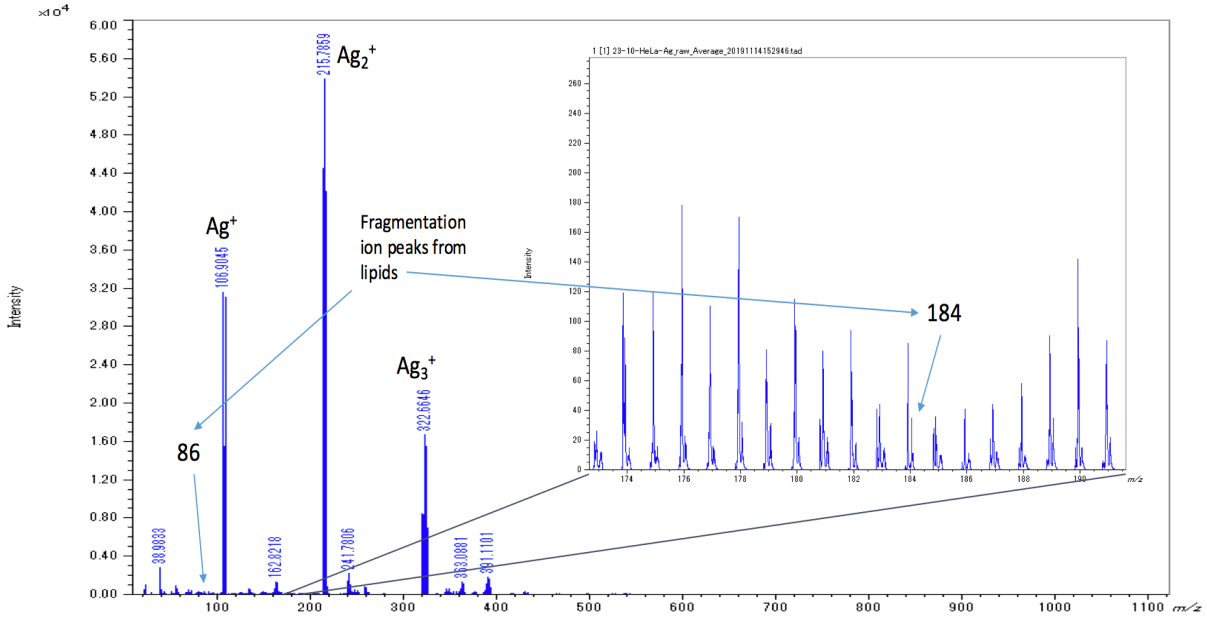

Fig. 4.17 – **Positive-ion mode average mass spectrum of the HeLa cells using Ag NPs as a matrix and analyzed by MALDI Spiral-TOF**

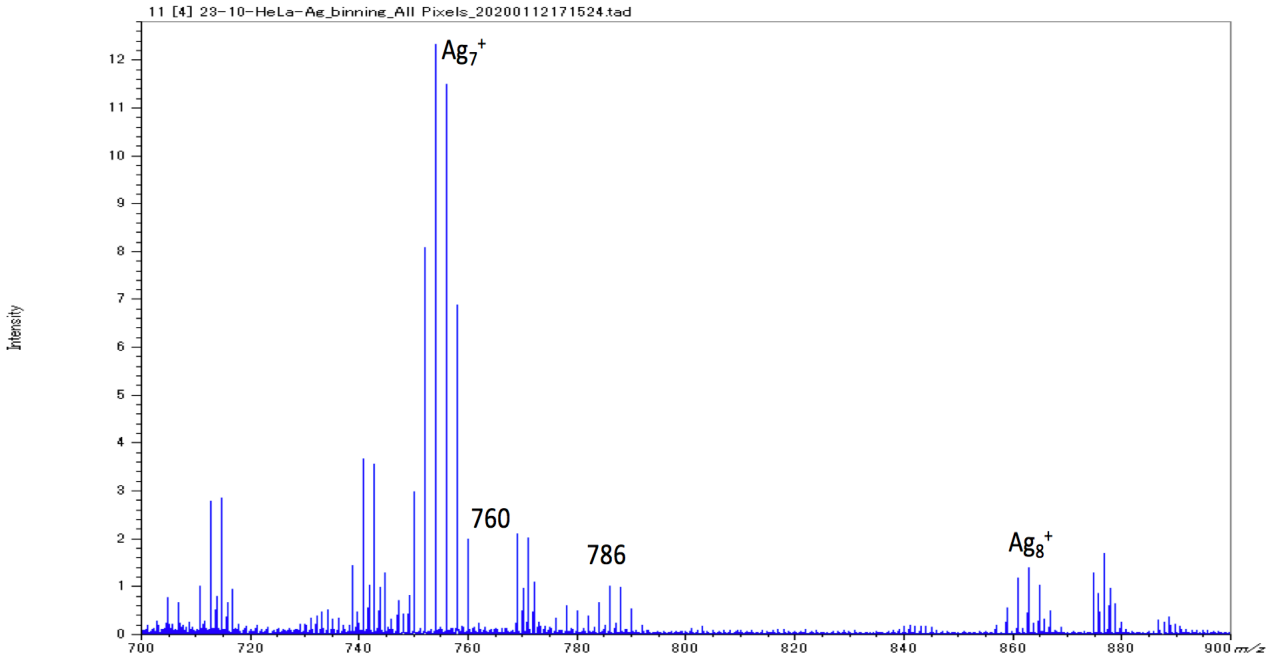

Fig. 4.18 - **Positive-ion mode average mass spectrum (mass range: *m/z* 173-191) of the HeLa cells using Ag NPs as a matrix and analyzed by MALDI Spiral-TOF**

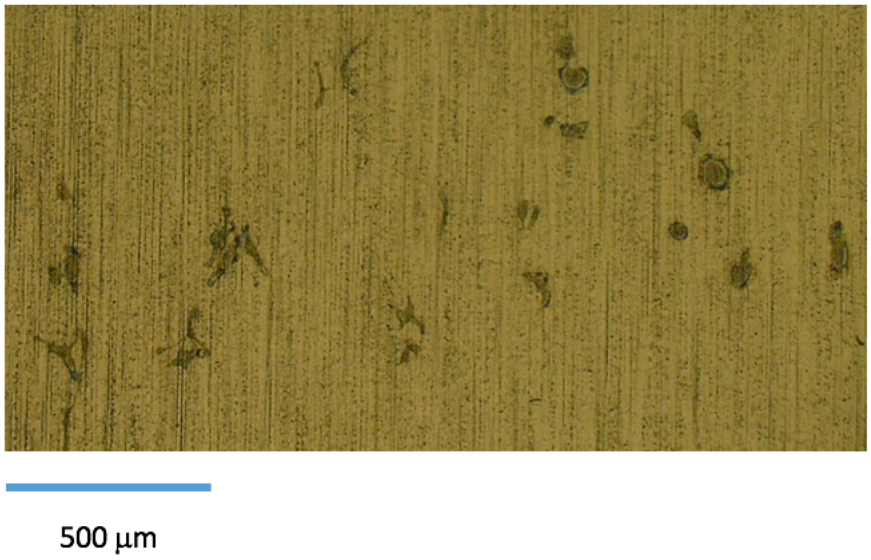

Fig. 4.19 – **Microscopic image of the analyzed single HeLa cells sample**

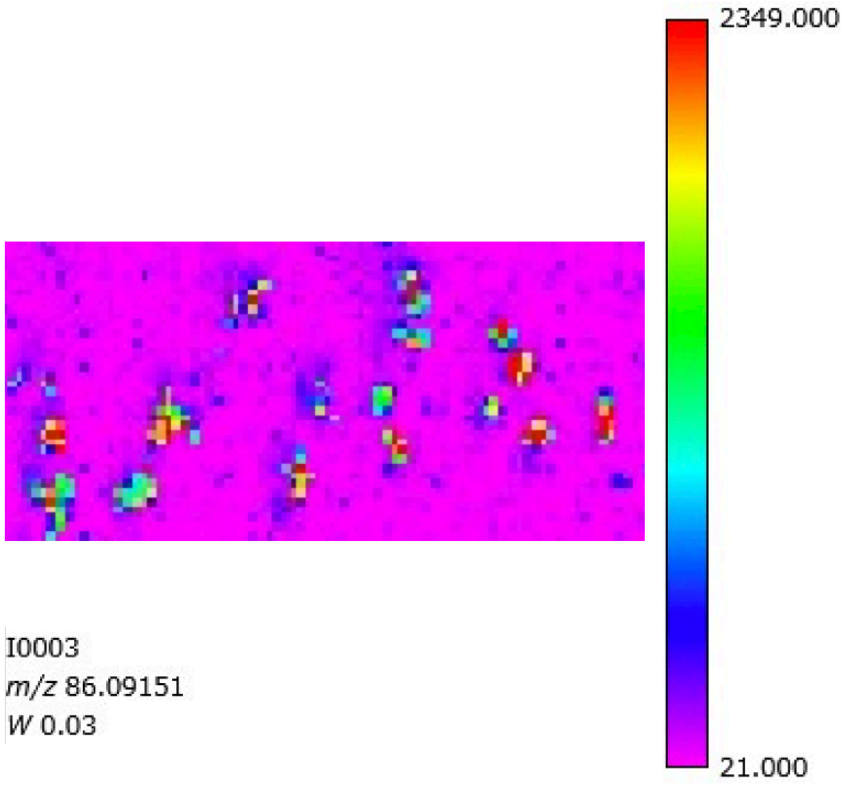

Fig. 4.20 – **Mass image of *m/z* 86**

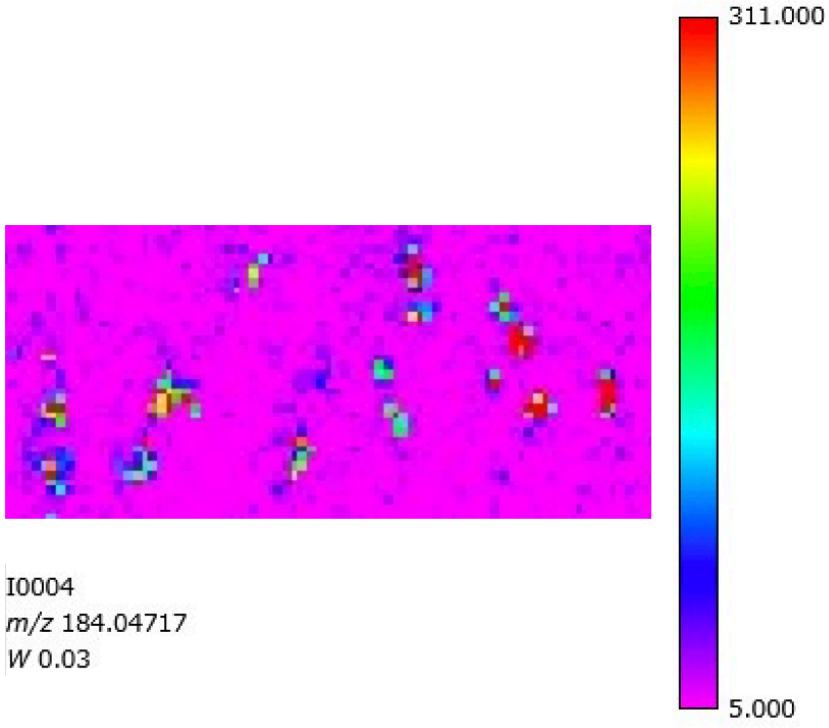

Fig. 4.21 – **Mass image of *m/z* 184**

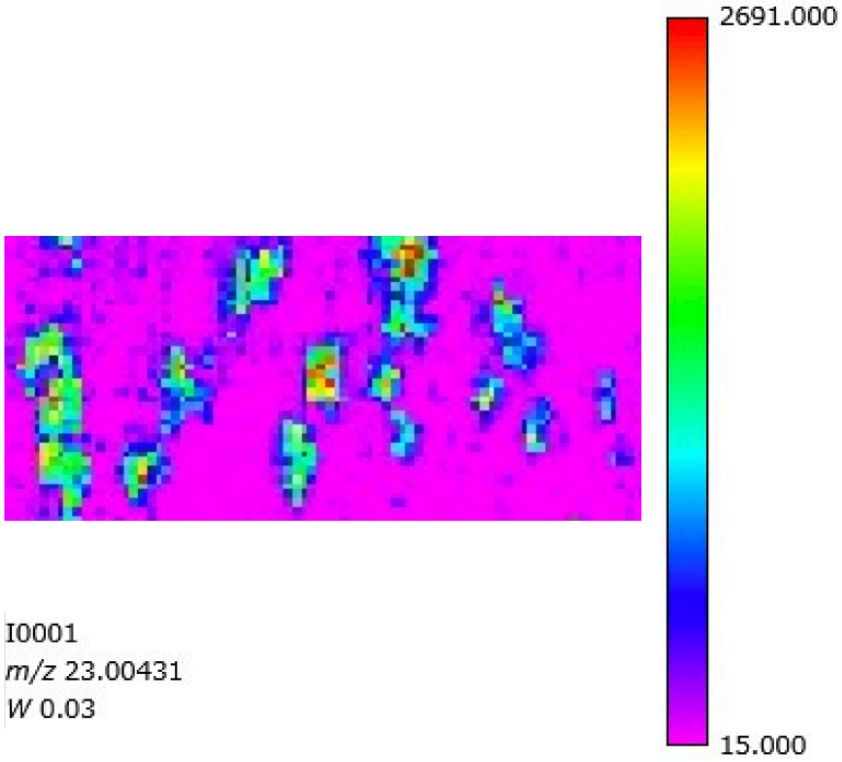

Fig. 4.22 – **Mass image of *m/z* 23**

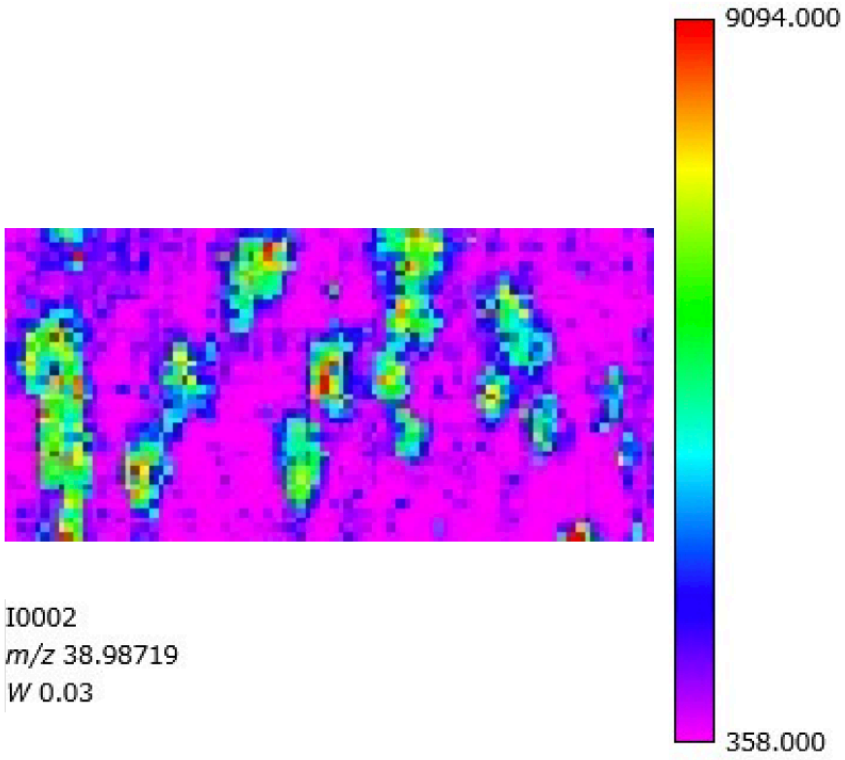

Fig. 4.23 – **Mass image of *m/z* 39**

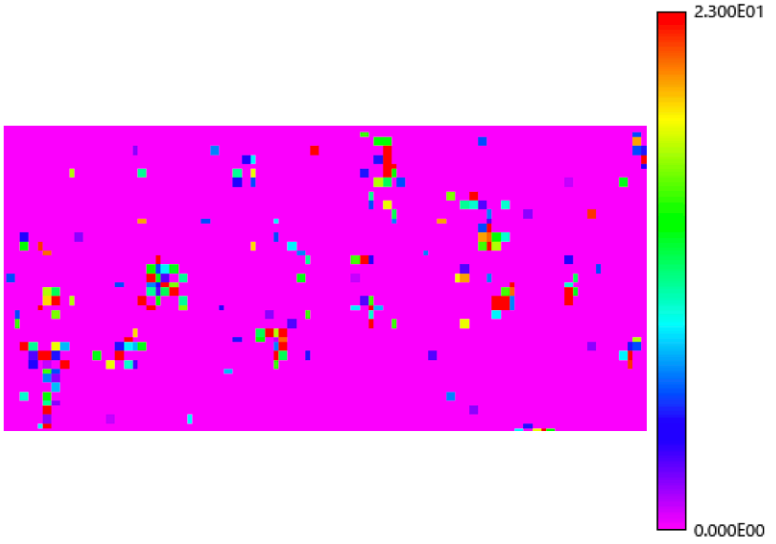

Fig. 4.24 – **Mass image of *m/z* 786**

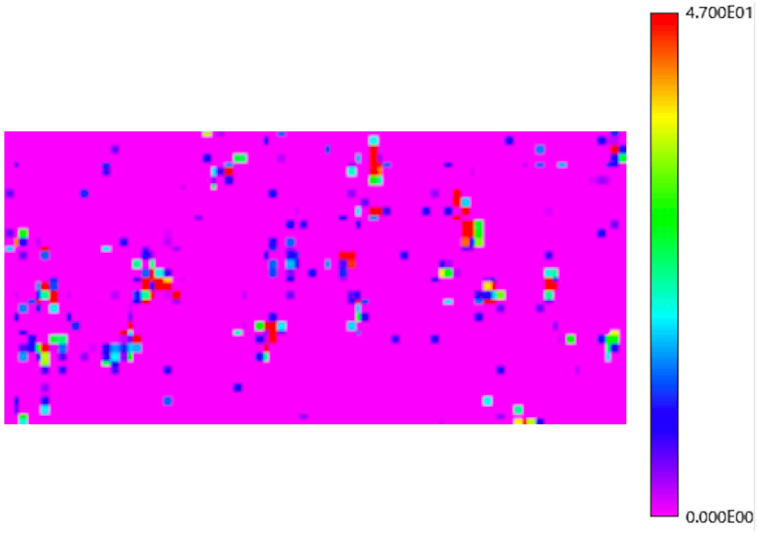

Fig. 4.25 – **Mass image of *m/z* 760**

References

[1] D. Watts, J.M. Ashworth *Biochem. J.* **1970**, 119, 171-174.

[2] Y. Fukui, S. Yumura, T. Yumura *Methods Cell Biol.* **1987**, 28, 347-356.

[3] K. Richter, N. Revelo *EMBO J.* **2018**, 37(1), 139-159.

Chapter 5

Single Cell Imaging Analysis by a Stigmatic-type Imaging Mass Spectrometer

5.1 Introduction

As mentioned in Chapter 1 and shown in the previous chapter, the conventional scanning type MALDI Spiral-TOF mass spectrometer is not suitable for the single-cell imaging analysis because the spatial resolution is roughly equal to the laser spot size and the laser spot size is typically 10-100 μm. To overcome this limitation, a stigmatic-type MALDI mass spectrometer[1,2], which has the potential to achieve sub-micron level spatial resolution independent of the laser spot size was used.

In this chapter, imaging analysis of single HeLa using Ag NPs by a stigmatic-type MALDI mass spectrometer is described. This is the first time the stigmatic-type MALDI mass spectrometer is used for the single-cell imaging analysis.

5.2 Sample Preparation

HeLa is an immortal cell line derived from cervical cancer cells. HeLa cells were grown directly on the MALDI plate in DMEM (high glucose, Wako Chemical Industries Ltd., Osaka, Japan) containing 10% fetal bovine serum (FBS) for 24 hours at 37 °C in a 5% CO_2 atmosphere. The cells were washed with phosphate buffer saline (PBS, Nacalai Tesque) and fixed with 3% glyoxal (40%, Nacalai Tesque) for 30 mins on ice. The MALDI plate was washed with purified water and air-dried. Samples were prepared by our collaborator Dr. Satomi Matsuoka of

Laboratory of Single Molecule Biology, Graduate School of Frontier Biosciences, Osaka University.

For the analysis, Ag nanoparticles were sputtered deposited directly on the cell samples by a sputtering instrument (MC1000 Ion Sputter Coater, Hitachi High-Technologies Corporation, Japan). The deposition current, time, distance between the silver specimen and the sample were 30 mA, 7 seconds, 30 mm respectively.

5.3 Experimental

A stigmatic-type MALDI TOF mass spectrometer equipped with MULTUM TOF mass analyzer build in our lab was used for the analysis. However, the MULTUM was used in the linear-mode. The instrument is equipped with a UV laser operating at 355 nm wavelength. The frequency of the laser was 1000 Hz. The laser energy is 600 μJ/pulse. The laser spot is square. The spot size of the laser was known to be about 750 μm. All the analyses were performed in the positive-ion mode.

After the nanoparticle deposition on the cells, the microscopic images of the cell samples were acquired with a microscope.

5.4 Results and Discussion

Figure 5.1 shows the mass spectrum (mass range: 0-400 Da) of HeLa cells obtained after the imaging analysis using Ag NPs. Enlarged view of the peaks can be seen in the Fig. B in the appendix. Again, as obtained in the imaging analysis of HeLa cells by Spiral-TOF mass spectrometer (mentioned in chapter 4), the most intense peaks were from the Ag nanoparticle cluster. The phosphocholine head group $PO_4H_2CH_2CH_2N(CH_3)_3^+$ at *m/z* 184 and the head

group fragmentation peak $(CH_3)_3NCH=CH_2^+$ at *m/z* 86 were also observed, but with very low intensity. The sodium and potassium were also detected at *m/z* 23 and 39 respectively. The intensity of the peaks at *m/z* 23 and 39 was higher than those of peaks at *m/z* 184 and *m/z* 86. And, the intensity of the peak at *m/z* 39 was higher than that of the peak at *m/z* 23. The calcium was also detected at *m/z* 40.

Figure 5.2 shows the microscopic image of the HeLa cells sample used for the imaging analysis. All the single cells can be seen as separated from each other. Figure 5.3, 5.4, 5.5, 5.6, 5.7 shows the distribution of sodium (*m/z* 23), calcium (*m/z* 40), potassium (*m/z* 39), phosphocholine head group fragmentation (*m/z* 86), phosphocholine head group (*m/z* 184) respectively. The intensity of the ion at *m/z* 39 is more as compared to other ions, which is also shown in the mass spectra. The distribution of potassium and sodium seems to be almost the same in all the cells while that of calcium and *m/z* 86 is different in different cells. The intensity of ion at *m/z* 184 is very low which is insufficient to determine its distribution in the cells. The size of the HeLa cells used was roughly equal to 50-150 μm. As expected, more spatially resolved images were obtained with stigmatic-type imaging mass spectrometer than the scanning type Spiral-TOF MALDI mass spectrometer. The pixel size or the spatial resolution of the images is 2 μm, which is much better as compared to 20-30 μm of MALDI Spiral-TOF mass spectrometer. Although a spatial resolution of fewer than 2 μm was achieved in the past using SIMS and by optimizing the laser spot size to less than 2 μm in the conventional MALDI instruments, the measurement time can be greatly reduced in the case of stigmatic-type MALDI mass spectrometer. For example, the laser spot size of the stigmatic-type imaging mass spectrometer, used in this study, has a laser spot size of about 750 μm with a repetition rate of 1 kHz. Therefore, the laser can shoot an area of 750 μm^2, 1000 times in just 1 second. On the other hand, in a scanning-type imaging mass spectrometer with a laser having a spot size of 1 μm and a repetition rate of 1 kHz, it will take approximately 6.5 days to scan the 750 square meter

area, if the laser shoots every spot 1000 times and, it will take about 15 hours, 1.5 hours to scan the same area if the laser shoots every spot 100, 10 times respectively.

In this study, the stigmatic mass spectrometer was used without the magnification lens because it was difficult to align with the ion trajectory axis. In the current situation, only the Einzel lens was used to magnify the ion distribution and focus onto the detector and, the spatial resolution is determined by this magnification and the pixel size of the detector. In this experiment, the pixel size of the detector used was 50 μm and, the ion distribution was magnified by 50 times, so the maximum spatial resolution that can be achieved in this configuration is 1 μm, but the adjacent features were not resolved clearly in the images constructed with 1 μm resolution, so the 1 μm pixels were binned to generated the images with 2 μm resolution. In the future, the stigmatic mass spectrometer will be improved to use with the magnification lens. Using the magnification lens will further improve the spatial resolution to the sub-micron level. For example, with the pixel size of the detector equal to 50 μm, a 500 times magnification will provide a spatial resolution of 0.1 μm.

Although stigmatic-type imaging mass spectrometer has been used previously for imaging analysis of metal cation distribution in a fish[3], this was the first time the single-cell imaging analyses were performed by the stigmatic-type imaging mass spectrometer. Although a spatial resolution of 2 μm was achieved, no molecular ion peaks from the lipids were observed. Only some fragmentation peaks from lipids were observed. The following are some factors if taken into consideration may produce better results in the future in this regard: 1) The single HeLa cells were imaged with high spatial resolution, but the subcellular structures were not visible because the cell is covered by the membrane. A method that could remove the cell membrane before the matrix deposition and analysis may allow the observation of subcellular structures and more lipid classes. 2) The stigmatic-type MALDI mass spectrometer used in this study can only be operated in the positive-ion mode. However, some lipids classes can only be detected

in the negative-ion mode and, some nanoparticles are more effective in the negative-ion mode. Stigmatic-type MALDI mass spectrometer should be improved to operate in the negative-ion mode. 3) As shown in chapter 4, the Fe_2O_3 nanoparticles are more suitable for the analysis of lipids in the HeLa cells, but they were not used for the imaging analysis because they were deposited in the wet form in this study which reduced the image quality. The deposition of the Fe_2O_3 nanoparticles in dry form may be more suitable for observing more lipids and, it will not affect the spatial resolution.

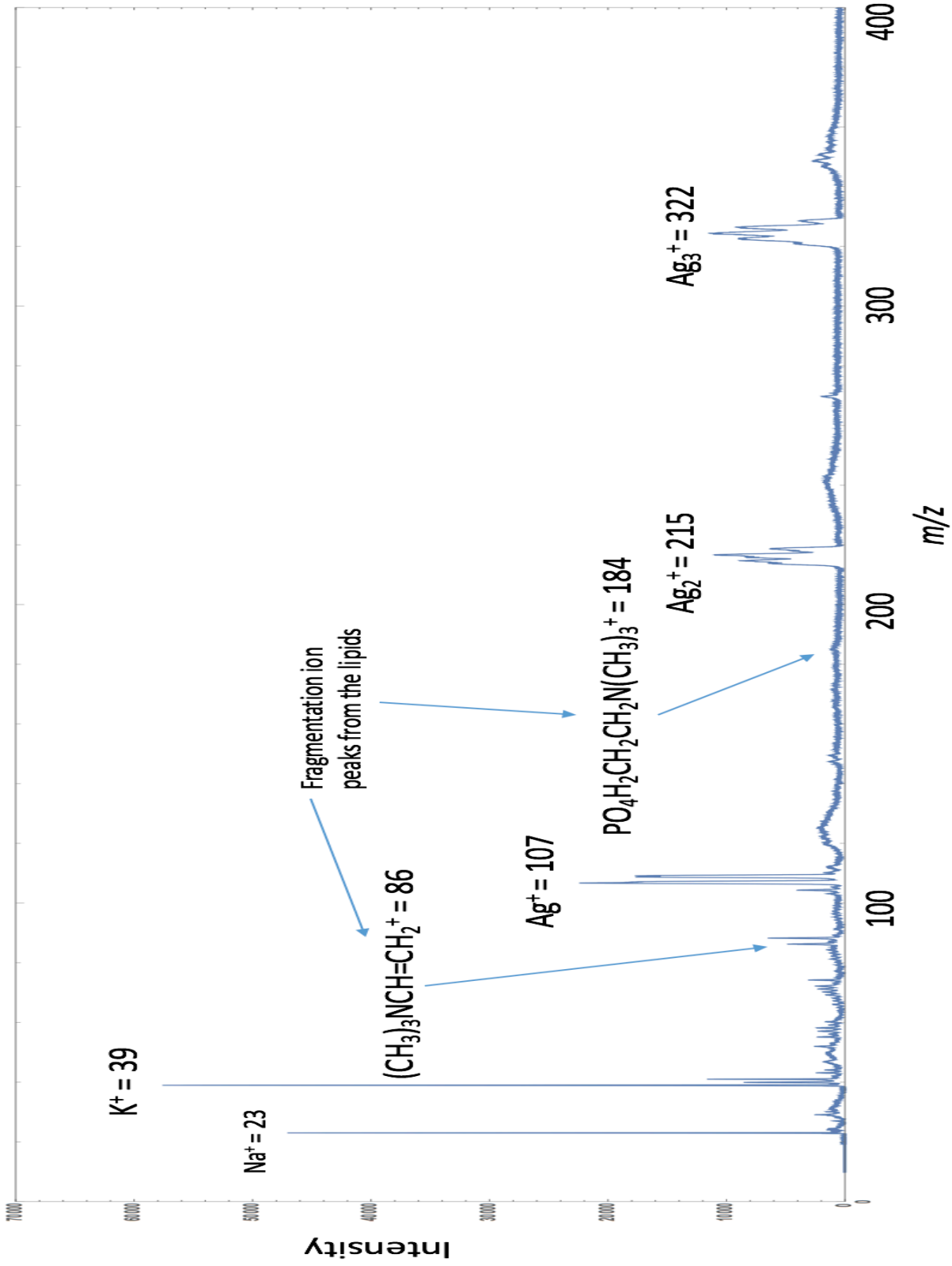

Fig. 5.1 - **Positive-ion mode single spot mass spectrum of the HeLa cells using Ag NPs as a matrix and analyzed by Stigmatic-type MALDI mass spectrometer**

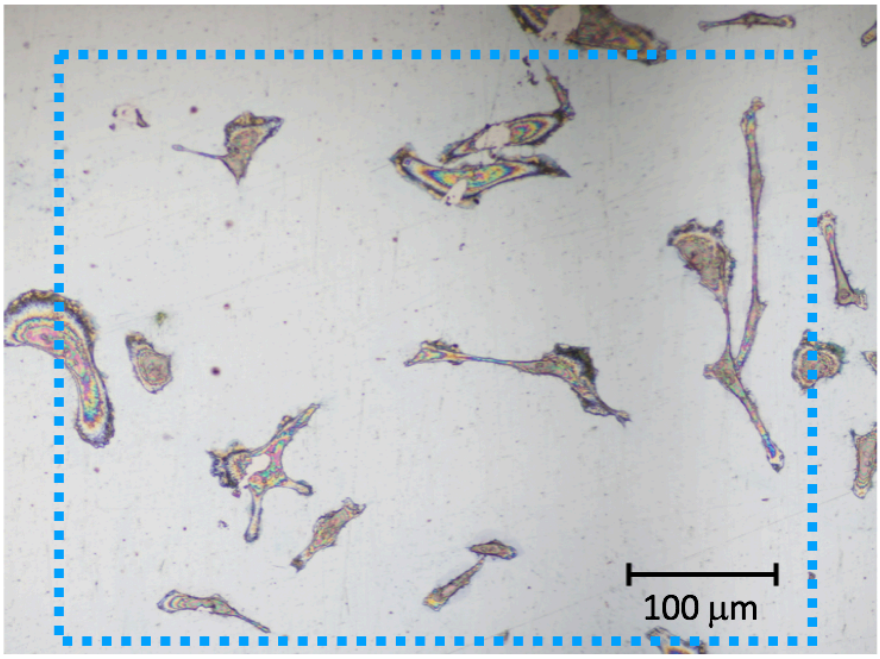

Fig. 5.2 – **Microscopic image of the analyzed sample**

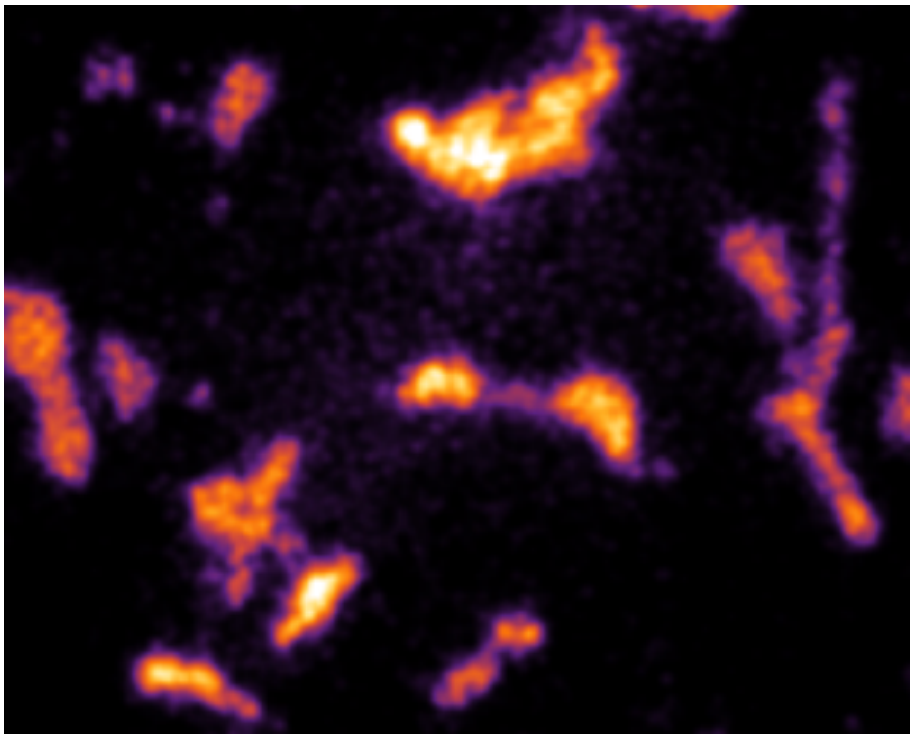

Fig. 5.3 – **Stigmatic mass image of the *m/z* 23 (Na)**

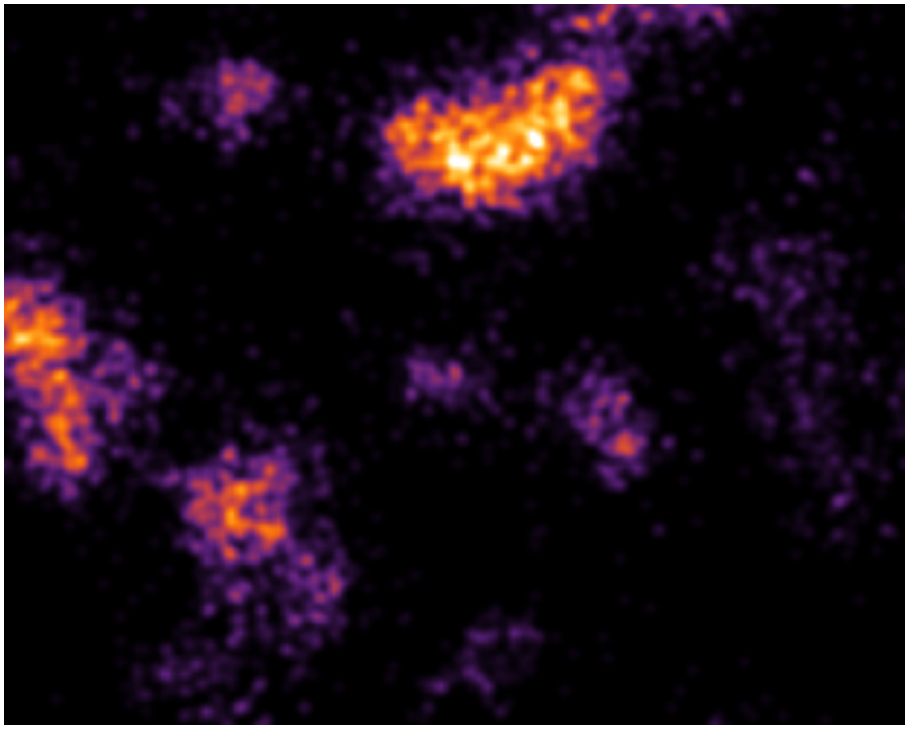

Fig. 5.4 **- Stigmatic mass image of the *m/z* 40 (Ca)**

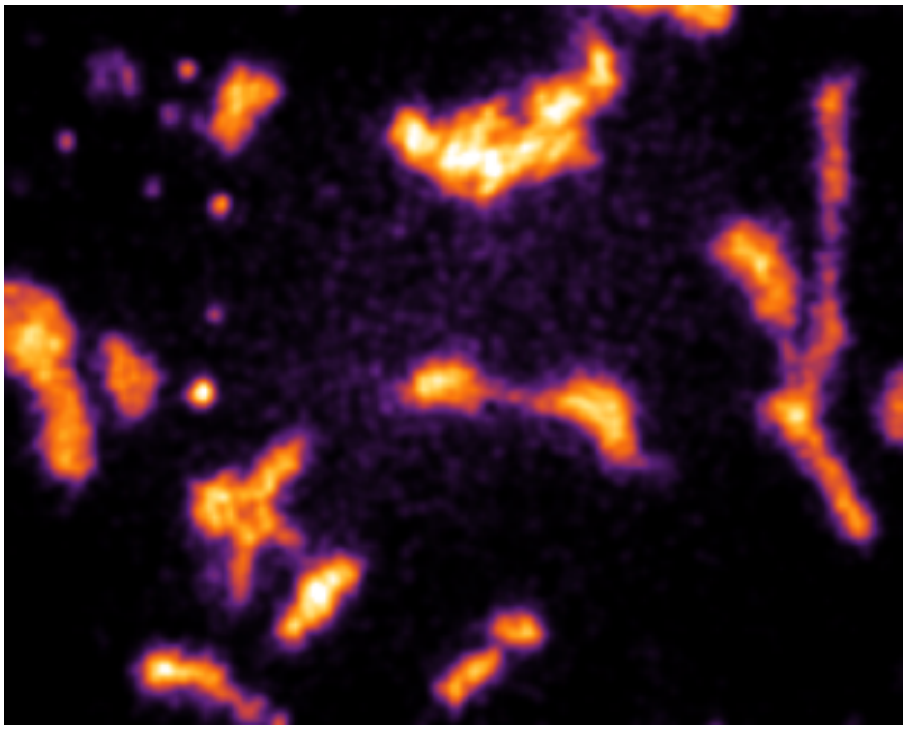

Fig. 5.5 **- Stigmatic mass image of the *m/z* 39 (K)**

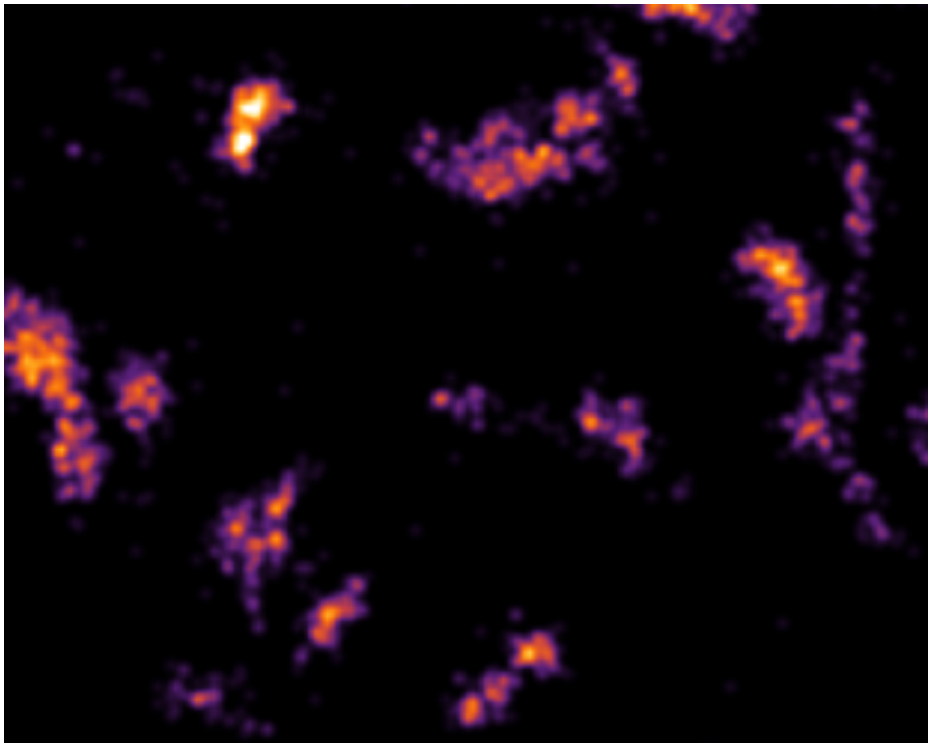

Fig. 5.6 **- Stigmatic mass image of the *m/z* 86**

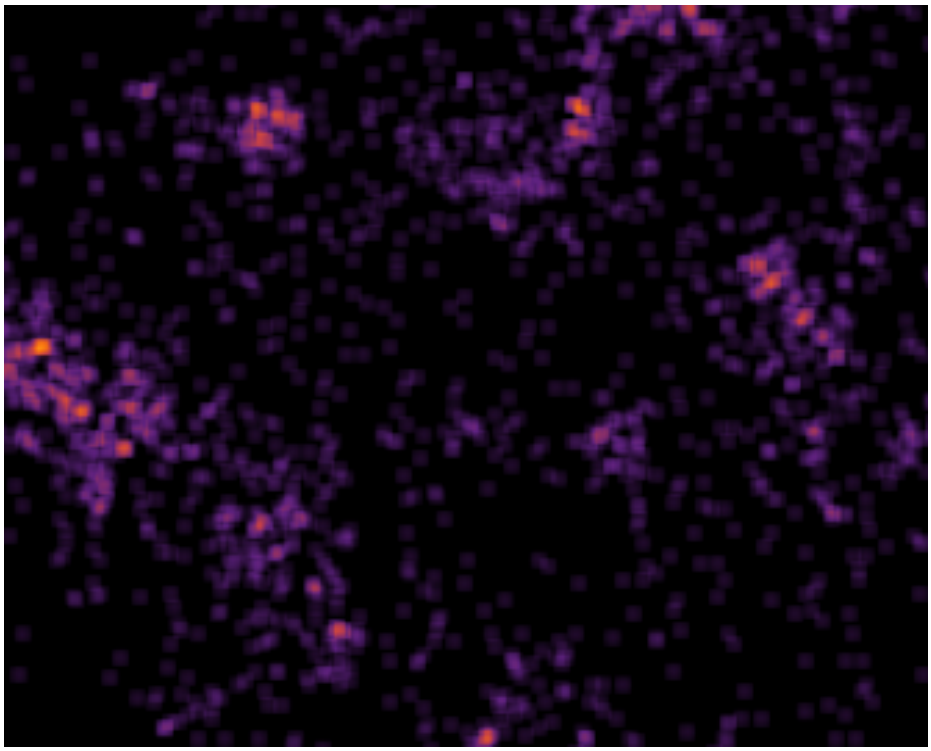

Fig. 5.7 **- Stigmatic mass image of the *m/z* 184**

References

[1] J. Aoki, M. Toyoda *J. Mass Spectrom. Soc. Jpn.* **2013**, 61(3).

[2] H. Hazama, J. Aoki, H. Nagao, R. Suzuki, T. Tashima, K. Fujii, K. Masuda, K. Awazu, M. Toyoda, Y. Naito *Applied Surface Science* **2008**, 255, 1257-1263.

[3] J. Aoki, S. Ikeda, M. Toyoda, *Journal of the Physical Society of Japan* 83, 023001 (**2014**).

Chapter 6

Conclusions and Future Directions

In commercially available conventional MALDI mass spectrometry instruments, the spatial resolution is dependent on the laser spot size which is roughly equal to 10 μm. This resolution is not sufficient for subcellular level imaging analysis. Many researchers have optimized MALDI to obtain a better spatial resolution, but in those instruments too, the spatial resolution is dependent on the laser spot size. In this study, a stigmatic-type MALDI mass spectrometer in which the lateral resolution is independent of the laser spot size is used for the single-cell imaging analysis. This study leads to the following conclusions:

1. Among the nanoparticles used in this study, Fe_2O_3 nanoparticles were most suitable for the analysis of lipids in cells.
2. The spectra obtained with Fe_2O_3 nanoparticles have almost no interference or unidentified peaks whereas a lot of them were observed in the mass spectra obtained using the DHB matrix. However, the intensity of the molecular ion peak, in the case of analysis of the standard phospholipid, is much higher with DHB matrix as compared to Fe_2O_3 nanoparticles and all other nanoparticles.
3. The Fe_2O_3 nanoparticles deposited in the wet form for the imaging analysis of amoeba cells reduced the image quality due to the migration of the analytes. Therefore, Ag NPs which can be deposited in the dry form were used for the final analysis, though they were less suitable for the lipid analysis in the cells.
4. This was the first time the single-cell imaging analyses were performed by the stigmatic-type imaging mass spectrometer. The pixel size or the spatial resolution of the images obtained using the stigmatic-type imaging mass spectrometer is found to be 2 μm which is far better as compared to 20-30 μm of MALDI Spiral-TOF mass

spectrometer. Although a spatial resolution of fewer than 2 μm was achieved in the past using SIMS and by optimizing the laser spot size to less than 2 μm in the conventional MALDI instruments, the measurement time can be greatly reduced in the case of stigmatic-type imaging mass spectrometer.

5. Although the single HeLa cells were imaged with a high spatial resolution by stigmatic-type MALDI mass spectrometer, the sub-cellular structures are not visible because the cell is covered by the membrane. A method that could remove the cell membrane before the matrix deposition and mass spectrometry analysis may allow the observation of subcellular structures.

The following points will be taken into consideration for the better results in the future:

1. In this study, the 7 nanoparticles were selected based on the literature survey and then the nanoparticles for single-cell imaging analysis were selected based on the results obtained. In the future, a better understanding of the SALDI mechanism is necessary for the better selection of the nanoparticles and the synthesis of more suitable nanoparticles for the single-cell analysis. In this study, only 7 nanoparticles were screened. In the future, more nanoparticles will be screened and research for the more suitable nanoparticle will continue. The physical and chemical properties of the nanoparticles such as heat capacity, density, melting point and nanoparticle size might play a role in selecting the better nanoparticle. The absorption spectra of the nanoparticles might also be useful for selecting suitable nanoparticles.
2. The Fe_2O_3 nanoparticles were deposited in the wet form in this study which reduced the image quality. The deposition of the Fe_2O_3 nanoparticles in dry form may produce better images.

3. The stigmatic-type imaging mass spectrometer was used without the MULTUM mass analyzer and PEDA method, which in result led to a low mass resolution. Using the PEDA method and MULTUM mass analyzer will improve the mass resolution and thus, the distribution of the ions can be observed more precisely in the images.
4. The stigmatic-type MALDI mass spectrometer used in this study can only be operated in the positive-ion mode. However, some lipids classes can only be detected in the negative-ion mode and, some nanoparticles are more effective in the negative-ion mode. Stigmatic-type MALDI mass spectrometer will be improved to operate in the negative-ion mode.
5. In this study, the stigmatic mass spectrometer was used without the magnification lens because it was difficult to align with the ion trajectory axis. Only the Einzel lens was used to magnify the ion distribution and focus it onto the detector and, the spatial resolution is determined by this magnification and the pixel size of the detector. In the future, the stigmatic mass spectrometer will be improved to use with the magnification lens. Using the magnification lens will further improve the spatial resolution to the sub-micron level.

The nanoparticle screening performed in this study may come handy in the future for the selection of nanoparticles for the single-cell analysis. The stigmatic-type imaging mass spectrometer showed the potential for high-resolution single-cell imaging. The spatial resolution and mass resolution can be improved further by making some improvements in the instrument. Since single-cell analysis is very important, this study will be of great importance for the single-cell biologist and mass spectrometry researchers and, inspire them to perform single-cell analysis using stigmatic-type imaging mass spectrometer.

Appendix

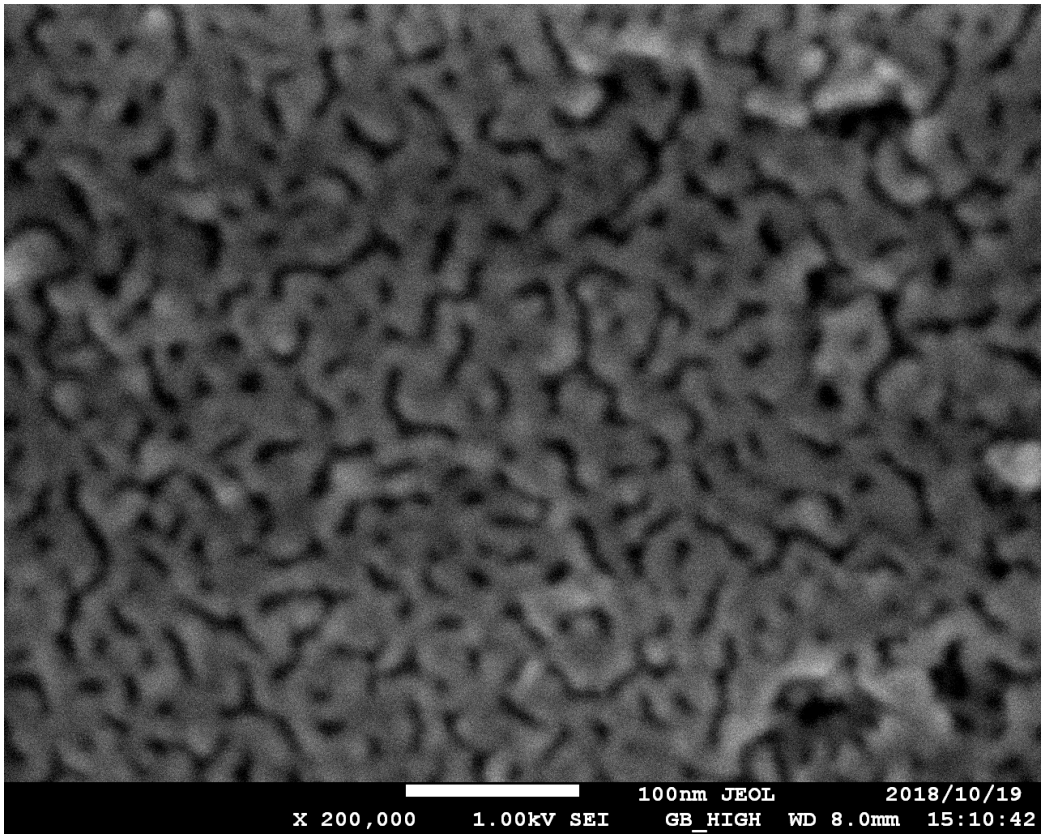

Fig. A – **SEM image of the Ag NPs deposited on a 0.1 mm thin stainless steel plate using an ion sputtering instrument**

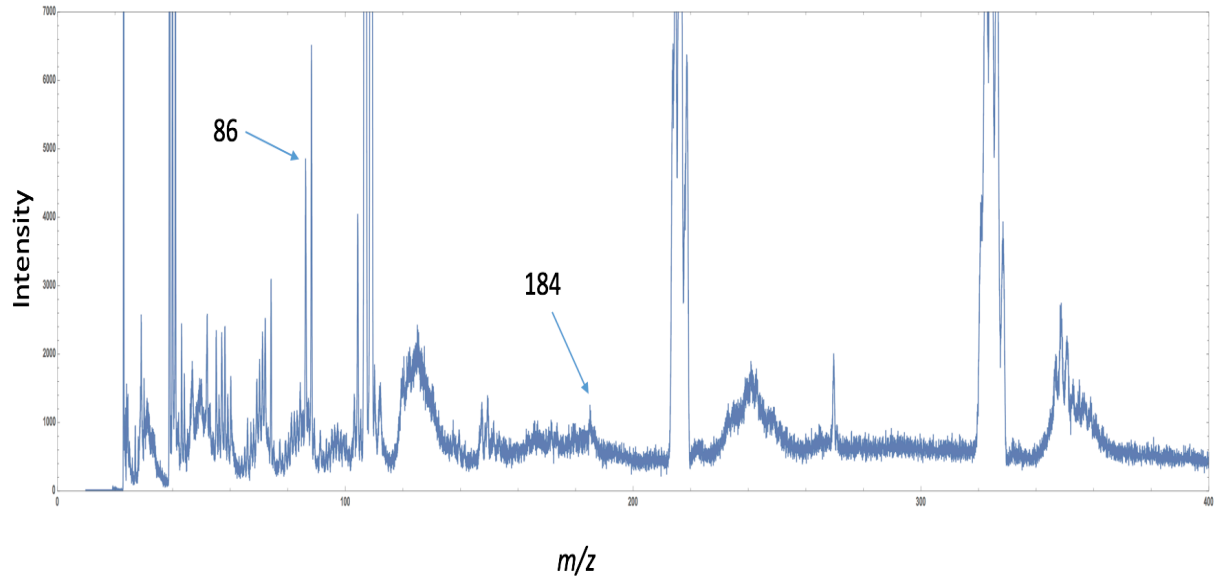

Fig. B – **Enlarged view of peaks in Positive-ion mode single spot mass spectrum of the HeLa cells using Ag NPs as a matrix and analyzed by Stigmatic-type MALDI mass spectrometer**

Acknowledgements

First of all, I would like to express my gratitude to Professor Michisato Toyoda who gave me the opportunity to work in on this project. I also express my gratitude to Assistant Professor Jun Aoki who supervised me in this project. I want to thank him for the useful discussions whenever needed. I also thank him for the experiments with the stigmatic mass spectrometer. A great thanks to Professor Yasuo Kanematsu for reviewing this thesis and useful discussions during the lab meetings.

A heartfelt thanks to Professor Masahiro Ueda from Laboratory of Single Molecule Biology, Graduate School of Frontier Biosciences, Osaka University for collaborating in this project and, to Assistant Professor Satomi Matsuoka of the same lab for preparing the cell samples and useful discussions. I would also like to thank a past member of the same lab, Dr. Yukihiro Miyanaga for preparing amoeba cell samples and useful discussions.

A big thanks to the past member of our lab Dr. Kirk Jensen for teaching me the operation of the MALDI instrument and useful discussions.

I would like to thank Mr. Junichi Osuga for the useful discussions and his help during the experiments with Spiral-TOF mass spectrometer. I would also like to thank Ms. Yumi Miyake for the useful discussions and suggestions for the experiments with amoeba cells.
I would like to thank Professor Hideya Kawasaki of Kansai University for the useful discussions on nanoparticles.

I also want to thank Assistant Professor Yosuke Kawai from the earth and space science department of Osaka University for the useful discussions and, for the SEM analysis and, for letting me use the digital microscope.

I would like to thank my colleague Mr. Naruaki Imaoka for the useful discussions. I also want to thank him and my other past colleagues Mr. Syuhei Takagi, Mr. Takumi Funatsu, Mr. Akira Oba, Mr. Koki Maeda, Mr. Yusuke Iwai and current colleagues Mr. Shinya Kawai, Ms. Moe Okuyama, Ms. Kana Kato, Mr. Ikuo Kashihara, Mr. Tomohiko Yasukura for their support with Japanese language which made my stay in Japan more convenient and enjoyable.

This work was supported by the Advanced Research and Development Programs for Medical Innovation (AMED-CREST) from the Japan Agency for Medical Research and Development, AMED JP17gm0910001. I would like to thank JICA (Japan International Cooperation Agency) for daily life financial support.

Finally, I would like to express my gratitude to my parents. Without their blessings and efforts, I wouldn't have been here at this platform.